ACTION SPECTRUM OF THE "SECOND EMERSON EFFECT"

GOVINDJEE *and* EUGENE RABINOWITCH
From the Photosynthesis Research Laboratory, Department of Botany, University of Illinois, Urbana

ABSTRACT A peak is found at 670 mμ in the action spectrum of the "second Emerson effect"[1] (22, 33), in the green alga *Chlorella pyrenoidosa,* and in the diatom *Navicula minima;* a shoulder appears in about the same location in the blue-green alga *Anacystis nidulans* and less clearly in the red alga *Porphyridium cruentum.* This peak (or shoulder) corresponds to an absorption band belonging to a form of chlorophyll *a in vivo,* which can be designated as "Chl *a* 670." Light absorption by this form can enhance the yield of photosynthesis caused by far red light (680 to 720 mμ), as effectively as does light absorption by chlorophyll *b,* chlorophyll *c,* fucoxanthol, phycocyanin, or phycoerythrin. The action spectrum of the second Emerson effect in *Anacystis nidulans* shows three peaks attributable to phycocyanin, at 570, 600, and 640 mμ. These correspond well to peaks on the curve, calculated by Emerson (17), which shows the fraction of total absorbed light absorbed by phycocyanin as function of wavelength. Intensity relation between the two participating beams has an important bearing on the second Emerson effect. In *Anacystis,* the "negative effect," described in (17), can be converted into a positive effect by change in this relation. In *Anacystis,* the saturation of photosynthesis occurs, at 700 mμ, in weaker light and on a lower level than at 680 mμ, and even more so, than at 600 mμ. This may explain, at least in part, the negative Emerson effect observed in this alga.

INTRODUCTION

It has been—and still is—generally accepted that chlorophyll *a* is the primary sensitizer in photosynthesis (*cf.* Duysens (6) and Rabinowitch (32*a*)). Until recently, it was assumed that absorption of light by chlorophyll *a* is fully sufficient for photosynthesis, and that it gives a constant quantum yield throughout the spectrum. However, Emerson and Lewis (15, 16), and later Haxo and Blinks (26), noted that the quantum yield of photosynthesis drops in the far red region, well within the main red absorption band of chlorophyll *a* ("red drop"). Later, Emerson

[1] The second Emerson effect is the enhancement of the yield of photosynthesis caused by far red light, by simultaneous illumination with light of shorter wavelengths. The first one is the "burst" of carbon dioxide released by plants in the first minutes of illumination.

(7, 8) and Emerson and coworkers (10, 12, 13, 17) found that the quantum yield of photosynthesis attributable to far red light can be enhanced by supplying simultaneously substantial amounts of "supplementary" light of shorter wavelengths. ("Catalytic" amounts of supplementary light give no enhancement, contrary to the findings of Warburg (41).) Emerson (17) plotted the action spectrum of this enhancement (which became known as the "second Emerson effect") and found it to follow closely the curve showing the fraction of total absorbed light absorbed by the accessory pigments (be it chlorophyll *b* in *Chlorella,* fucoxanthol and chlorophyll *c* in *Navicula,* phycocyanin in *Anacystis,* or phycoerythrin in *Porphyridium*). Thus it appeared to Emerson (7, 8, 17) that excitation of chlorophyll *a* alone may not be enough to produce photosynthesis (or, at least, to do this with a high quantum yield); to obtain a full yield, it appeared necessary to excite simultaneously an accessory pigment, absorbing at shorter wavelengths.

The red drop begins much earlier in red than in green algae; but Emerson (7, 8, 12) noted that in this case, too, it starts when chlorophyll *a* begins to take up most (and ultimately all) of the absorbed light.

The conclusion that photosynthesis requires the excitation of an accessory pigment (in addition to that of chlorophyll *a*) seemed, however, to contradict the conclusions, drawn from experiments on sensitized fluorescence of chlorophyll *a in vivo* (*cf.* Duysens (6)), that accessory pigments contribute to photosynthesis to the extent to which their excitation is transferred, by resonance, to chlorophyll *a*. Franck (18) suggested that what is really necessary for full yield of photosynthesis, is balanced formation of two excited forms of chlorophyll *a*. Only one of these forms is obtained by absorption beyond the threshold of the red drop, while the other can be formed either by direct absorption by chlorophyll *a* at shorter wavelengths, or by resonance transfer of excitation energy from the accessory pigments. The difference between the two types of excitations is associated, according to Franck, with one part of chlorophyll *a* being present in the cells in a hydrophilic, and another part, in a hydrophobic surrounding. Lavorel (30), Krasnovsky (27, 28, 40), and Brody (3) suggested, as an alternative (or supplementary) interpretation, that the two forms of chlorophyll *a* are monomeric and dimeric, respectively. The development up to this point was summarized in a paper by Emerson and Rabinowitch (17).

French and coworkers (4, 19) confirmed, by differential spectroscopy, what was often surmised before—that several spectroscopically different forms of chlorophyll *a* exist in algae, flagellates, and leaves. Two forms of Chl *a in vivo* were noted also by Halldal (25) in *Anacystis nidulans,* Thomas and Marsman in *Porphyra* (39) and Thomas and Govindjee (38) and Cederstrand (5) in *Porphyridium cruentum.* Krasnovsky and coworkers (27, 28, 40) reported that two forms of chlorophyll *a in vivo* are photooxidized at different rates.

Govindjee and Rabinowitch (22) and Rabinowitch and Govindjee (33) reported in a preliminary note that absorption in the form "Chl *a* 670" enhances the yield of photosynthesis produced by absorption in other chlorophyll forms (Chl *a*

680 and Chl *a* 690). These results are described in more detail in the present paper. It also presents evidence concerning the "negative Emerson effect" (17), and new features of the action spectrum of the second Emerson effect in *Anacystis* and *Porphyridium*.

Rajni Govindjee *et al.* (24) recently observed the second Emerson effect also in the photoreduction of quinone by *Chlorella* cells; while Govindjee *et al.* (21) reported that the yield of fluorescence of chlorophyll *a* in a mixture of far red and blue light is smaller than the average of the yields in the two separate beams. These observations provide additional evidence of differences in the immediate consequences of excitation of the several forms of Chl *a in vivo*, and of their mutual interaction.

MATERIALS AND METHODS

The studied organisms were *Chlorella pyrenoidosa* Chick strain 3, *Navicula minima* Grun, *Porphyridium cruentum*, and *Anacystis nidulans*. All four species were cultured in 300 ml Erlenmeyer flasks with sealed-in tubes for passing air (or air containing 5 per cent carbon dioxide). These flasks were charged with 200 ml of culture medium, plugged with cotton, and sterilized in an autoclave for 10 to 30 minutes at 15 pounds per square inch before inoculation. Care was taken to use always the same amount of inoculum from the same stock when working with a given species. All the cultures used were single strain cultures free from bacteria and molds. Details of their growing conditions are given in Table I.

Cells were harvested and washed twice in cold (10°C) buffer (Warburg's buffer No. 11 with added NaCl for *Porphyridium;* buffer No. 9 for *Chlorella, Anacystis,* and *Navicula*). Cell suspensions were made up to 7 ml in their respective buffers. We adjusted them to identical optical density of 0.500 at the chlorophyll *a* absorption peak (rather than to identical cell density). Measurements were made in closed differential manometers (*cf.* Emerson and Chalmers (9), for detailed description of the method). The levels of the liquid in both arms of the manometer were read simultaneously to hundredths of a millimeter, using two cathetometers. Seven readings were taken at intervals of 1 minute in each measuring period; the first three were discarded because the steady rate was reached only after 2 minutes. The water bath was maintained at 10°C.

"Far red" light was obtained, in the earlier experiments, by means of a combination of sharp cut-off filters (Schott RG5, Schott RG8, and a Corning filter). Fig. 1 shows the resulting transmission curve. In later experiments we used instead an interference filter (Farrand No. 109556), with maximum transmission at 700 mμ (half-band width, 16 mμ).

The optical system used to isolate far red light was described by Thomas and Govindjee (see Fig. 1, (38)). "Supplementary" light was obtained from the Emerson-Lewis monochromator (f 1.5) with a 225 watt tungsten ribbon filament lamp operated at full capacity. Both the supplementary light, and the far red light were projected at the manometer vessel from below. The following sequence of readings was used in most of the experiments: *Dark, Far Red, Dark, Far Red, Supplementary, Supplementary + Far Red, Supplementary, Supplementary + Far Red.* The action of the far red light was checked at the end of each experiment; but if there was reason to think that this action

TABLE I

SUMMARY OF CULTURING CONDITIONS

	Chlorella pyrenoidosa	*Navicula minima*	*Anacystis nidulans*	*Porphyridium cruentum*
Strain isolated by	Emerson	Tanada	Kratz and Allen	Lewin
Inoculum, in μl/200 ml	15–20	100	15–20	100
Culture medium described by	Emerson and Chalmers* (11)	Tanada (36)	Kratz and Myers (29)	Brody and Emerson (1)
Illumination	4 tungsten lamps and 1 white fluorescent ring	10 white fluorescent rods	4 white fluorescent rods and 1 tungsten bulb	10 fluorescent rods. See Thomas and Govindjee (38)
Wattage of each lamp or rod	60 watt tungsten and 32 watt white fluorescent	15 watt white fluorescent	40 watt white fluorescent and 100 watt tungsten	15 watt white fluorescent
Distance from the bottom of flask	6 inches (tungsten) 4 inches (fluorescent ring)	6 inches	7½ inches	6 inches
Axis to axis distance of the fluorescent rods	Distance between the axes of the tungsten bulbs = 3 inches	1 1/16 inches	3 1/16 inches	2¼ inches
No. of days culture flasks were on line	2–3	3–4	2–3	6–7
Temperature of culture bath	20°C ± 2°C	25°C ± 2°C	27°C ± 2°C	19°C ± 2°C
Gas mixture	5% CO_2 in air	Filtered room air or 5% CO_2 in air	Filtered room air or 5% CO_2 in air	5% CO_2 in air
Growth (x-fold)	40	20	40	40

Growth (x-fold)	40	20	40	40

FOOTNOTES TO TABLE I

* $MgSO_4.7H_2O$: 1.017×10^{-3} M; KH_2PO_4 : 13.79×10^{-3} M; $CaCO_3$: 0.1598×10^{-3} M; KNO_3 : 12.38×10^{-3} M; Na_2HPO_4 : 0.2498×10^{-3} M; KCl: 0.335×10^{-3} M; $FeSO_4.7H_2O$: 2.05×10^{-3} M; A_2 : 0.2 ml/200 ml; ABC : 0.1 ml/200 ml.
[A_2 contains $MnCl_2.4H_2O$: 1.8 gm/1; H_3BO_3 : 2.86 gm/1.]
[ABC contains 5 ml A_3, 1 ml B_9, and 5 ml C_{10} made up to 100 ml.]
[A_3 contains $(NH_4)_6Mo_7O_{24}.4H_2O$: 0.188 gm/1; $ZnSO_4.7H_2O$: 0.22 gm/1; $CuSO_4.5H_2O$: 0.079 gm/1.]
[B_9 : refer to Brody and Emerson (1).]
[C_{10} contains As_2O_3 : 6.61 mg/1; $SrSO_4$: 10.49 mg/1; $HgCl_2$: 6.77 mg/1; $PbCl_2$: 6.71 mg/1; LiCl : 30.55 mg/1; RbCl : 14.2 mg/1; $K_2TiF_6.H_2O$: 5.0 mg/1; $NaSeO_4$: 11.96 mg/1; $Be(NO_3)_2.3\ H_2O$: 103.7 mg/1; uranyl nitrate : 10.0 mg/1.]

Special Care.

Chlorella. (*a*) The illumination was reduced to two 15 watt tungsten bulbs for the final 24 hours preceding the manometric experiments as advised by Emerson (14) to reduce the rate of respiration. (*b*) Culture flasks were shaken once a day to avoid settling of algae on the bottom of the flask.

Navicula. (*a*) On the last day, the culture flask "saw" essentially only one 15 watt fluorescent light. (*b*) A magnetic rod wrapped in teflon was sterilized with alcohol, dried by keeping it near a flame and aseptically introduced into the flask on the last day. The culture flask was left overnight (12 to 16 hours) on the magnetic stirrer. Both (*a*) and (*b*) were necessary to get homogeneous cultures having convenient rates of respiration for manometry.

Anacystis. Culture flasks were shaken once a day; the illumination was reduced to one 40 watt fluorescent rod on the last day.

Porphyridium. (*a*) On the last 2 days, illumination was reduced to a single 15 watt fluorescent rod. (*b*) Cultures were shaken continuously by a wrist action shaker to prevent settling of the algae and to get homogeneous cultures.

was not constant, it was checked repeatedly during the experiment. The light action of far red light in the presence of accessory light of various wavelengths was expressed in per cents of that of far red light alone. Values above 100 mean a "positive" second Emerson effect; values lower than 100 suggest a "negative" effect. The results are plotted in Figs. 2, 4, 6, 8, and 9.

Absorption measurements were done either with the integrating sphere of Cederstrand (5); or by the wet filter paper technique described by Thomas and Govindjee (38), or by a modified technique of Shibata, using oiled filter paper instead of opal glass (35).

RESULTS AND DISCUSSION

A. *Different Photochemical Activity of Two Forms of Chlorophyll a in vivo.* Supplementary monochromatic light used in these experiments was varied between 640 and 700 mμ, by increments of 10 mμ, the band width being 10 mμ. Fig. 2 shows the resulting action spectrum of *Chlorella.* In the range studied, there are two sharp peaks: at 650 and 670 mμ. The former was noted by Emerson and coworkers (10, 17) and ascribed to chlorophyll *b;* it was also observed by

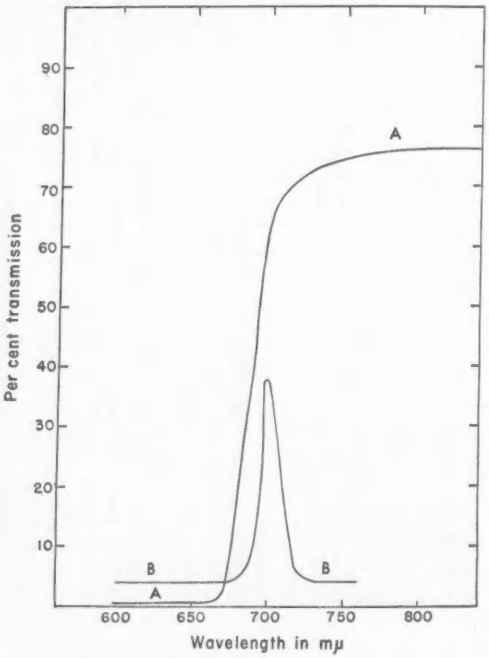

FIGURE 1 *A,* transmission curve of the combination of Schott glass filters RG5, and RG8, and a red Corning filter. *B,* transmission curve of a Farrand interference filter (No. 109556) used to produce far red light (~ 700 mμ).

Myers and French (31). The peak at 670 mμ was not noted before. The ratio of the heights of the two peaks changed from culture to culture (between 0.86 and 1.20) probably owing to variations in the relative amounts of chlorophyll *b* and chlorophyll *a* 670.

When the absorption spectra of the same cultures were measured, two peaks, which must be both due to chlorophyll *a*, could be seen, at 670 to 672 mμ and at 678 to 680 mμ respectively (Fig. 3).

These results provide clear evidence of the existence and a specific photochemical function of a form Chl *a* 670 *in vivo*. This function is not shared by Chl *a* 680. (There is evidence of the existence of a third form, Chl *a* 690; but our action spectra did not permit us to differentiate between the contributions to photosynthesis due to Chl *a* 680 and Chl *a* 690. In order to obtain a full yield of photosynthesis

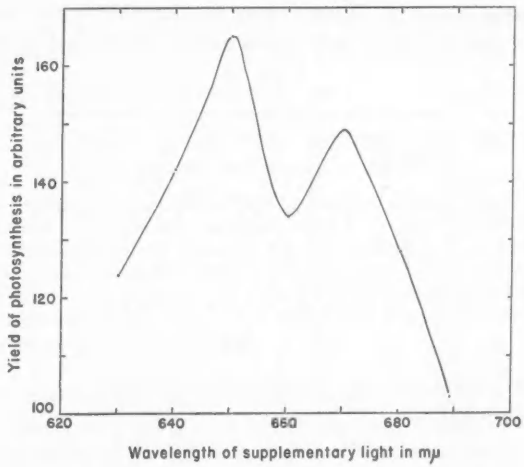

FIGURE 2 Action spectrum of the second Emerson effect in *Chlorella pyrenoidosa*. Light action of far red light alone is taken as 100. Light action of the far red light alone was 3.0 μl/hour and the ratio of far red:supplementary light actions was 1:1. Far red light was > 680 mμ. Similar results were obtained by using light that was ~ 700 mμ.

from excitation of Chl *a* 680, the Chl *a* 670 must be also excited in appropriate proportion, and failure to do so is the reason for the red drop. It can be postulated that when Chl *a* 670 alone is excited, it transfers enough energy to Chl *a* 680 to achieve balanced excitation of both forms; but the reverse transfer is negligible for energetic reasons. Therefore, as soon as quanta become prefrentially absorbed by Chl *a* 680, the quantum yield begins to decline (*cf.* Franck (18) and Emerson and Rabinowitch (17)).

After having observed the 670 mμ peak, we reexamined the original curves of Emerson and coworkers and noticed that Emerson's figure for *Chlorella* (17) already suggested the existence of this peak.

Fig. 4 shows the action spectrum of *Navicula minima.* We clearly recognize a peak of 670 mμ (Chl *a* 670), in addition to the peaks at 630 mμ (Chl *c*) and 540 mμ (fucoxanthol). The position and shape of the fucoxanthol band in the action spectrum should be analyzed in terms of relative contribution of this pigment to the total light absorption by the cells at different wavelengths. Emerson's calculation (17) suggests only one peak in the latter curve, at 535 mμ; but this result cannot be reliable because of the strong change the absorption curve of fucoxanthol undergoes *in vivo* compared to its shape *in vitro.*

The absorption spectrum of *Navicula* (Fig. 5) again shows evidence of two peaks attributable to chlorophyll *a.* The ratio of the optical densities due to Chl *a* 670 and Chl *a* 680 appears higher in *Navicula* than in *Chlorella;* it remains to be seen whether this is a general rule, or only applies to the cultures used by us.

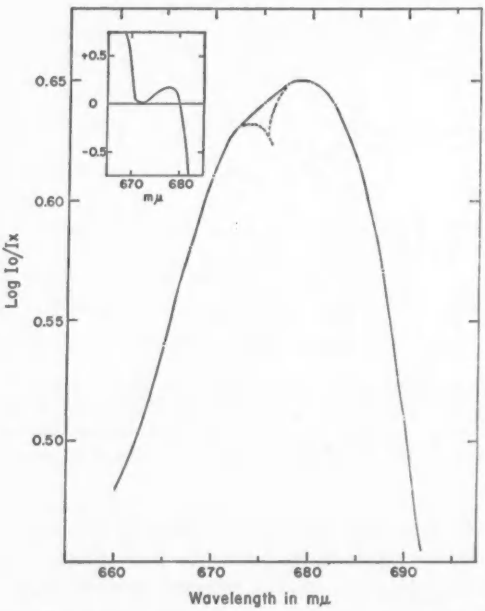

FIGURE 3 Absorption spectrum of a culture of *Chlorella pyrenoidosa,* measured by Beckman spectrophotometer using the oiled filter paper technique. Dotted lines are drawn to emphasize the existence of two peaks of chlorophyll *a.* Insert shows a first derivative absorption spectrum of *Chlorella* (a different culture). All samples measured showed a double peak of chlorophyll *a.*

Fig. 6 represents the action spectrum of the second Emerson effect in the blue-green alga *Anacystis nidulans*. The main peak is clearly due to phycocyanin; the results in the chlorophyll absorption region are not very clear, and vary from culture to culture. In nearly all experiments with this alga, at least a shoulder could be noted in the 670 to 680 mμ region. In one experiment, (Fig. 6*C*) a peak was present at 665 mμ, in another (Fig. 6*D*) at 675 mμ. This suggests that the Chl *a* 670

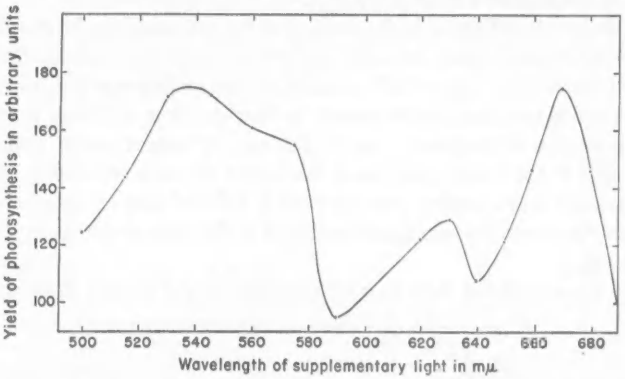

FIGURE 4 Action spectrum of the second Emerson effect in *Navicula minima*. Light action of far red light alone is taken as 100. Measurements were made only in the region 600 to 700 mμ; the action spectrum of Emerson (17) is shown from 500 mμ to 600 mμ (we have confirmed the approximate shape of this section). Light action of the far red light alone was 8.0 μl/hour and the ratio of far red light to supplementary light actions was 1:2. Far red light was $>$ 680 mμ. Similar results were obtained by using light that was $\sim$ 700 mμ.

form may exist and be active also in this species. The variability of the action spectrum of *Anacystis* in this region (670 to 700 mμ) may be related to the fact that *Anacystis* often shows in this region a negative Emerson effect (to be discussed later); but the nature of the relation we do not yet understand.

Fig. 7 shows the absorption spectrum of *Anacystis nidulans*. In addition to the phycocyanin maximum at 627 mμ, it shows an apparently triple band of chlorophyll *a*, with peaks located at approximately 672, 675, and 680 mμ. However, not in all cultures was such a triple peak observed.

Fig. 8 represents the action spectrum of the red alga *Porphyridium;* it shows a less clear shoulder at about 675 mμ.

Red algae, such as *Porphyridium*, exhibit a red drop much earlier than *Chlorella*, *Navicula*, and *Anacystis* (at $\sim$ 650 mμ instead of at $\sim$ 680 mμ). Despite the early red drop, Brody and Emerson (2) found, in *Porphyridium*, measurable photosynthesis in monochromatic light even at 680, 690, and 700 mμ (confirmed by us). The reason for earlier drop may be that the ratio of absorptions by Chl *a* 670 and Chl *a* 680 in these organisms falls earlier than in *Chlorella* below the minimum

required for full photosynthesis. This hypothesis should be checked by quantitative analysis of the red absorption bands of the different algae and calculation of the relative contributions of several Chl *a* components to the total absorption. The amount of Chl *a* 670 in red algae may be sufficient to serve as acceptor for energy transfer from auxiliary pigments, but not enough for significant direct absorption. The absorption spectrum of *Porphyridium* (see Figs. 2, 4 (38)) suggests a doublet nature of the chlorophyll *a* band in this alga.

Alternatively, the difference in the position of the red drop may be due to spatial separation of Chl *a* 670 and Chl *a* 680 in *Porphyridium*, with phycoerythrin being closely associated with "Chl *a* 680" (along the lines of Duysens' original theory).

Phycocyanin is not prominently present in *Porphyridium*, but there is indication in our experiments of its presence in the existence of several peaks in the 600 to 660 mμ region in the action spectrum of the second Emerson effect (Fig. 8). However, the amount is too small to raise the yield to its maximum value; otherwise, the red drop in *Porphyridium* would have occurred in the same region as in *Anacystis*, (*i.e.* at 680 mμ).

B. *Photochemical Activity of Phycobilins in the Second Emerson Effect.*

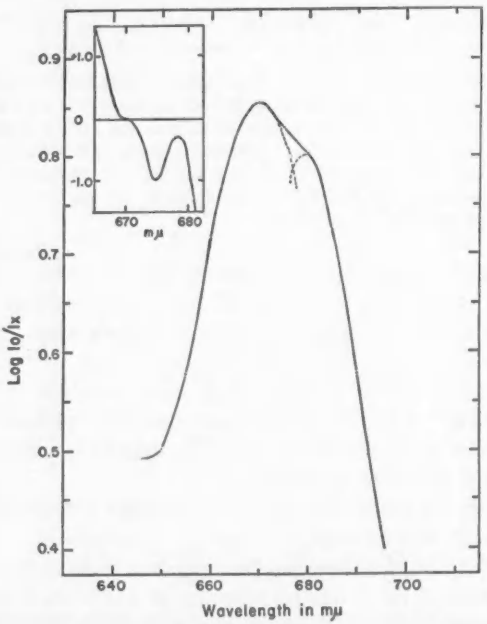

FIGURE 5 Absorption spectrum of *Navicula minima* obtained with Cederstrand's integrating sphere spectrophotometer. Dotted lines are drawn to emphasize the presence of two peaks of chlorophyll *a*. Insert shows a first derivative absorption spectrum of *Navicula*. All samples measured showed a double peak of chlorophyll *a*.

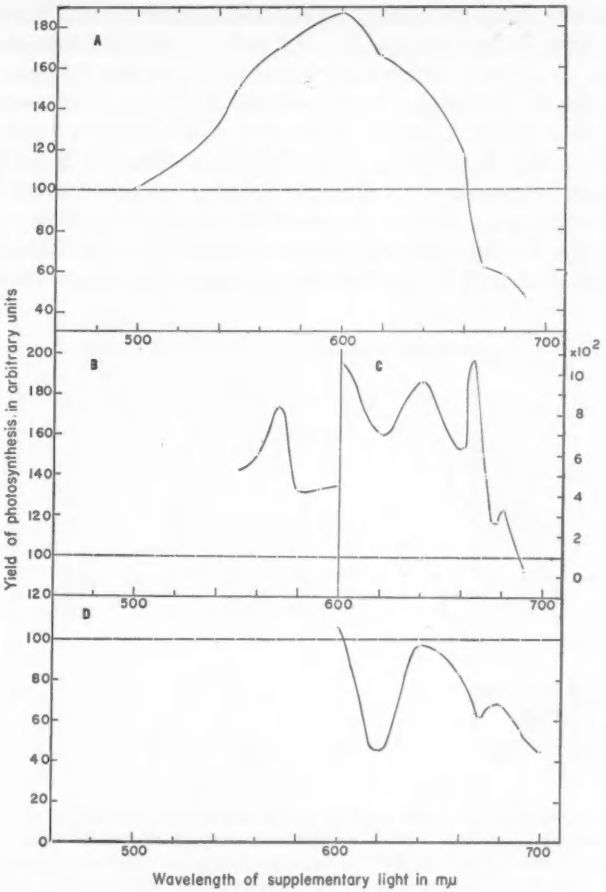

FIGURE 6 Action spectra of the second Emerson effect in *Anacystis nidulans*. *A*, intensity of far red light comparable to that used by Emerson (10, 17). Light action of the far red light alone was 8.5 μl/hour and the ratio of far red to supplementary light actions was 1:1. Curve drawn to suggest a triple peak, although this particular experiment does not justify it. Note points which confirm Emerson's findings. *B*, a different intensity of far red light; note peak at 570 mμ. Light action of far red light alone was 1.5 μl/hour and the ratio of far red to supplementary light actions was 1:2. *C*, intensity of far red light lower than in *A*, *B*, and *D*. Light action of far red light alone was 0.25 μl/hour and the ratio of far red to supplementary light actions was 1:20. Nearly all values are positive; note peaks at 640 and 665 mμ. *D*, intensity of far red light higher than in *A*, *B*, and *C*. Light action of far red light alone was 15.0 μl/hour and the ratio of far red to supplementary light actions was 1:1. All values are negative, and there are peaks at 640 and 675 mμ. (Scale of ordinates is different for different curves. Far red light was ~ 700 mμ.)

Fig. 6 nows the action spectrum of the second Emerson effect in *Anacystis nidulans*. It confirms the conclusions of Emerson and coworkers that light absorbed by phycocyanin (or rather, by the several phycocyanins) can raise the yield in far red light. The phycocyanin peak is not single but often triple (Fig. 6), corresponding to three maxima in the curve showing the fraction of light absorbed by phycocyanin as function of wavelength (17). These peaks lie at 570, 600, and 640 mμ. In *Porphyridium* (Fig. 8) we noted in two experiments a new peak (not noted by Emerson and coworkers) at 650 mμ. It cannot be due to Chl *b*—which is absent—but may be due to phycocyanin or allophycocyanin. The height of this peak relatively to that of the peak at about 510 mμ (not shown in Fig. 8; *cf.* Emerson (10,

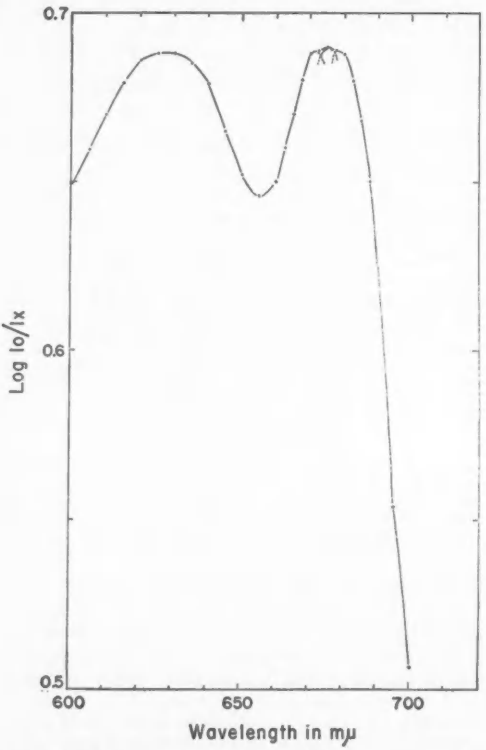

FIGURE 7 Absorption spectrum of *Anacystis nidulans* measured by Beckman spectrophotometer, using oiled filter paper technique. The spectrum was confirmed by wet filter paper technique. All samples did not show the triple peak. Some samples had two peaks and some appeared to have only one. This may be due to variability in the relative amounts of the three forms in different samples.

17)) is usually 1:6. We do not know the exact absorption spectrum of the phycocyanin in *Porphyridium* and therefore cannot calculate the fraction of light absorbed by this pigment. The 650 mμ peak was not observed in two other experiments on *Porphyridium;* this could be due to the very low concentration of phycocyanin in some cultures.

C. *Negative Emerson Effect.* The action spectrum of *Chlorella* (Emerson and Rabinowitch (17); and Fig. 2) shows no negative effects in *Chlorella.* However, some of our experiments with this alga did show a negative effect when 680 to 700 mμ supplementary light was used (see Fig. 9). We asked ourselves whether it could be associated with an early saturation of photosynthesis in 700 mμ

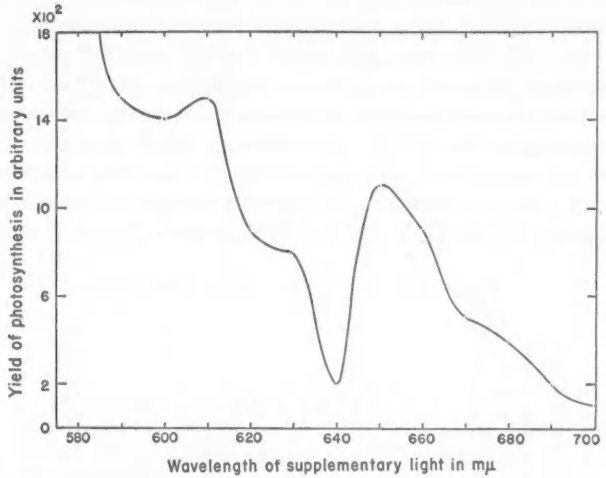

FIGURE 8 Action spectrum of the second Emerson effect in *Porphyridium cruentum.* Intensity of far red light used in this experiment was very low. Only two experiments of this type were made. Light action of the far red light alone was 0.09 μl/hour and the ratio of far red to supplementary light actions was 1:60. Far red light was ~ 700 mμ.

light. It was at first difficult to believe that saturation could occur, at certain wavelengths, below compensation; but this turned out to be the case. Data in the literature did not indicate (*cf.* Rabinowitch (32*b*)) that saturation levels can vary with wavelength. However, preliminary results with *Anacystis nidulans* (33) and the findings of French (20) with *Chlorella,* revealed that the saturation levels at 700 mμ are much lower than at 680 mμ; while the saturation levels at 600 mμ are much higher than at 680 mμ (Fig. 10). The negative effects could be generally associated with early light saturation of photosynthesis in one of the two beams. We noticed that by reducing the intensity of far red light, a positive Emerson effect can be

obtained in the spectral region where negative effects were observed at the higher intensities (*cf.* Table II and Fig. 6 for *Anacystis*).

Rajni Govindjee (unpublished data), working on the second Emerson effect in the Hill reaction, also found that by reducing the light intensity in the region where the initially observed effect was negative, its sign could be changed.

Relation of the negative Emerson effect to light saturation is plausible. Owing to early saturation, addition of a certain amount of far red light (700 mμ) to background light of the same wavelength, naturally causes a negative effect (*i.e.*, the total light action is smaller than the sum of the light actions of the two separate beams). It seems plausible that the same effect may result from combination of two beams of different wavelength, one of which is characterized by early saturation. However, if the two beams have different primary photochemical functions—and this is what we have postulated as our working hypothesis—this conclusion becomes uncertain. Obviously, a satisfactory explanation would have to begin with explaining how the saturation level of photosynthesis can be different in light of different wavelengths, since this fact contradicts the simple hypothesis that saturation level of photosynthesis is the measure of the maximum rate of a certain physical process or enzymatic reaction unrelated to the primary photochemical process.

The discovery (23, 34, 37, 38) of the inhibitory effect of extreme red light (740

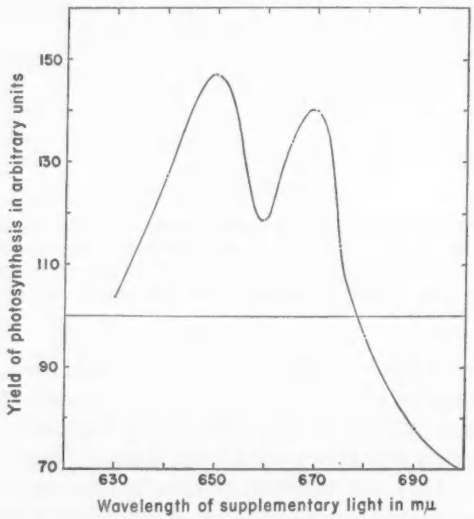

FIGURE 9 Action spectrum of second Emerson effect in *Chlorella pyrenoidosa*. Note negative Emerson effect in 680 to 700 mμ region. Light action of the far red light alone was 15.0 μl/hour and the ratio of far red to supplementary light actions was 1:3. Far red light was ~ 700 mμ.

TABLE II

CHANGE FROM POSITIVE TO NEGATIVE EMERSON EFFECT WITH INCREASING LIGHT INTENSITY

A Light action of far red light alone	B Light action of supplementary light (680 mμ)	C Light action of far red light + 680 mμ light given simultaneously	D = C − B Light action of far red light in presence of supplementary light	A:B Ratio of far red light action: Supplementary light action	100 × D/A Emerson effect (Far red light action alone = 100)
μl/hr.	*μl/hr.*	*μl/hr.*	*μl/hr.*		
1.89	2.34	5.52	3.18	1:1.2	168
3.42	2.16	5.22	3.06	1:1.0	90
7.38	7.64	13.50	5.86	1:1.10	80
9.90	13.68	20.15	6.47	1:1.4	66
12.24	13.86	21.80	7.94	1:1.11	65
18.00	19.80	26.80	7.00	1:1.10	39

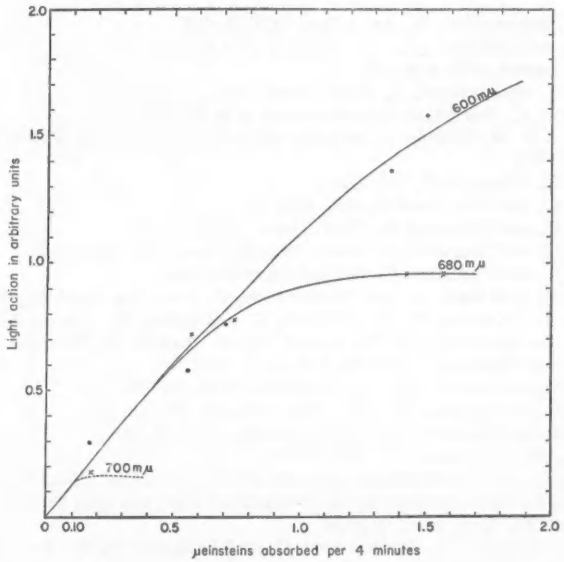

FIGURE 10 Light curves of *Anacystis nidulans* in light of 600, 680, and 700 mμ. Different saturation levels are approached at these three wavelengths. Initial slope of 700 mμ curve could not be determined with certainty. Saturation at this wavelength was reached at a very low level as indicated by dotted line. Abscissae are energies in μeinsteins per 4 minutes per 14 cm².

to 750 mμ) on the rate of photosynthesis in far red light (680 to 700 mμ) suggests a possible relation between this effect and the negative Emerson effect observed when monochromatic light > 670 mμ is added to "far red" light obtained by means of sharp cut-off filters (and therefore containing some of the "inhibitory extreme red" light).

The negative Emerson effect obviously requires further study.

We are grateful to Visiting Research Professor Jan B. Thomas for stimulating discussions and to Mr. Carl Cederstrand for help in the absorption measurements with the integrating sphere. We also thank Mrs. Rajni Govindjee and Mrs. Judy Twarog for help.

One of the authors (Govindjee) owes gratitude to the late Professor Robert Emerson for making it possible for him to come to this laboratory, and for his encouragement and guidance in the earlier stages of this research.

This work was supported by the National Science Foundation, and is part of a thesis presented by Govindjee to the University of Illinois in partial fulfillment of requirements for a Ph.D. degree in Biophysics.

Received for publication, July 18, 1960.

REFERENCES

1. BRODY, M., and EMERSON, R., *Am. J. Bot.*, 1959, **46**, 433.
2. BRODY, M., and EMERSON, R., *J. Gen. Physiol.*, 1959, **43**, 251.
3. BRODY, S., *Science*, 1958, **128**, 838.
4. BROWN, J. S., and FRENCH, C. S., *Plant Physiol.*, 1959, **34**, 305.
5. CEDERSTRAND, C., description of the instrument to be published.
6. DUYSENS, L. N. M., Transfer of excitation energy in photosynthesis. Thesis, University of Utrecht, 1952.
7. EMERSON, R., *Science*, 1957, **125**, 746.
8. EMERSON, R., *Ann. Rev. Plant Physiol.*, 1958, **9**, 1.
9. EMERSON, R., and CHALMERS, R., *Plant Physiol.*, 1955, **30**, 504.
10. EMERSON, R., and CHALMERS, R., *Phycol. Soc. Am. News Bull.*, 1958, **11**, 51.
11. EMERSON, R., and CHALMERS, R., personal communication.
12. EMERSON, R., CHALMERS, R., and CEDERSTRAND, C., *Proc. Nat. Acad. Sc.*, 1957, **43**, 133.
13. EMERSON, R., CHALMERS, R., CEDERSTRAND, C., and BRODY, M., *Science*, 1956, **123**, 673.
14. EMERSON, R., and LEWIS, C. M., Annual Report, Division of Plant Biology, *Carnegie Institution of Washington*, 1939, **38**, 118 (see p. 122).
15. EMERSON, R., and LEWIS, C. M., *J. Gen. Physiol.*, 1942, **25**, 579.
16. EMERSON, R., and LEWIS, C. M., *Am. J. Bot.*, 1943, **30**, 165.
17. EMERSON, R., and RABINOWITCH, E., *Plant Physiol.*, 1960, **35**, 477.
18. FRANCK, J., *Proc. Nat. Acad. Sc.*, 1958, **44**, 941.
19. FRENCH, C. S., *in* Photochemical Apparatus, *Brookhaven Symp. Biol.*, 1958, **11**, 65.
20. FRENCH, C. S., Paper presented at the conference on Light and Life, Baltimore, McCollum Pratt Institute, April, 1960, in press.
21. GOVINDJEE, ICHIMURA, S., CEDERSTRAND, C., and RABINOWITCH, E., *Arch. Biochem. and Biophysics*, 1960, **89**, 322.
22. GOVINDJEE, and RABINOWITCH, E., *Science*, 1960, **132**, 355.
23. GOVINDJEE, RABINOWITCH, E., and THOMAS, J. B., *Biophysic. J.*, 1960, **1**, 91.
24. GOVINDJEE, R., THOMAS, J. B., and RABINOWITCH, E., *Science*, 1960, **132**, 421.
25. HALLDAL, P., *Physiol. Plantarum*, 1958, **11**, 401.
26. HAXO, F., and BLINKS, L. R., *J. Gen. Physiol.*, 1950, **33**, 389.
27. KRASNOVSKY, A. A., and KOSOBUTSKAYA, L. M., *Doklady Akad. Sc.*, 1955, **104**, 440.

28. KRASNOVSKY, A. A., VOROBYOVA, L. M., and PAKSHINA, E. V., *Fizio. Rastenii*, 1957, **4**, 124.
29. KRATZ, W. A., and MYERS, J., *Am. J. Bot.*, 1955, **42**, 282.
30. LAVOREL, J., *J. Physic. Chem.*, 1957, **61**, 1600.
31. MYERS, J., and FRENCH, C. S., *J. Gen. Physiol.*, 1960, **43**, 723.
32. RABINOWITCH, E., Photosynthesis and Related Processes, New York, Interscience Publishers, Inc., **1** (1945) and **2**, (pts. 1 (1951) and 2 (1956)), (*a*) 1300; (*b*) 1161.
33. RABINOWITCH, E., and GOVINDJEE, Paper presented at the conference on Light and Life, Baltimore, McCollum Pratt Institute, April, 1960, in press.
34. RABINOWITCH, E., GOVINDJEE, and THOMAS, J. B., *Science*, 1960, **132**, 422.
35. SHIBATA, K., BENSON, A. A., and CALVIN, M., *Biochim. et Biophysica Acta*, 1954, **15**, 461.
36. TANADA, T., *Am. J. Bot.*, 1951, **38**, 276.
37. THOMAS, J. B., and GOVINDJEE, Paper presented at the conference on Light and Life, Baltimore, McCollum Pratt Institute, April, 1960, in press.
38. THOMAS, J. B., and GOVINDJEE, *Biophysic. J.*, 1960, **1**, 63.
39. THOMAS, J. B., and MARSMAN, J. W., *Biochim. et Biophysica Acta*, 1959, **35**, 316.
40. VOROBYOVA, L. M., and KRASNOVSKY, A. A., *Biokhimiya*, 1956, **21**, 126; 1958, **23**, 760.
41. WARBURG, O., KRIPPAHL, G., SCHROEDER, W., BUCHOLZ, W., and THEEL, E., *Z. Naturforsch., pt. B*, 1954, **98**, 164.

INHIBITION OF PHOTOSYNTHESIS IN CERTAIN ALGAE BY EXTREME RED LIGHT

GOVINDJEE, EUGENE RABINOWITCH, *and* JAN B. THOMAS

From the Photosynthesis Research Laboratory, Department of Botany, University of Illinois, Urbana. Dr. Thomas's present address is Biophysical Research Group, Physical Institute of the State University, Utrecht, The Netherlands

ABSTRACT This paper shows that in *Porphyridium cruentum* and in *Chlorella pyrenoidosa* (but apparently not in *Anacystis nidulans*) "extreme red" light (> 720 mμ) can inhibit photosynthesis produced by "far red" light (up to 720 mμ). From the action spectrum of this phenomenon, it appears that an unknown pigment with an absorption band around 745 mμ must be responsible for it.

INTRODUCTION

It was shown in preceding papers (9, 10) that when the unicellular red alga *Porphyridium cruentum* is illuminated with light filtered through a sufficiently dense aqueous solution of mixed phycobilins (filter PB-95), no photosynthesis can be observed.[1] However, the addition of orange supplementary light induces a definite photosynthetic activity attributable to this "far red" light (9, 10): the rate of photosynthesis in orange + far red light is found to be markedly greater than in orange light alone. The occurrence of this effect (5, 6) indicates that phycobilin-filtered light does produce some excitation of chlorophyll *a*. As a matter of fact, PB-95-filtered light contains wavelengths down to about 660 mμ (9, 10), while chlorophyll *a in vivo* absorbs up to 720 mμ. According to Emerson and co-workers (1, 5, 6), these algae, when exposed to monochromatic light (bands isolated by a grating monochromator, band half-width about 10 mμ), do in fact produce measurable photosynthesis up to 700 mμ.

To resolve this apparent discrepancy, it was suggested that the "extreme red" radiation,[2] which is present in the PB-95-filtered light, may be able to *inhibit* photo-

[1] For the transmission spectrum of this filter, see reference 10.

[2] In order to distinguish between the "long-wave" light used in the study of the Emerson effect, and the inhibitory radiation of still longer wavelengths, we define as "far red" the radiations with wavelengths 680 to 720 mμ (the long-wave limit of chlorophyll *a* absorption), and as "extreme red" the radiations extending from 720 up to 800 mμ.

synthesis caused by shorter-wave light. To check this assumption, we investigated the effect of monochromatic "extreme red" light on photosynthesis produced by "far red" light.

METHODS

Algae were cultivated as described in earlier papers from this laboratory (for a summary, see Govindjee *et al.* (7)) and photosynthesis was measured with Emerson's differential manometer (4).

Two light beams were projected onto the bottom of the manometric vessel. The far red beam, isolated from the light of an incandescent lamp by an interference filter (Farrand filter with maximum transmission at 700 mμ), served to produce photosynthesis. The extreme red beam consisted of monochromatic bands (band half-width, about 10 mμ) emerging from the Emerson and Lewis grating monochromator. Light energy was measured with a bolometer, as described by Emerson and Chalmers (4).

The results in Tables I and II were reduced to equal numbers of absorbed quanta by means of absorption measurement with an integrating spectrophotometer built and operated by C. Cederstrand.

RESULTS

A. *Preliminary Experiments.* To make sure that the apparent discrepancy described in the introduction, was not due to differences in the algal material used in the two sets of experiments, we made an experiment in which the same cell suspension was irradiated alternatively with a 10-mμ wide band of 680-mμ light, and with light transmitted through the PB-95 filter. The results, adjusted to equal numbers of quanta absorbed from both beams, are given in Table I.

Table I shows that, in one and the same cell suspension, 680-mμ light produces substantial photosynthesis while absorption of the same amount of light filtered through the PB-95 filter, is unable to do so.

With this point established, we proceeded to check the hypothesis attributing

TABLE I

PHOTOSYNTHESIS OF *Porphyridium cruentum* IN LIGHT OF 680 mμ AND IN LIGHT TRANSMITTED BY PB-95 PHYCOBILIN FILTER

Oxygen evolution, μl/hr.	
In 680-mμ light	In light transmitted by PB-95
+0.26	−0.55
+0.32	−0.26
+0.39	+0.22
+0.74	+0.18
+0.73	+0.21
Mean +0.49 ± 0.10	−0.04 ± 0.15

The actual rate of absorption of light transmitted through filter PB-95 was 0.1 to 0.2 μeinstein/hour, depending on the density of the cell suspension; the rate of absorption of light from the 680-mμ beam was about six times higher. After ascertaining that light saturation was not approached in the latter case, the values obtained in the 680-mμ beam were divided by a factor of 6 for comparison with those obtained in the PB-95-filtered beam.

the inefficiency of phycobilin-filtered light to inhibition of photosynthesis produced by far red light, by extreme red radiation. Radiation at 750 mμ was found in fact to have a marked depressing effect on photosynthesis produced by light of 680 to 720 mμ; this was reported in a preliminary note (8). The extent of inhibition varied for different cultures, as shown in Table II. These variations presumably are due to slight differences in the culturing conditions. Although these conditions were kept as constant as possible, minor variations undoubtedly have occurred, as indicated by perceptibly different growth rates of the various cultures. The physiological age of the cells used was therefore not exactly the same, despite equal periods of cultivation.

B. *Action Spectrum of the Inhibition Effect.* The action spectrum of the inhibitory effect was then studied. First, the rate of photosynthesis in far red light was determined as follows. Two series of measurements, each consisting of eight 1-minute readings in the dark, were alternated with two similar series of readings in the presence of far red light. The first three readings in each set were always discarded. If after 3 minutes, the steady state was not reached, the measuring period was extended until five consistent readings were obtained. The photosynthetic rate in far red light was calculated by subtracting the average of the dark readings from that of the readings in far red light. During each inhibition experiment, this result was checked at regular intervals—as a rule, once an hour.

Two series of readings with extreme red light were then alternated with two series of readings in which this light was combined with far red light. The difference between the averages of the two series was assumed to be the "light action" of the

TABLE II

INHIBITION BY EXTREME RED LIGHT OF PHOTOSYNTHESIS PRODUCED BY FAR RED LIGHT

The pairs of values in each horizontal line are reduced to equal rates of absorption of light quanta.

Rate of photosynthesis, μl O_2/hour		
Far red light 680 to 720 mμ	Far red light + extreme red light 750 mμ	Inhibition per cent
Porphyridium cruentum		
4.01	2.23	44
1.87	0.29	85
1.85	0.29	84
3.30	2.04	38
1.08	0.84	22
Chlorella pyrenoidosa		
2.61	1.98	24
2.52	1.80	29
2.52	2.07	18

far red light in the presence of extreme red light. The per cent difference between this light action and that measured in far red light alone is plotted for the red alga *Porphyridium cruentum* in Fig. 1 as function of wavelength. All the experiments performed with this species are included in this figure.

The efficiency of far red light appears in Fig. 1 to be *enhanced* by supplementary light of 700 to 720 mμ. This is readily explained because our "far red" light, trans-

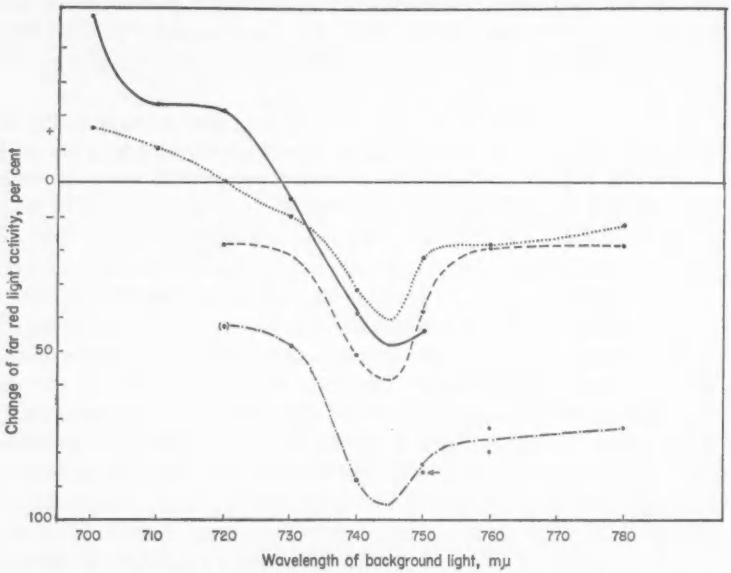

FIGURE 1 Action spectra of stimulation and inhibition of photosynthesis in *Porphyridium cruentum* caused by the addition of monochromatic light bands (half-width, 10 mμ) of different wavelengths, to far red light of about 700 mμ. Arrow indicates a separate experiment. Brackets (.) designate a less reliable measurement. Curves are drawn through the experimental points in as symmetrical way as consistent with the data. The suggested location of the minima is therefore somewhat arbitrary.

mitted by the 700-mμ interference filter, represents a relatively broad band (half-width, about 20 mμ), which includes some light considerably below 700 mμ. In other words, what is measured between 700 and 720 mμ in Fig. 1 is simply the previously known "Emerson effect."

Supplementary light of 730 to 780 mμ, on the other hand, *decreases* the photosynthetic efficiency of far red light; the effect is strongest at 740 to 750 mμ. The reason why the inhibition does not entirely disappear at still longer wavelengths may lie in the distortion of the spectrum in this region, where the resolving power of our grating becomes increasingly poor.

Similar observations with *Chlorella pyrenoidosa* are illustrated by Fig. 2, which

shows three typical experiments. Why the minimum in the curves is sometimes shallow and sometimes deep (between 20 and 100 per cent inhibition) and why it is sometimes found at 740 mμ and sometimes at 745 mμ, we do not know, except that the results suggest differences between individual cultures.

So far, no similar inhibition effect could be observed with suspensions of the blue-green alga *Anacystis nidulans*.

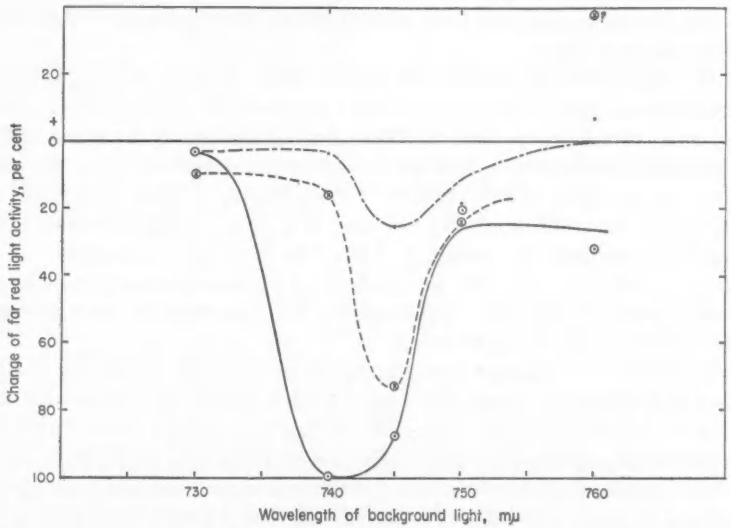

FIGURE 2 Action spectra of the inhibition of photosynthesis in *Chlorella pyrenoidosa* caused by the addition of monochromatic light of different wavelengths to "far red" light of about 700 mμ. ⊗ ? is a questionable point. Curves are drawn in the same way as in Fig. 1.

DISCUSSION

The above described experiments suggest the existence in some algae of a pigment with an absorption maximum at 740 to 750 mμ, whose excitation can inhibit photosynthesis caused by far red light (680 to 720 mμ).

The question arises: how can cells photosynthesize with high yield in white light, which usually contains considerable amounts of the "inhibitory" 740 to 750 mμ radiation? In the first place, it remains to be seen whether the inhibition affects only the photosynthetic action of far red light (> 680 mμ), or extends to shorter wavelengths. A preliminary experiment suggested that no inhibition occurs when photosynthesis is produced by *blue* light. Shorter-wave radiations may conceivably counteract the inhibitory effect of the 740 to 750 mμ radiation. At least, this conclusion is suggested by earlier experiments (*cf.* reference 10), in which light trans-

mitted through either a solution of phycocyanin (without phycoerythrin) or a solution of phycoerythrin (without phycocyanin) was found to produce measurable photosynthesis in *Porphyridium,* even though about the same amount of extreme red radiation was transmitted through these filters as through the filter PB-95 behind which no measurable photosynthesis could be observed. This difference, left unexplained in (10), can be now explained by assuming that the much larger amount of shorter-wave light (< 650 mμ), transmitted by the filters containing only one phycobilin, counteracts the inhibitory effect of the extreme red light transmitted by all three filters.

A few preliminary experiments that we have done in which photosynthesis was produced by red light < 680 mμ suggested a decline in the inhibitory effect. Measurements of the inhibitory effect of 750 mμ light as function of the wavelength of the photosynthesis-producing light are needed to decide whether this inhibition is restricted to the region of the "red drop" (above 680 mμ in green, blue-green, and brown algae, above 650 mμ in red algae) or is a more general phenomenon, and to check the hypothesis of "counter inhibition" by short-wave visible light.

In our preliminary note (8) we stated that no absorption band could be observed in the investigated algae in the region of 750 mμ, where the action spectrum of the inhibition effect has its maximum.

Experiments we have made since, on highly concentrated suspensions of *Chlorella, Porphyridium,* and *Anacystis,* suggested the existence of absorption bands in the region 720 to 780 mμ; but their exact position and intensity varied widely, and it seems as yet premature to discuss their possible relation to the inhibition effect. The most consistent observations were those with *Anacystis,* where a sharp absorption band at about 750 mμ was observed with Cederstrand's integrating sphere spectrophotometer[3] and with the Beckman DU spectrophotometer; but this was the alga in which we have not yet found any evidence of an inhibition effect.

Using the Cary spectrophotometer to compare the absorption spectra before and after illumination with light of different wavelengths, we have observed increases of absorption in the region of 700 to 780 mμ and decreases in absorption in region of 620 to 680 mμ caused by preillumination with red light (660 mμ). This made us think of the findings of Butler and co-workers (2, 3) who reported that a "phototropic" pigment, absorbing at 660 or at 730 mμ, depending on light exposure, is present in (and can be extracted from) plant organs showing photomorphogenic effects. However, the position of the peaks in the difference spectrum and their intensity varied too much to warrant speculations on the existence of a similar "phototropic" pigment in the investigated algae without further systematic study.

The inhibitory effect of extreme red light on photosynthesis suggests that this light creates some kind of an "energy sink." A "physical" energy sink might be

[3] Details of instrument will be published later by Cederstrand.

created by chlorophyll being converted to an inactive form, with a lower excited energy level; or by a pigment other than chlorophyll being converted to a form suitable for trapping the excitation energy. A "chemical" energy sink might be due to deactivation, by extreme red light, of some enzyme or another catalytic component involved in photosynthesis; or to activation of an agent catalyzing some back or side reactions. Perhaps, crystalline chlorophyll, which has an absorption band around 740 mμ, is present in these algae in minute quantities, and provides the "energy sink" responsible for inhibition.

Our thanks are due to Mrs. Rajni Govindjee, Mrs. Judith Twarog, and Mr. Carl Cederstrand for valuable assistance.

This work was supported by the National Science Foundation under Grant G4969.
This work is part of the thesis presented by Govindjee in partial fulfillment of the requirements for a Ph.D. degree in Biophysics at the University of Illinois.
Received for publication, June 22, 1960.

REFERENCES

1. BRODY, M., and EMERSON, R., *J. Gen. Physiol.*, 1959, **43**, 251.
2. BUTLER, W. L., and NORRIS, K. H., *Arch. Biochem. and Biophysics*, 1960, **87**, 31.
3. BUTLER, W. L., NORRIS, K. H., SIEGELMAN, H. W., and HENDRICKS, S. B., *Proc. Nat. Acad. Sc.*, 1959, **45**, 1703.
4. EMERSON, R., and CHALMERS, R., *Plant Physiol.*, 1955, **30**, 504.
5. EMERSON, R., CHALMERS, R., and CEDERSTRAND, C., *Proc. Nat. Acad. Sc.*, 1957, **43**, 133.
6. EMERSON, R., CHALMERS, R., CEDERSTRAND, C., and BRODY, M., *Science*, 1956, **123**, 673.
7. GOVINDJEE, and RABINOWITCH, E., *Biophysic. J.*, 1960, **1**, 73.
8. RABINOWITCH, E. I., GOVINDJEE, and THOMAS, J. B., *Science*, 1960, **132**, 422.
9. THOMAS, J. B., and GOVINDJEE, Conference on Light and Life, sponsored by McCollum-Pratt Institute, April, 1960, Baltimore, Maryland, in press.
10. THOMAS, J. B., and GOVINDJEE, *Biophysic. J.*, 1960, **1**, 63.

THE PHOTOCONDUCTIVITY OF CHLOROPLASTS AND THE FAR RED LIGHT EFFECT

SHOJI ICHIMURA

From the Photosynthesis Research Laboratory, Department of Botany, University of Illinois, Urbana

ABSTRACT The photoconductivity of chloroplast films in the dry and the wet state has been investigated. These films were found to behave like typical semiconductors, in agreement with the results of Arnold and co-workers, who have used only dry films. It was found that a steady photocurrent produced in a chloroplast film by blue or red light, can be either stimulated or quenched—depending on the intensity of the illumination—by simultaneous application of far red or near infrared light. This reminds one of the quenching of the photoconductivity of phosphors by infrared light. The interaction of long wave light with light of shorter wavelength in the production of photoconductivity is of interest in relation to the "second Emerson effect," which suggests a similar interaction in photosynthesis.

INTRODUCTION

The studies of Emerson and Arnold (1, 2) and of Gaffron and Wohl (3) indicated that the primary photochemical act in photosynthesis is carried out not by a single chlorophyll molecule, but by cooperation of several hundred such molecules. These results suggested the occurrence in photosynthesis of excitation energy migration over several hundred pigment molecules; in other words, the absorption of light by chlorophyll in a chloroplast seems to lead to the creation of an exciton. Resonance energy transfer accounts also for the experimentally established fact (4-17) that light energy absorbed by accessory pigments is transferred, often with high efficiency, to chlorophyll *a* (or, in purple bacteria, to bacteriochlorophyll B-890).

In 1949, Katz (18) discussed the possibility that chlorophyll molecules in the chloroplasts may form a two-dimensional crystal, possessing conduction bands in which excited electrons or holes could migrate. In 1955, Bassham and Calvin (19) discussed the same idea and pointed out that a semiconducting structure could facilitate spatial separation of the oxidizing and reducing agents—free electrons and holes—and that this may help photosynthesis by preventing back reactions between these agents.

In 1956, the investigations of Commoner, Heise, and Townsend (20) and of Sogo, Pon, and Calvin (21) gave evidence of the formation of unpaired electron

spins in illuminated spinach chloroplasts, while Arnold and Sherwood (22-24) found in 1957 that dried chloroplast films exhibit thermoluminescence as well as other typical properties of semiconductors.

In addition, studies by Arnold, Strehler, and co-workers (25-28) have demonstrated the occurrence of a temperature-dependent, long-lived phosphorescence in algae and in chloroplasts, which could be attributed to a slow recombination of trapped electrons and holes.

However, the concept of photosynthesis as a "solid state process" has been opposed, particularly by Rabinowitch (17), mainly for the following reasons.

The chlorophyll monolayers, which appear to be present in chloroplasts, are *not* crystalline (as suggested by Katz). If they were, the absorption band of chlorophyll *in vivo* would lie beyond 730 mμ, and not at 675 to 680 mμ, in a position typical of chlorophyll in the amorphous state. The absence in the spectrum of chlorophyll *in vivo* of an absorption band, which could be attributed to transition into a conductance level, also argues against the assumption that electron excitation into such a level is the primary result of light absorption. Furthermore, in a monomolecular layer, the separation of the primary oxidation product from the primary reduction product does not require electric "conduction" over distances longer than the diameter of a single molecule; therefore, it could be achieved by a mesomeric transformation (electron loss on one end of the chlorophyll molecule and electron acquisition at the other end; the cycle can be closed by a tautomerization).

Rosenberg (29) objected to Rabinowitch's argument by quoting observations of strong photoelectric currents in noncrystalline hydrocarbon melts, and the absence of a separate band leading into a photoconducting level in organic photoconductors.

Rosenberg suggested that the long-lived triplet levels of molecules in a noncrystalline solid can merge into a conductance band, while the short-lived singlet excited levels remain associated with individual molecules; photoconductance may then result from a secondary singlet-triplet transformation and not affect the absorption spectrum.

The alternative: exciton (*i.e.*, electron *and* hole) migration in illuminated chloroplasts *versus* separate migration of electrons and holes, thus remains open. The following experiments are a contribution to the study of this problem. They confirm the observations of Arnold and Sherwood on dry chloroplast films and add some data on wet chloroplast films. The main new finding is the effect of far red light ($\lambda > 700$ mμ) on the photocurrent produced in dry chloroplast films by light of shorter wavelength.

MATERIALS AND METHODS

Spinach chloroplast fragments were prepared by the method of Spikes (30).[1] The chloroplasts, sedimented in the final centrifugation, were rinsed twice with glass-distilled water, resuspended in this medium, frozen rapidly at −78°C, and lyophilized. The material was then stored at −25°C in the dark.

[1] Obtained from Dr. Bishop.

To prepare the films, chloroplasts were resuspended in a small amount of water, the suspension painted onto a copper plate (2 X 3 cm), and dried in a stream of nitrogen. The chloroplast-painted plates were kept in a desiccator over drierite.

Sandwiches, 3 X 2 cm in size, were made from a copper electrode carrying the chloroplast film (about 0.2 mm thick), and a glass plate with an electrically conducting layer facing the chloroplast film (obtained from Liberty Mirror Division, Libby-Owens-Ford Glass Co.) and serving as the second electrode. The use of a transparent glass electrode permitted the illumination of a large area of the chloroplast film.

Fig. 1 is a schematic diagram of the apparatus used for the investigation of photoconductivity.

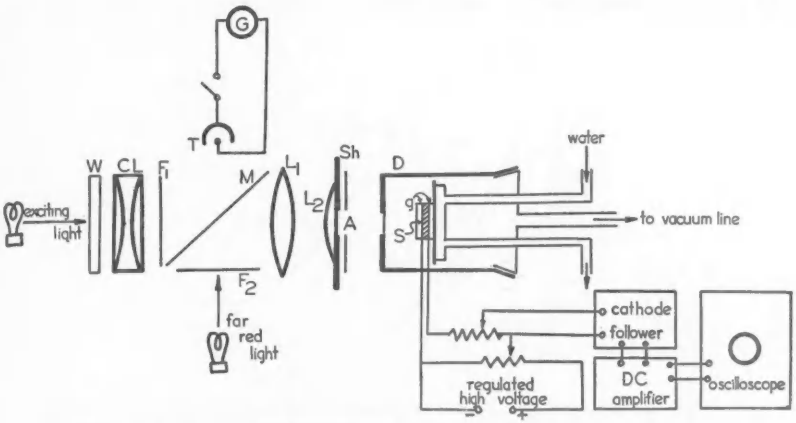

FIGURE 1 Block diagram of apparatus. L_1, L_2, lenses; W, 5-cm water cell; CL, condenser lens; T, thermocouple; F_1, F_2, filters; M, 50 per cent transmittance mirror; G, galvanometer; S, sample; Sh, shutter with aperture A; D, Dewar vessel; g, glass conduction electrode.

The photocurrent generated by light passed through a resistor ranging from 10^8 to 10^{10} ohms, and the voltage developed across the resistor was fed through a cathode follower and a D.C. amplifier (gain = 10^6) into an oscilloscope. In this way, it was possible to follow the decay curve of the photocurrent from about 10 μsec. to about 100 sec. after the light was switched off. The oscilloscope sweep was triggered by the photosignal; thus, it was possible to observe the rise of the photocurrent as well as its decay.

For the measurement of steady state photoconductivity, a 1000-watt incandescent lamp was used. The filament of the lamp was projected on the chloroplast film by a glass condenser lens. A water layer 5 cm thick served to absorb infrared light above 1.4 μ.

Action spectrum measurements were made with the same system by using a Bausch and Lomb grating monochromator.

The chloroplast films were illuminated parallel to the direction of the applied field. A screen with an aperture for the passage of light separated the lamp and the condenser from the glass vessel containing the chloroplast films. In order to protect the films from scattering light, the glass vessel was painted with black ink, with a hole opposite the film layer.

For the measurement of far red light effect on steady state photocurrent excited in chloroplast films by blue or red light, a Corning color filter (No. 7-59) was used in combination with a narrow band pass filter 2412, and Bausch and Lomb 2nd order filter.

RESULTS AND DISCUSSION

1. *Dark Conductivity of Chloroplasts.* The apparatus can easily measure 10^{-15} ampere flowing through the 10^{10}—ohm resistor. This permitted the measurement of the dark current caused in the chloroplast films by a potential of 1000 volts. Fig. 2 shows the resistance of dry and wet films as a function of temperature. The heating rate was 10°C per minute. The resistance of wet chloroplast film de-

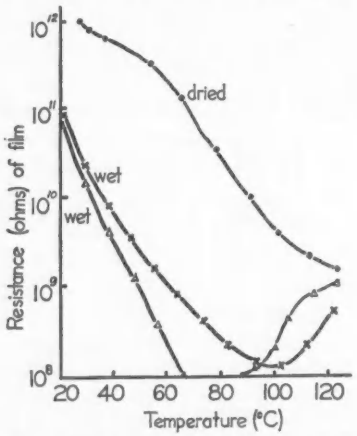

FIGURE 2 Resistance of dried and wet chloroplasts as a function of temperature.

creased in a way typical of semiconductors, but later increased again, probably because of the loss of water by heating (which was carried out in an atmosphere saturated with water vapor at 20°C).

The specific resistance of dried films was never less than 10^{12} ohms at room temperature (20°C); but that of the wet films ranged from 10^{11} to 10^{8} ohms, depending upon the amount of water in the films.

Experiments showed that the conductivity of dry chloroplast films depends not only on temperature but also on the duration of the passage of the dark current, often manifesting hysteresis.

On the whole, the dark conductivity of chloroplast films behaves like that of other organic semiconductors, as already shown by Tollin and Kearns (31).

2. *The Photoconductivity of Chloroplasts.* When dry chloroplast films ($R_d \cong 10^{13}$ ohms) were illuminated *in vacuo* with an incandescent lamp, with a potential of 1000 volts applied to the electrodes, a photocurrent was observed, the

strength of which depended upon the temperature and the intensity of illumination. The direction of the field applied to the chloroplast films did not influence the current, either during the illumination or after it was stopped. No photocurrent was observed when the two electrodes were illuminated without a chloroplast layer between them. Increasing the thickness of the chloroplast film up to 0.5 mm caused the current to rise.

3. *Action Spectrum.* When the chloroplast film was illuminated with monochromatic light obtained from a Bausch and Lomb grating monochromator, the maximum photocurrent was produced by wavelengths corresponding roughly to the visible absorption bands of chlorophyll in the chloroplast. Fig. 3 shows a

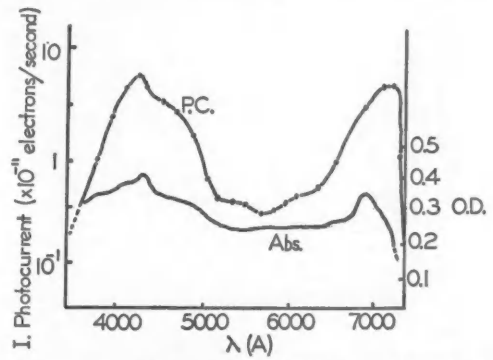

FIGURE 3 Action spectrum of the photoconductivity of chloroplast (at room temperature). Intensity of exciting light: 10^{15} quanta/sec/6 cm^2.

typical action spectrum of the steady state photoconductivity in a dry chloroplast film at room temperature, at a light intensity of 10^{15} quanta per second per 6 cm^2. In this curve, the peak of the conductivity curve appears at or above 700 mμ, whereas the absorption peak lies at 685 mμ; it remains to be seen whether this shift is significant; if so, it could be taken as evidence that photoconductivity is due to the chlorophyll *a* component absorbing at or beyond 690 mμ—perhaps a polymeric form of the pigment (32).

4. *Dependence of the Photocurrent upon Duration of Illumination and Its Decay.* Fig. 4 is a typical curve showing the current as function of time during and after the illumination.

At the beginning of illumination, the conductivity of the dry film *in vacuo* rises approximately linearly. After reaching a maximum, the photocurrent does not become constant, as expected for a pure photoconducting crystal, but begins to decline while the light is still on.

The time required to reach the maximum photocurrent depends upon the thickness of the film, the intensity and spectral composition of light, and the temperature

of the film. The rise and decay times were several times longer than those reported for pure chlorophyll (33). When the light was turned off, the current decreased to a steady level somewhat lower than the initial one (Fig. 4); the latter was re-established if the film was left in the dark for several hours.

The maximum photoconductivity of the chloroplast film did not depend upon previous illumination of the layer; but an after effect was manifested by more rapid establishment of maximum conductivity after repeated illumination (Fig. 5). This proves that the internal state of the pigment in the chloroplast film may be different even if photoconductivity is the same during illumination or after it.

The dependence of the decay on temperature has been investigated from 0° to

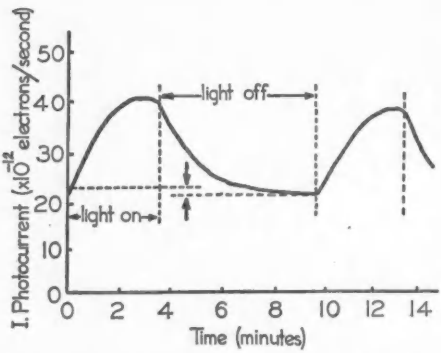

FIGURE 4 Dependence of the photoconducivity upon the duration of illumination and decay of the current after the illumination is stopped (at room temperature). Intensity of light: 10^{15} quanta/sec/6 cm^2.

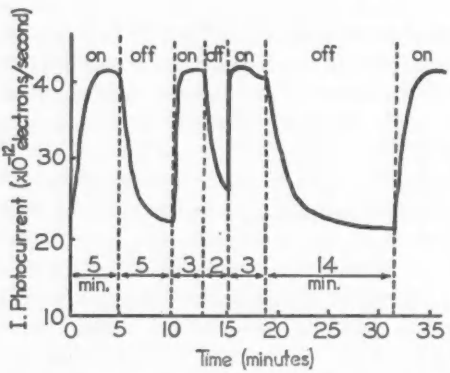

FIGURE 5 Independence of the maximum conductivity of chloroplast films from after effect.

50°C (Fig. 6). (The maximum conductivities at different temperatures were arbitrarily set at 100.) With rising temperature, the decay is accelerated.

5. *Dependence of the Photoconductivity upon Water Content of the Films.* If dried chloroplast films are wetted with a drop of water, the dark current increases, but the photocurrent decreases. Fig. 7 shows that the rise of the photoconductivity in a wet chloroplast film is faster than in a dry film; after the maximum photoconductivity is reached, photocurrent does not decline while light is still on, as it does in a dry film. This suggests that the excitation of conduction electrons may go in dry and in wet films through different excited states, as suggested by Franck (34).

The photoconductivity decreases with increasing water content of the chloroplast

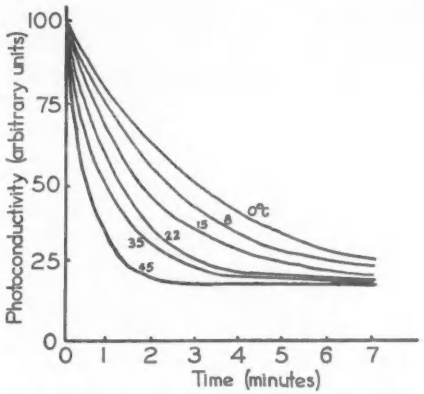

FIGURE 6 Decay of the photoconductivity of chloroplast films at different temperatures.

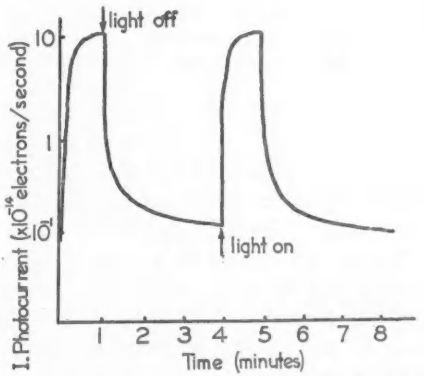

FIGURE 7 Time dependence of the photoconductivity of wet chloroplast of films.

films; at a certain content, no photocurrent is observed at all. It can be surmised that photoconductivity occurs as long as all water is "bound water," but disappears when some of it becomes "free water." Introduction of water molecules into chloroplast films may interrupt the ordered hydrogen bond structure in the protein, leading to the destruction of the conductance band.

6. *Influence of Far Red or Infrared Light on the Photoconductivity of Chloroplasts.* A change in the photocurrent caused by actinic light in a chloroplast film can be produced by simultaneous illumination of the film with far red or near infrared light, which in itself produces no photocurrent. As long as the actinic "short wave" light is comparatively weak, a *stimulation* of photocurrent by far red or near infrared light is observed, but if the intensity of the "short wave" light is increased, the photocurrent is, to the contrary, *quenched* by near infrared light ($\lambda > 850$ mμ). For a certain critical ratio of the two light intensities, the addition of light >850 mμ has no effect on the photocurrent at all (*cf.* Fig. 8). Far red light of

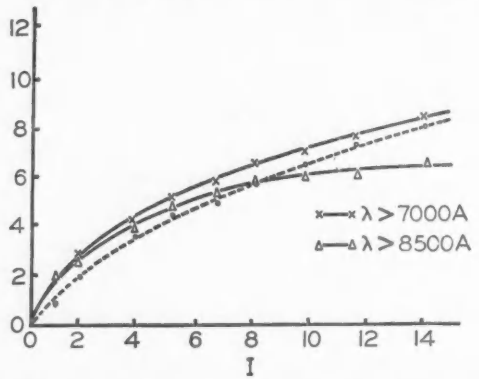

FIGURE 8 Dependence of photocurrent on intensity: dotted line . . . exciting light only; solid line ——, simultaneous illumation with far red light at $\lambda > 7000$ A; *I*, intensity of exciting light in arbitrary units; *i*, photocurrent in arbitrary units.

wavelength >750 mμ produces a stimulation effect even if actinic light is relatively strong. The photoconductivity due to weak visible radiation can be stimulated, by 10 per cent or more, by the addition of far red or near infrared radiation.

In these measurements, the chloroplast films have been made conductive by weak illumination with blue (430 mμ) or red (680 mμ) light obtained by means of an interference filter; after the photocurrent has reached a stationary value, the effect of additional illumination with far red or near infrared light of constant energy has been measured. The energy has been kept constant over the whole investigated region by determining in advance the lamp current needed to produce a given energy flux at the different wavelengths.

Fig. 9 shows the time dependence of the increase and decrease of photoconduc-

tivity, produced by visible light, as the >700-mμ light of different intensity (marked in arbitrary units) is applied for 30 sec. and then cut off. With increasing intensity of long-wave radiation the saturation is reached faster. No similar acceleration was observed in quenching.

When quenching occurs, one observes first a rapid rise in photocurrent immediately after the far red light is applied, and later, a slower decay as shown in Fig. 10. The transient stimulation becomes more significant with decreasing temperature, but disappears at temperatures above 35°C. This suggests that the transient stimulation is due to electrons ejected into the conduction band from shallow traps, which are not stable at temperatures higher than 35°C.

CONCLUSION

This paper gives experimental evidence that a purely electronic primary photo-

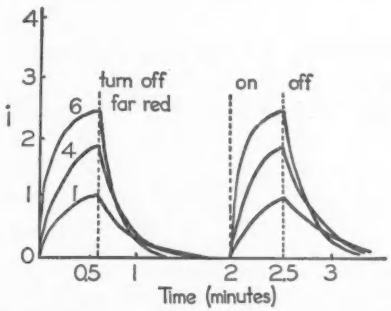

FIGURE 9 Time dependence of the increase and decrease of photoconductivity (i) of chloroplasts by additional illumination with far red light.

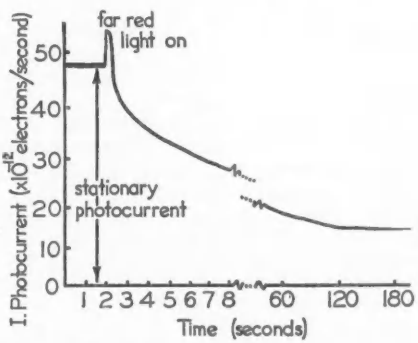

FIGURE 10 Transient change of photoconductivity and its decay resulting from the quenching by far red light.

physical process can occur in chloroplast films. These results are in close agreement with those obtained by Arnold and co-worker.

The main new finding of the present paper is the influence of far red light on photoconductivity of chloroplasts caused by light of shorter wavelength. The photocurrent produced by weak blue or red light can be stimulated when far red or near infrared light ($\lambda > 850$ mμ) is applied simultaneously. The near infrared light can cause quenching instead of stimulation when added to stronger blue or red light. In the case of quenching, a transient increase in photoconductivity immediately after the application of far red light is followed by decay. Many authors have reported quenching of photoconductivity of inorganic phosphors by infrared light, as well as some stimulation phenomena of a transient character (35–39). To explain the rapid transient stimulation, followed by quenching, as observed in CdS, Rose (40) has proposed a model which involves the creation of free holes by infrared radiation.

The dependence of the stimulation or quenching effect on the ratio of the intensities of the exciting light and of the infrared supplementary light, found in the present experiments, could be explained perhaps by using Rose's model. Further study of these phenomena may assist in the understanding of the energy migration in the photosynthetic unit and of the role of electron migration in it.

The interaction of long wave light with light of shorter wavelength in the production of photoconductivity is of interest in its possible relation to the "second Emerson effect" which suggests a similar interaction in photosynthesis (*cf.* Govindjee and Rabinowitch (41)).

The author would like to express his gratitude to Professor E. Rabinowitch for the privilege he gave him to work in the Photosynthesis Laboratory at the University of Illinois and for numerous discussions; to Dr. Bishop of the Department of Biochemistry, University of Chicago, for a sample of spinach chloroplasts, and to members of Solid State Physics Laboratory, in the Department of Physics of the University of Illinois, for assistance in carrying out the measurements.

Received for publication, August 8, 1960.

REFERENCES

1. EMERSON, R., and ARNOLD, W., *J. Gen. Physiol.*, 1932, **15**, 391.
2. EMERSON, R., and ARNOLD, W., *J. Gen. Physiol.*, 1932, **16**, 191.
3. GAFFRON, H., and WOHL, K., *Naturwissenschaften*, 1936, **24**, 81.
4. EMERSON, R., and LEWIS, C. M., *J. Gen. Physiol.*, 1942, **25**, 579.
5. DUTTON, H. J., MANNING, W. M., and DUGGAR, B. M. G., *J. Physic. Chem.*, 1943, **47**, 308.
6. WASSINK, E. C., and KERSTEN, J. A. H., *Enzymologia*, 1946, **12**, 3.
7. FRANCK, J., and LIVINGSTON, R., *Revs. Mod. Physics*, 1949, **21**, 505.
8. ARNOLD, W., and OPPENHEIMER, J. R., *J. Gen. Physiol.*, 1950, **33**, 423.
9. TERENIN, A. N., *Uspekhi Fiz. Nauk*, 1951, **43**, 367.
10. DUYSENS, L. N. M., *Nature*, 1951, **168**, 548.
11. DUYSENS, L. N. M., Transfer of Excitation Energy in Photosynthesis, Thesis, University of Utrecht, Netherlands, 1952.

12. FRENCH, C. S., and YOUNG, V., *J. Gen. Physiol.*, 1952, **35**, 873.
13. BANNISTER, T. T., *Arch. Biochem. and Biophysics*, 1954, **49**, 222.
14. ARNOLD, W., and MECK, E. S., *Arch. Biochem. and Biophysics*, 1956, **60**, 82.
15. LIVINGSTON, R., *J. Physic. Chem.*, 1957, **61**, 860.
16. RABINOWITCH, E. I., *J. Physic. Chem.*, 1957, **61**, 870.
17. RABINOWITCH, E. I., *Tr. Faraday Soc.*, 1959, **27**, 161.
18. KATZ, E., *in* Photosynthesis in Plants, (W. E. Loomis and J. Franck, editors), Ames, Iowa State College Press, 1949, Chapter 15, 291.
19. BASSHAM, J. A., and CALVIN, M., United States Atomic Energy Commission Unclassified Report UCRL–2853, 1955.
20. COMMONER, B., HEISE, J. J., and TOWNSEND, J., *Proc. Nat. Acad. Sc.*, 1956, **42**, 710. COMMONER, B., HEISE, J. J., LIPPINCOTT, B. B., NORBERG, R. E., PASSONEAU, J. V., and TOWNSEND, J., *Science*, 1957, **126**, 57.
21. SOGO, P. B., PON, N. G., and CALVIN, M., *Proc. Nat. Acad. Sc.*, 1957, **43**, 387.
22. ARNOLD, W., and SHERWOOD, H. K., *Proc. Nat. Acad. Sc.*, 1957, **43**, 105.
23. ARNOLD, W., and MACLAY, H. K., the photochemical apparatus—its structure and function, *Brookhaven Symp. Biol.*, 1958, **11**, 1.
24. ARNOLD, W., and SHERWOOD, H. K., *J. Phys. Chem.*, 1959, **63**, 2.
25. STREHLER, B. L., and ARNOLD, W., *J. Gen. Physiol.*, 1951, **34**, 809.
26. STREHLER, B. L., 1951, *Arch. Biochem. and Biophysics* 1951, **34**, 239.
27. ARTHUR, W. E., and STREHLER, B. L., *Arch. Biochem. and Biophysics*, 1957, **70**, 507.
28. STREHLER, B. L., and LYNCH, V. K., *Arch. Biochem. and Biophysics*, 1957, **70**, 527.
29. ROSENBERG, B., *Discussions Faraday Soc.*, 1959, **27**, 254.
30. SPIKES, J. D., *Arch. Biochem. and Biophysics*, 1952, **35**, 101.
31. TOLLIN, G., and KEARNS, D. R., United States Atomic Energy Commission Unclassified Report UCRL–8848, 1959.
32. BRODY, S. S., *Science*, 1958, **128**, 838.
33. ARNOLD, W., and MACLAY, H. K., see reference 24.
34. FRANCK, J., *Proc. Nat. Acad. Sc.*, 1958, **44**, 941.
35. FRERICHS, R., *Physic. Rev.*, 1947, **72**, 594.
36. FASSBENDER, J., *Ann. Physic.* 1949, **5**, 33.
37. KALLMAN, H., KRAMER, B., and PERLMUTTER, A., *Physic. Rev.* 1955, **90**, 39.
38. TAFT, E. A., and HEBB, M. H., *J. Opt. Soc. Am.*, 1952, **42**, 249.
39. TUTIHASHI, S., *J. Opt. Soc. Am.* 1956, **46**, 443.
40. ROSE, A., *Physic. Rev.*, 1955, **97**, 322.
41. GOVINDJEE and RABINOWITCH, E., *Biophysic. J.*, 1960, **1**, 73.

THE KINETICS OF DISTRIBUTION OF THE FAT-SOLUBLE INERT GAS CYCLOPROPANE IN THE BODY

W. PERL, G. T. LESSER, *and* J. M. STEELE

From the New York University Research Service, Department of Medicine, New York University College of Medicine, Goldwater Memorial Hospital, Welfare Island, New York

ABSTRACT A kinetic analysis is made of the experimentally measured time course of respiratory uptake of the highly fat-soluble, inert gas cyclopropane by normal human subjects. The analysis is based on the well-known perfusion-limited model in which a number of body compartments are arranged in parallel with the lungs *via* the circulating blood. Three distinct body compartments are derived from the data. These are tentatively identified as: (*a*) adipose tissue (*b*) fat-poor tissue of low perfusion such as resting muscle, skin, and connective tissue (*c*) fat-poor tissue of high perfusion such as brain, heart, gut, liver, and kidney. Blood flow rates to the several compartments are also derived from the data. The rates to compartments (*a*) and (*b*) are each approximately 10 per cent of the estimated total cardiac output. The derived perfusion (blood flow rate/compartment weight) of the three compartments are in the range, respectively, (*a*) 2 to 4, (*b*) 1 to 2.5, (*c*) 25 to 75 ml/min/100 gm. Uncertainties arising from the experimental data and from simplifications of the model (neglect of lung fill-up phase of uptake and gross diffusion of cyclopropane from one tissue into another) are discussed. The present type of uptake experiment is significant for the problems of total body fat determination, of gross body composition in relation to weight change, of gross shunting of blood flow from one compartment to another, of anesthesia by fat-soluble substances, and of decompression sickness.

INTRODUCTION

The purpose of the experiments conducted by Lesser, Blumberg, and Steele (1, 2) was to determine the total body fat of living animals by uptake of the highly fat-soluble inert gas, cyclopropane. Although the method proved successful in rats, a rather fortunate difficulty was encountered in its application to human subjects. A direct calculation of the total body fat requires knowledge of the amount of cyclopropane taken up when equilibrium has occurred. In the rat, gaseous equilibrium

was observed to occur in 90 to 120 min. and only cursory observation was made of the approach to equilibrium. In human subjects, however, absorption of the gas was much slower, equilibrium not being reached even at the end of 8 hrs. As a consequence, detailed observations were made of the approach to equilibrium. In analyzing such data for a series of six normal human subjects (Figs. 1, 2)[1] to de-

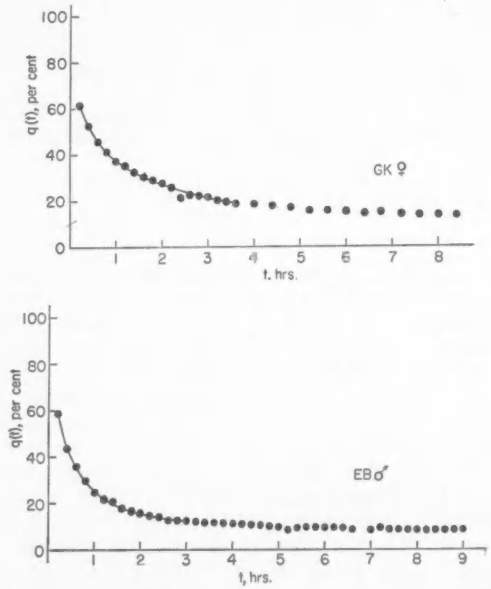

FIGURE 1*a* and *b* Cyclopropane uptake of two normal human subjects from a closed respiratory circuit. Ordinate: $q(t)$, ratio, in per cent, of amount of cyclopropane in respiratory circuit volume to total cyclopropane in subject plus external volume, at time t. Abscissa, time, t. Circles denote experimental data points. Solid lines are curves drawn "by eye" through data. Graphically measured slopes of solid line portions shown give time rate of change, $\dot{q}(t)$. Measurement of $\dot{q}(t)$ continued on solid lines drawn through data on enlarged scale of Fig. 2.

termine an equilibrium value of cyclopropane uptake (3, 4), it became apparent that a test could also be made of certain features of the well-known perfusion-limited physiological model of inert gas exchange in body tissues (5–7).

In this model (Fig. 3) the body is regarded as a group of tissues or organs each connected separately with the lungs, *i.e.*, in parallel, *via* the circulating blood (the

[1] Figs. 1 and 2 show the experimental data for two typical cases. The data for all six subjects are given in numerical form in reference 3.

liver is an exceptional case). Introduction of a foreign inert gas into the lung volume results in diffuson of this gas across the alveolar and pulmonary capillary membranes, its solution in the blood, its transport by the arterial blood into the various capillary beds, and its diffusion across the capillary membranes and throughout the extra- and intracellular tissue components. Mixed venous blood at reduced cyclo-

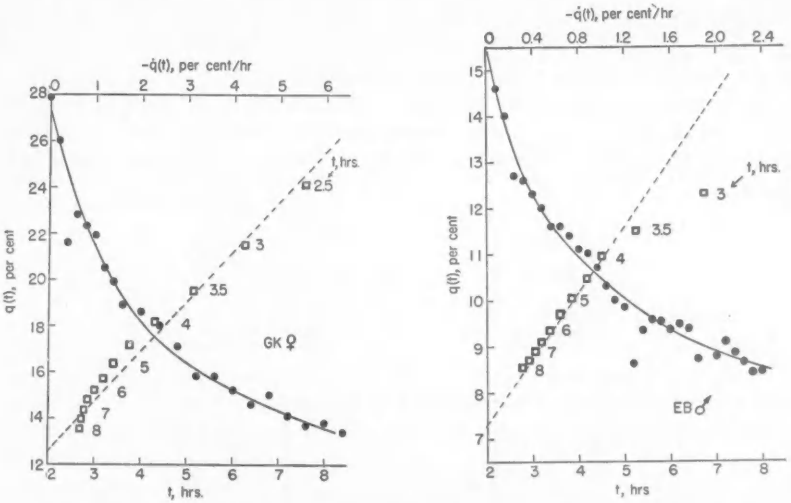

FIGURE 2*a* and *b* Circles denote enlarged plots of data of Fig. 1 in last 4 hrs. Solid lines are curves drawn "by eye" through data for graphical measurement of time rate of change of $q(t)$. Square points are plot of $q(t)$ against $-\dot{q}(t)$, the negative time rate of change of $q(t)$ (upper scale). Dashed lines are straight lines drawn "by eye" to represent the equilibrium constant q_∞ plus the slowest exponential $a_1e^{-k_1t}$ to fit the data. The q-axis intercept of the dashed line is q_∞. The slope of the dashed line is $1/k_1$. A slight displacement of the dashed lines from best visual fit with the square points was made to provide a somewhat better over-all fit of the derived q_∞ plus three exponentials to the data.

propane concentration returns to the lungs and the circulatory cycle is repeated. In this uptake process the different partial pressures of gas in the various tissues approach the partial pressure of the gas in the alveolar volume and equilibrium, or saturation, is reached when all partial pressures have become equal. Desaturation of body tissues in response to a decrease of inert gas concentration in the lungs occurs in a similar manner.

In terms of this model, respiratory measurement of rate of uptake or elimination of inert gases from the body yields information on various aspects of the transport process. If, for example, it is known or assumed that the various diffusion processes in the alveoli and in the tissues are rapid compared to the blood circulation

time, then from such measurements one can, in principle, deduce blood flow rates to the various tissues. Jones (5), in particular, has offered evidence in favor of this assumption (similar uptake and elimination rates for gases of differing diffusion constants) and has made extensive use of this model in the preceding manner. The present experiments offer a test of the model under two conditions different from those used by Jones. The gas used, cyclopropane, possesses different diffusion and solubility coefficients from the gases (nitrogen, xenon, krypton, etc.) of Jones's experiments. Secondly, a closed external rebreathing volume was employed in place of the constant external concentration arrangement of Jones.

In the following sections the calculations made from the experimental data using the above described model are described. The results are compared with existing ones, and the significance of the experiment for various physiological problems is assessed.

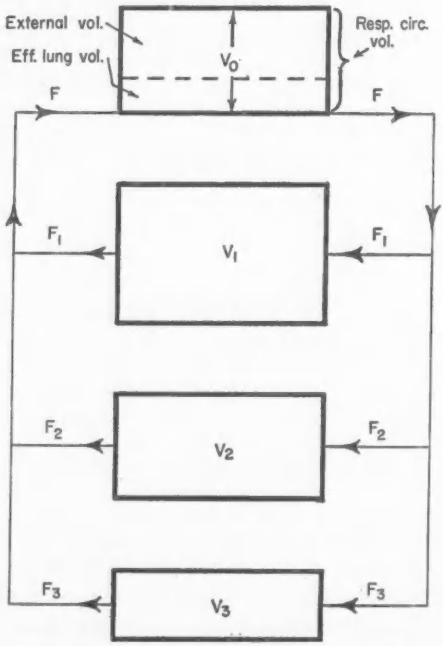

FIGURE 3 Schematic representation of physiological model. Three body compartments 1, 2, 3 are shown and a respiratory circuit compartment consisting of the external volume plus an effective lung volume. The physiological parameters of the model are: the rates of blood flow, F or F_1, through the compartments and the solubility volumes v_0 or v_1 of the compartments. The solubility volumes or "cyclopropane spaces" are proportional to the relative amounts of cyclopropane in the several compartments at equilibrium.

EXPERIMENTAL ARRANGEMENT

The experimental procedure is presented in detail elsewhere (2,3). Briefly, the subject's head and neck are enclosed by a helmet which is part of a closed respiratory circuit of known fixed volume. This volume, external to the subject, will be called the "external volume." It does not include the lung volume. Oxygen is admitted into the external volume at the rate utilized by the subject, and carbon dioxide is absorbed within it by soda lime. Pressure and temperature in the external volume are constant. A small amount of cyclopropane, to give a concentration level of the order of 1 per cent, is introduced into the external volume. At intervals thereafter, small samples of gas are withdrawn from the external volume and analyzed for cyclopropane content. In a separate experiment for each subject the "respiratory circuit volume" consisting of the external volume plus an effective lung volume (see Appendix B) is measured by a nitrogen dilution technique (2). The experimental data are expressed as the ratio $q(t)$ of the amount of cyclopropane in the respiratory circuit volume to total cyclopropane in subject plus external volume, at time t.

THE PHYSIOLOGICAL MODEL

The physiological model is considered to be a number of body compartments connected in parallel with an external compartment *via* the circulating blood (Fig. 3). Any body compartment, denoted as the ith compartment, is defined as a group of tissues, not necessarily contiguous, characterized by two quantities: a rate of flow of blood to, or blood plus lymph from, the compartment, F_i, liters/minute, and a solubility volume v_i, defined as,

$$v_i = \lambda_i V_i \tag{1}$$

in which V_i is the total volume, liters, of the compartment, and λ_i is an average solubility partition coefficient (in the sense defined below) of cyclopropane between the tissues of the compartment and blood; *i.e.*, the ratio of an average concentration of cyclopropane in the tissues of the compartment to an average concentration of cyclopropane in blood which is in solubility equilibrium with the tissues of the compartment. It is convenient to define the "solubility volume perfusion,"[2] ϕ_i, as the rate of blood flow per unit solubility volume of the ith compartment, or

$$\phi_i = \frac{F_i}{v_i} = \frac{F_i}{\lambda_i V_i} \tag{2}$$

The two independent quantities which characterize a compartment can then be taken as any two of the three quantities F_i, v_i, ϕ_i.

The anatomical justification for this physiological model is that most small pieces of tissue are presumed to be arranged in parallel; *i.e.*, a small volume of blood

---

[2] The term "solubility volume perfusion" is to be distinguished from the commonly used term perfusion which is rate of blood flow per unit weight of tissue.

passes through just one such piece of tissue in making one complete circuit. The parts of the body which cannot be characterized in this way, such as portions of the liver, intestinal contents, blood, and other fluids in the larger vessels, may be neglected in the present problem.[3] As can be shown from later analysis of the model, those small pieces of tissue having the same solubility volume perfusion ϕ_i have the same gas uptake rate under the conditions of the present experiment and, hence, are separately indistinguishable. Consequently, the sum of their individual solubility volumes can be considered as the solubility volume v_i of a single larger compartment and the sum of their individual spatial volumes as the spatial volume V_i of the same larger compartment. The ratio of these two volumes, v_i/V_i, defines the average implied in the definition of the partition coefficient λ_i, equation (1).

The basic relation used to analyze the model is the principle of perfuson (Fick), which states that the rate of net delivery (moles/minute) *via* the blood of a substance, in the present case cyclopropane, to a compartment is the product of the arteriovenous difference in concentration of that substance (moles/liter) and the rate of blood flow through the compartment (liters/minute). If in addition the following three assumptions are valid, a conventional compartment analysis becomes possible:

Assumption (*a*): Rate of net delivery of substance equals rate of increase of substance in a compartment. This assumption requires not only that the transported substance be not metabolized, which is apparently true for the inert gas cyclopropane, but also that it not enter or leave a compartment by any route other than the blood plus lymph. One such possible additional route in the present case is *via* direct diffusion of gas from one compartment to contiguous parts of another compartment. Thus, if a piece of muscle in compartment 2 lies next to a piece of adipose tissue in compartment 1, and the partial pressure of gas in compartment 2 increases faster than in compartment 1, gas will diffuse from the region of high partial pressure (muscle) directly across into the region of low partial pressure (adipose tissue). This compartment-to-compartment diffusion operates at distances of the order of centimeters, the presumed dimensions of gross adipose or lean tissue. This type of gross diffusion is to be distinguished from the diffusion between capillary blood and neighboring cells since the latter operates at distances of the order of 10^{-3} cm (several cell diameters).

As previously mentioned, Jones (5) has offered the observations of similar uptake and elimination rates of different gases in body tissues as evidence for the general negligibility of gross diffusion relative to blood perfusion as a kinetic mechanism for the distribution of inert gases to body tissues. However, a theoretical estimate of the rate of gross diffusion of cyclopropane into a slab of adipose tissue of

[3] Cyclopropane is about 33 times as soluble in fat as in fat-free body, weight for weight (1,3,8), so that in a normal subject in equilibrium, about 90 per cent of the absorbed cyclopropane is in the total body fat and about 10 per cent in the entire fat-free body.

thickness 1 cm indicates a non-negligible rate of uptake of gas relative to that due to perfusion. The estimate was based on a diffusion constant of cyclopropane in adipose tissue of 10^{-6} cm²/sec. This value is indicated by the diffusion constant measurements of Davidson, Eggleton, and Foggie (9) who obtained 2.1×10^{-6} cm²/sec. for nitrogen in lard at 25°C and by measurements in this laboratory (10) by the same method as in (9) on cyclopropane in freshly excised rat adipose tissue. Inasmuch as we have not convinced ourselves of the negligibility of gross diffusion *versus* perfusion as a mechanism of uptake of cyclopropane in adipose tissue, the calculated results by the present perfusion-limited model are offered as valid only in order of magnitude. In particular, the derived rate of blood flow to the total body adipose tissue derived by neglecting gross diffusion is too high and consequently should be considered as an upper-limiting value.

Assumption (*b*): Concentrations of substance in blood can be related by appropriate partition coefficients to concentrations of substance in compartments. This assumption is applied in the following form. Blood leaving a compartment is assumed to be in solubility equilibrium with the average concentration of gas existing at that time in the tissues of the compartment. If this assumption is not valid, *i.e.*, if less cyclopropane is being transferred from blood to compartment than is given by using an equilibrium tissue-blood partition coefficient at the venous end of the compartment (owing to possible slowness of local diffusion relative to speed of blood flow through capillaries), then the primary error of the model will be to yield from the data too low values of the blood flow rates to the several body compartments.

Assumption (*c*): A steady physiological state exists, *i.e.*, all blood flow rates and solubility volumes are constant in time. Certain indications in the data of possible deviation from a steady physiological state will be pointed out later.

One other major simplification of the analysis is made. The alveolar volume should be treated as a separate body compartment in series with the external volume. However, it equilibrates with an external concentration of foreign gas so rapidly that this phase of body uptake can be regarded as essentially instantaneous in deriving quantities which depend on long times of uptake. Sechzer, Dripps, and Price (11) have observed experimentally that approximately 90 per cent of a constant external concentration of cyclopropane is reached in the alveolar volume in less than 10 min. Of primary interest in the present experiments are the "slowest" uptake half-times which were in the range 90 to 150 min. Moreover, preliminary calculation of the effect of the alveolar volume as a separate compartment, by using the formulation of Kety (7) but extended to the present multi-compartment model, indicates that the effect on the calculated blood flow rate to the "slowest" compartment is less than 5 per cent from this source. Therefore, the simplification of combining the lung volume with the external volume as a single "respiratory circuit volume" compartment appears permissible.

APPLICATION OF MODEL TO EXPERIMENT

The simplified model that emerges from the preceding considerations is the well-known closed n-compartment mammillary model in which a central compartment, here the respiratory circuit volume, exchanges with $n-1$ other compartments, which do not exchange with each other (12, 13). A general feature of compartment models, of which the details pertinent to the present case are given in Appendix A, is that the theoretical quantity which is identified with the experimentally measured quantity $q(t)$ is the sum of a number n of decay-type exponential functions of time. Accordingly, the experimental data (Figs. 1, 2) were examined as to the possibility of being curve-fitted by exponentials. They were found to be representable within experimental error by a constant (regarded as an exponential with rate constant zero) plus a minimum of three additional exponentials, as follows:

$$q(t) = q_\infty + a_1 e^{-k_1 t} + a_2 e^{-k_2 t} + a_3 e^{-k_3 t} \tag{3}$$

Thus, the first result yielded by application of the model is that a minimum of three distinct body compartments exists for the respiratory uptake of cyclopropane. Of the seven numbers q_∞, a_j, k_j ($j = 1, 2, 3$), which represent the results of an experiment, however, a_3 is not an independent number, having been derived to satisfy the theoretical model relationship for zero time (see Appendix B)

$$1 = q_\infty + a_1 + a_2 + a_3 \tag{4}$$

In addition, the fastest rate constant k_3 is considered unreliable and unusable because of scantiness of experimental data in the initial period in which this exponential makes its greatest contribution. Therefore, only five numbers are available in each experiment from which to derive *via* the model specific values characterizing the body compartments.

The parameters characterizing the four compartments of the model are eight in number, the four solubility volumes v_0, v_i ($i = 1,2,3$) and the four blood flow rates F, F_i ($i = 1,2,3$). Of these, $v_0 = \lambda_0 V_0$ is known from the experimental arrangement and the solubility properties of cyclopropane (see equations (A13), (A14)). The blood flow rate F is identified with the total cardiac output, which is estimated for each subject (see next section). Furthermore, F is equated to the sum $F_1 + F_2 + F_3$ of the blood flow rates to the body compartments, by the assumption that circulatory shunts across the lungs and tissues may be neglected. The number of unknown model parameters has now been reduced to five, namely, the three solubility volumes v_i ($i = 1,2,3$) and any two of the three blood flow rates F_i ($i = 1,2,3$). The mathematical relationships of the model connect the model parameters with the exponential parameters which represent the data. The five model parameters can be determined uniquely in terms of the five exponential parameters. Some details relevant to this determination are given in Appendices A, B. The results are given in the next section.

RESULTS

Basic Data. The basic data for the six normal subjects are given in Table I. The respiratory circuit volume V_0 was measured by a nitrogen dilution technique (2,3). The respiratory circuit solubility volume v_0 is defined in Appendix A, equations (A13), (A14) as $\lambda_0 V_0$ where $\lambda_0 \approx 2.3$ is approximately the reciprocal of the Bunsen solubility coefficient of cyclopropane in blood.[4] The estimated total

TABLE I

BASIC DATA FOR SIX NORMAL SUBJECTS

Subject, age, sex	Height H, cm	Weight W, kg	Respiratory circuit volume V_0, liter	Respiratory circuit solubility volume v_0, liter	Estimated total cardiac output F, liter/min.*	Total body fat W_f, kg†
VL, 19 ♀	160.7	52.40	19.6	45.6	5.16	13.9
GK, 38 ♀	155.6	53.30	21.0	48.5	5.07	10.7
TJ, 32 ♂	168.3	70.08	19.0	44.1	6.02	12.9
FK, 29 ♂	170.2	73.26	18.5	42.7	6.19	15.9
EB, 36 ♂	183.0	76.0	19.7	45.6	6.64	18.9
PD, 30 ♂	177.2	80.29	18.6	43.4	6.62	19.7

* $F = 3.35 \times 71.84 \times 10^{-4}$ (H, cm)$^{0.725}$ (W, kg)$^{0.425}$, see (15, 16).
† See (3).

cardiac output F was obtained by multiplying an assumed average cardiac index for the sitting position, 3.35 liters/min.M^2 (15), by the body surface area, M^2, calculated from height and weight by the DuBois formula (16). Total body fat, W_f, was calculated from the equilibrium uptake of cyclopropane as given by q_∞, Table II (see reference 3 and equations (C4), (C5) in Appendix C).

Exponential Parameters from Curve-Fitting Experimental Data. The experimental data were curve-fitted by exponential functions by a method apparently first used for this purpose by Greville (17) and described in detail elsewhere (4). In this method the quantity $q(t)$ is plotted against its negative time derivative, $-\dot{q}(t)$. In the present case $\dot{q}(t)$ was obtained as the slope of a smooth curve drawn "by eye" through the experimental data (the solid lines in Fig. 1, continued as the solid lines in Fig. 2). The linear appearance of the plot at large time (the square points of Fig. 2) indicated that a straight line (the dashed lines of Fig. 2) could fit the data adequately in this region. The q-axis intercept and the slope of this straight line are respectively the constant q_∞ and the reciprocal of the rate constant

[4] A Bunsen solubility coefficient of cyclopropane in blood of 0.40 ± 0.04 ml STP cyclopropane/ml blood at 37°C is used in this paper. This coefficient can be calculated additively from an assumed normal composition of blood, using measured solubility coefficients of cyclopropane in isosmotic saline and protein suspensions (1) and in fat (8). The calculated value compares well with the mean of measured solubility coefficients of cyclopropane in blood (14). The indicated uncertainty of ± 10 per cent is ascribed to variations in the plasma-cell ratio and in the lipid content of blood (14).

TABLE II

EXPONENTIAL PARAMETERS FROM CURVE-FITTING CYCLOPROPANE UPTAKE DATA BY $q\dot{q}$ METHOD

Subject	Equilibrium value, %	Amplitudes, %			Rate constants, min.$^{-1}$			Half-lives, min.		
	q_∞	a_1	a_2	a_3	k_1	k_2	k_3	T_1	T_2	T_3
VL ♀	9.75	33.8	28.3	28.2	0.00807	0.0328	0.108	85.9	21.1	6.42
GK ♀	12.60	37.2	28.7	21.5	0.00772	0.0487	0.146	89.8	14.2	4.74
TJ ♂	9.68	13.5	28.9	48.0	0.00400	0.0199	0.101	173	34.8	6.84
FK ♂	7.93	11.8	44.8	35.5	0.00363	0.0244	0.183	191	28.4	3.79
EB ♂	7.30	11.0	47.6	34.1	0.00466	0.0263	0.123	149	26.3	5.62
PD ♂	6.70	21.4	48.3	23.7	0.00527	0.0291	0.220	131	23.8	3.16

k_1 of the "slowest" exponential, equation (3). The exponential amplitude q_1 is obtained as the slope of the straight line portion of a plot of $q(t)$ *versus* $e^{-k_1 t}$. The exponential $q_1 e^{-k_1 t}$ is then subtracted from $q(t)$, and the process is repeated to give the parameters of a second, "faster" exponential $q_2 e^{-k_2 t}$ etc.

In each of the present experiments the method yielded, in addition to the constant q_∞, three exponentials as the minimum number required to fit the data within the experimental uncertainty (Table II). The reliability of the two most important exponential parameters, q_∞ and k_1, is indicated by the possible variations in drawing the straight (dashed) lines in Fig. 2. Two independent measures of reliability of the exponential parameters were available in two additional curve-fit solutions for each case.[5] The first was a least squares fit to the logarithm of the given unsmoothed data (the circles of Fig. 1). The second was a least squares fit to the logarithm of the smoothed data (values taken from the solid lines of Figs. 1 and 2). Detailed comparison between these solutions and the present solution is given for cases GK and EB in reference 4. From comparison among these solutions and from the graphical display yielded at all stages of the present method, the uncertainty of q_∞ was judged to be of the order of 5 per cent and that of the parameters of the two slower exponentials of the order of 20 per cent. As previously discussed, the fastest rate constant k_3 is not used to derive physiological results, and a_3 is used by way of a correction to results which depend primarily on the two slower exponentials.

Worthy of note are the differences between the results for the two female subjects and the four male subjects (Table II). The half-lives T_2 and especially T_1 are smaller, and the amplitude a_1 larger, for the females than for the males. Also the q *versus* $-\dot{q}$ plots (Fig. 2) seem more "oscillatory" for the females than for the males. Such "oscillations" may conceivably correspond to deviations from a steady internal state in the subject, perhaps due to shunting of blood flow from one type of body tissue to another during the course of the experiment (3).

[5] These solutions were kindly derived and supplied by Dr. Mones Berman, of the National Institutes of Health, using IBM punch card computers.

TABLE III

PHYSIOLOGICAL PARAMETERS OF MODEL DERIVED FROM EXPONENTIAL PARAMETERS OF EXPERIMENTAL DATA

Subject	Solubility volumes, liters			Blood flow rates, liters/min.			Half-life, min.
	v_1	v_2	v_3	F_1	F_2	F_3	T_{α_3}
VL ♀	386	20.4	15.6	0.61	0.46	4.10	1.93
GK ♀	301	23.9	11.5	0.54	0.79	3.74	1.70
TJ ♂	321	58.6	32.3	0.45	0.57	4.99	2.49
FK ♂	399	75.7	20.1	0.47	0.69	5.04	1.84
EB ♂	488	70.9	20.1	0.67	0.68	5.29	1.78
PD ♂	550	42.9	12.3	0.54	0.58	5.50	1.20

Physiological Parameters Derived from Exponential Parameters. With q_∞, a_1, a_2, k_1, k_2 (Table II), and v_0, F (Table I) as input data for the mathematical relationships of the model (Appendix A), the solubility volumes v_1, v_2, v_3, and blood flow rates F_1, F_2, F_3 were derived (Table III). An auxiliary quantity α_3 is also determined in this derivation. This quantity, see equation (A17), is the rate constant of the fastest exponential occurring in the model. It has only limited physical significance in that if the initial mixing and lung fill-up phenomena were negligible, and sufficient experimental data were available in the initial period to yield a reliable rate constant k_3 by curve-fitting, then this k_3 would equal α_3. For completeness and convenience in checking the calculations the derived values of α_3 are included in Table III as the half-times $T_{\alpha_3} = 0.693/\alpha_3$.

Particularly striking is the large value of v_1 in comparison with v_2 and v_3 and the approximately equal and low values of F_1 and F_2 in comparison with F_3. The first result, in view of the approximately 33 times greater solubility of cyclopropane in fat than in fat-free tissue indicates that compartment 1 must contain most of the body adipose tissue. Compartments 2 and 3 must therefore contain mostly fat-poor tissues. Since the blood flow rate F_3 is much greater than F_2, compartment 3 may be tentatively identified with highly perfused viscera and compartment 2 with lesser perfused non-adipose tissue such as resting muscle, skin, and connective tissue. A more detailed version of this argument is given in Appendix C. If this identification is not grossly in error the conclusion is indicated that, at rest, the body adipose tissue of a normal subject takes about as much of the total cardiac output as all the less well-perfused fat-poor tissue combined (such as resting muscle, skin, and connective tissue).

An important practical feature of the present experiment is the so-called speeding-up effect. The solubility volume perfusion $\phi_i = F_i/v_i$ has the physical significance, in the present perfusion-limited model, of being the rate constant of the ith exponential which can be curve-fitted to the uptake or elimination curve that would be obtained under conditions of constant external gas concentration (or infinite external volume). For compartment 1 the model solution (Table III)

yields a half-time $0.693/\phi_1$ in the range 400 to 700 min. On the other hand, the present experiment yielded a slowest observed half-time T_1 in the range 90 to 200 min. (Table II). A similar but lesser speeding-up effect exists for the "faster" half-times. Thus, the present perfusion-limited model shows that the smaller the respiratory circuit volume, the faster will equilibrium be approached. Consequently, a given period of experimental observation will yield a more complete record of the approach to equilibrium and will permit more accurate resolution of this record into exponentials, under small external volume conditions than under constant external concentration conditions.

Weight of Body Compartments. The weight of the three body compartments can be derived, and the fat to fat-free weight ratio of any one of them, if the fat to fat-free weight ratios of the other two are known or assumed. The solubility volume of a body compartment is essentially the product of the solubility coefficient of cyclopropane in that compartment and the weight of the compartment (Appendix C). The solubility coefficient can be determined from the known solubility coefficients of cyclopropane in fat and in fat-free lean mass if the fat to fat-free ratio is known. The solubility volume divided by this solubility coefficient then yields the weight of the compartment. Since the weights of all body compartments should add up to the known total body weight (if all parts of the body are represented in the experimental data in the manner described by the model), the fat to fat-free ratio need be known or assumed for only two compartments. The weight and fat to fat-free ratio for the remaining compartment can then be deduced.

This type of calculation is illustrated for subject EB in Table IV. It is seen that the fat ratio of compartment 2 goes down as the fat ratio of compartment 3 goes up and that the two are equal at approximately 3 per cent, a not unreasonable order of magnitude for lipid content of non-adipose tissues such as muscle and viscera (18). The assumption of 80 per cent rather than 60 per cent fat content for compartment 1 (probably largely adipose tissue) gives a greater fat-free weight in compartment 2. Too low an assumption of fat content in compartment 1 (below about 30 per cent) would produce negative values for fat-free weight in compartment 2.

The particular assumptions of 80 per cent fat content in compartment 1 and 3 per cent fat content in compartment 3 for normal humans are suggested by the work of Pitts (18) and others and were used to calculate compartment compositions for all the subjects (Table V). The results in all cases are qualitatively similar. The slightly negative values of W_{f2} for the two female subjects could be changed to positive values by assuming slightly less fat in the other compartments, in particular compartment 1. The results in Tables IV and V tend to support the qualitative interpretation of the anatomical nature of the three derived body compartments.

The nature of the changes in gross body composition as a result of loss or gain of body weight is of obvious physiologic interest. The preceding possibility resulting from the cyclopropane uptake experiment, of dividing up total body fat and total

fat-free body weight into portions assignable to anatomically distinct types of tissues, appears to be capable of yielding information relevant to this problem. Specifically, information as to the degree to which adipose and other tissues change in weight and in relative composition of fat to fat-free components for a given change in body weight, might be derived by applying the present model to precise gas uptake experiments on a given subject before and after weight change.

Perfusion of Body Compartments. It has been seen how blood flow rates and solubility volumes of the several body compartments can be derived (Table III) from the exponential parameters of the observed uptake curves. From

TABLE IV

COMPOSITION OF THE THREE BODY COMPARTMENTS FOR VARIOUS ASSUMED RELATIVE COMPOSITIONS OF COMPARTMENTS 1 AND 3

Subject EB♂, $W = 76.0$ kg, $W_f = 18.9$ kg, $W_l = 57.1$ kg

$\frac{W_{f1}}{W_1}$	W_{f1}	W_{l1}	$\frac{W_{f3}}{W_3}$	W_{f3}	W_{l3}	W_{f2}	W_{l2}	$\frac{W_{f2}}{W_2}$
1.0	17.3	0	0	0	24.3	1.6	32.7	.046
0.8	17.2	4.3	0	0	24.3	1.7	28.5	.056
0.6	17.0	11.3	0	0	24.3	1.9	21.5	.081
1.0	17.3	0	0.03	0.4	11.8	1.2	45.3	.026
0.8	17.2	4.3	0.03	0.4	11.8	1.3	41.0	.031
0.6	17.0	11.3	0.03	0.4	11.8	1.5	34.0	.042
1.0	17.3	0	0.06	0.5	7.7	1.1	49.4	.022
0.8	17.2	4.3	0.06	0.5	7.7	1.2	45.1	.026
0.6	17.0	11.3	0.06	0.5	7.7	1.4	38.1	.035
1.0	17.3	0	0.09	0.6	5.6	1.0	51.5	.019
0.8	17.2	4.3	0.09	0.6	5.6	1.1	47.2	.023
0.6	17.0	11.3	0.09	0.6	5.6	1.3	40.2	.031

Notation: W_i = weight, W_{fi} = fat weight, W_{li} = fat-free weight, of compartment i, $W_i = W_{fi} + W_{li}$.

TABLE V

COMPOSITION OF BODY COMPARTMENTS ASSUMING 80 PER CENT FAT IN COMPARTMENT 1 AND 3 PER CENT FAT IN COMPARTMENT 3. NOTATION AS IN TABLE IV

Subject	W_{f1}	W_{l1}	W_{f2}	W_{l2}	W_{f3}	W_{l3}	W_1	W_2	W_3
VL ♀	13.6	3.41	−0.04	25.9	0.28	9.17	17.0	25.9	9.5
GK ♀	10.6	2.65	−0.12	33.2	0.21	6.79	13.3	33.0	7.0
TJ ♂	11.3	2.83	1.05	35.3	0.59	19.0	14.1	36.3	19.6
FK ♂	14.1	3.52	1.46	41.9	0.37	11.9	17.6	43.4	12.2
EB ♂	17.2	4.31	1.32	40.9	0.37	11.8	21.5	42.2	12.2
PD ♂	19.4	4.85	0.11	48.5	0.22	7.26	24.2	48.6	7.5

the solubility volumes have been deduced weights of tissues constituting the compartments, with the aid of plausible assumptions for fat to non-fat ratio of two of the body compartments (Tables IV and V). One can now divide blood flow rate, F_t, by compartment weight, W_t, to obtain the ratio denoted as perfusion of the compartment (Table VI). For comparison, the average perfusion of the whole body, which is not derived from the model, *i.e.*, the estimated total cardiac output F divided by body weight W (Table I), is included in the last column of Table VI. The perfusion of compartment 1 is in the range 2 to 4 ml/min./100 gm. The perfusion of compartment 2 is about half that of compartment 1. The perfusion of compartment 3 is in the range 25 to 73 ml/min./100 gm.

TABLE VI

PERFUSION OF BODY COMPARTMENTS

Subject	100 F_1/W_1*	100 F_2/W_2* ml/min./100 gm	100 F_3/W_3*	100 F/W† ml/min./100 gm
VL ♀	3.6	1.8	43	9.9
GK ♀	4.1	2.4	53	9.5
TJ ♂	3.2	1.6	25	8.6
FK ♂	2.6	1.6	41	8.4
EB ♂	3.1	1.6	43	8.7
PD ♂	2.2	1.2	73	8.2
Mean	3.1	1.7	46	8.9

* From Tables III, V. † From Table I.

These values of perfusion are not incompatible with reported values. The range of values derived for compartment 3 agrees in order-of-magnitude with the values quoted for well-perfused viscera (16). The perfusion of compartment 2 may be compared with the values $3.0\ ^{+3.5}_{-0.7}$ ml/min./100 gm for resting muscle (16). Jones (5) has given the values 1 to 2.5 ml/min./100 ml for perfusion of resting muscle and the value 1.3 ml/min./100 ml for perfusion of adipose tissue. The muscle values were obtained as the rate constants of exponentials determined by curve-fitting nitrogen, krypton, and xenon elimination and uptake data. The experiments were done under conditions of constant external concentration in which the model analysis reduces to identifying each exponential with one compartment. The adipose tissue value was obtained as the slowest rate constant of a sum of five exponential functions fitted to a nitrogen elimination curve for the whole body. In a recent paper Lundin (19) has derived from a series of nitrogen elimination experiments at constant external concentration the range of values 4.6 to 6.1 ml/min./100 ml for perfusion of resting muscle and the range of values 2.4 to 4.0 ml/min./100 ml for perfusion of adipose tissue. These ranges were derived respectively from the two rate constants (half-times 12 to 15 min. and 90 to 150 min. respectively) into which the data could be resolved by exponential curve-fitting.

The values of perfusion derived in this paper are valid if the perfusion-limited model by which they were derived is valid. In particular, the values derived for the compartment interpreted as adipose tissue are estimated as about ±20 per cent uncertain, largely on account of uncertainty in estimating the slowest rate constant k_1 from the data. If, however, the model is in error because of appreciable gross diffusion of cyclopropane into adipose tissue from more quickly saturated neighboring tissue, then the present values of perfusion of adipose tissue are overestimated and should be regarded as of the nature of upper-limiting values.

The Course of Cyclopropane Uptake in Body Compartments. The kinetic aspects of uptake of fat-soluble inert substances are known to be fundamental to various problems of anesthesia. Recent kinetic considerations have been set forth by Price and co-workers (20, 21) and by Goldstein and Aronow (22) for the cases of thiopental and pentobarbital injected into the blood (which acts as the external volume of the present model) and the subsequent different rates of uptake by the several body tissues. Also, decompression sickness requires for its understanding a knowledge of the kinetics of distribution in the body of a fat-soluble inert gas (nitrogen) (5,23). It is therefore of interest to illustrate the kinetic results of the present model analysis by exhibiting the calculated time course of cyclopropane uptake in the several body compartments.

The fractional amount of cyclopropane $q_i(t)$ in each body compartment as a function of time is given by equations (A17), (A21), (A22). As an example, for subject EB,

$$\begin{aligned} q_1(t) &= 78.2 - 48.9\,e^{-k_1 t} - 28.0\,e^{-k_2 t} - 1.3\,e^{-\alpha_3 t} \\ q_2(t) &= 11.3 + 33.0\,e^{-k_1 t} - 42.9\,e^{-k_2 t} - 1.4\,e^{-\alpha_3 t} \\ q_3(t) &= 3.2 + 4.9\,e^{-k_1 t} + 23.3\,e^{-k_2 t} - 31.4\,e^{-\alpha_3 t} \end{aligned} \tag{5}$$

in which $q_i(t)$ is expressed in units of per cent, k_1, k_2 are given in Table II, and α_3 is obtained from Table III. These $q_i(t)$ are shown graphically (Fig. 4*a*), together with the smoothed experimental curve $q(t)$ for the respiratory circuit volume. The results may also be exhibited as the partial pressure of cyclopropane in each compartment as a function of time. This quantity, expressed as a fraction of the initial partial pressure of cyclopropane in the alveolar volume, is given by

$$P_i(t) = \frac{v_0}{v_i}\, q_i(t) \tag{6}$$

$P_i(t)$ is plotted in Fig. 4*b*, together with the experimental $q(t)$, which may also be regarded as the partial pressure in the external volume divided by the initial partial pressure in the external volume (after mixing with the alveolar gases). The quantities $q(t)$ and $P_i(t)$, $i = 1, 2, 3$, all approach the same value at $t = \infty$. The curves show among other things how the two fast compartments (2 and 3) fill up rapidly to the partial pressure of the external volume and then "join with" the external volume in "feeding" the adipose tissue compartment. This behavior of the three

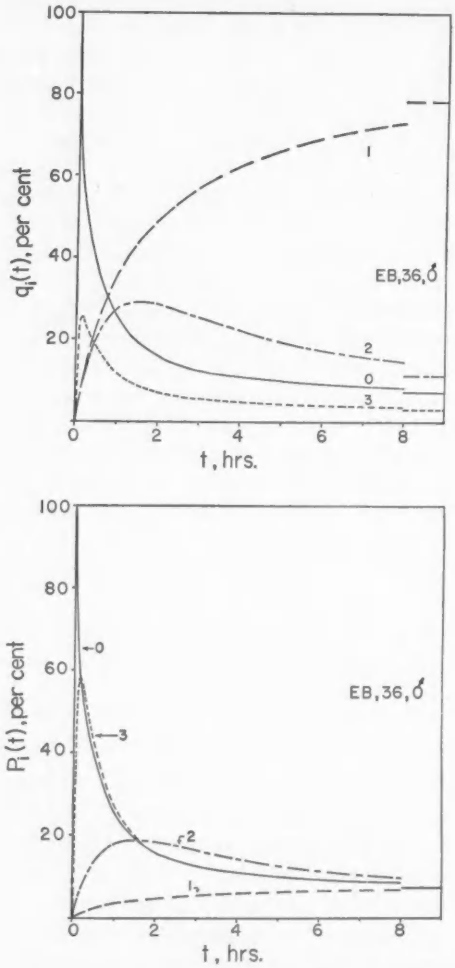

FIGURE 4*a* and *b* Time course of inert gas uptake by body compartments. Compartment numbers i indicated for each curve: $i = 0$, respiratory circuit volume; $i = 1$, 2, 3, body compartments. Horizontal lines at right of each curve are asymptotic values for $t \rightarrow \infty$.

(*a*) Ordinate: Amount of cyclopropane in compartment i at time t as percentage of total cyclopropane in system. Abscissa: time, t, hours.

(*b*) Ordinate: Partial pressure of cyclopropane in compartment i at time t as percentage of initial partial pressure of cyclopropane in respiratory circuit volume. Abscissa: time, t, hours.

body compartments is in sharp contrast to their course of uptake under the conditions of constant external concentration, in which case each compartment fills up to its equilibrium value independently of the others as a single exponential function of time.

CONCLUSIONS

1. The existing perfusion-limited model of inert gas exchange by the body is compatible with the present cyclopropane uptake experiments.
2. Analysis by this model of uptake data on six normal resting subjects yielded the following results:
   (*a*) The body is composed of three compartments, or cyclopropane spaces, which are anatomically compatible with (1) adipose tissue; (2) resting muscle, skin, and connective tissue; (3) highly perfused viscera.
   (*b*) The rates of blood flow to compartments 1 and 2 are approximately equal and are of the order of 10 per cent of the total cardiac output.
   (*c*) The rates of blood flow per unit compartment weight (perfusion) were in the following ranges: compartment 1, (adipose tissue), 2 to 4 ml/min./100 gm; compartment 2, (resting muscle, skin, etc.), 1 to 2.5 ml/min./100 gm; compartment 3, (highly perfused viscera), 25 to 75 ml/min./100 gm.
   (*d*) The time course of cyclopropane uptake in each body compartment is described by a constant plus three exponential functions of time.

   These results may be regarded as quantitative if the perfusion-limited model from which they were calculated proves valid. To the extent that tissue-to-tissue diffusion processes compete with perfusion processes, the quantitative significance of the results becomes more limited. At present the precise extent of such diffusion processes relating to adipose tissue is unknown.
3. Kinetic analysis of experiments on fat-soluble inert gas uptake would appear to be a useful tool in such problems as:
   (*a*) Gross body composition and its changes with body weight change.
   (*b*) rate of blood flow to total body adipose tissue and its variations under different conditions of the subject.
   (*c*) Narcotic action of fat-soluble anesthetics.
   (*d*) Decompression sickness.

The authors wish to thank Miss Edith Schreiber and Miss Mu Wan Sun for their painstaking performance of the computations.

This investigation was supported in part by a research grant (H-1288) from the National Heart Institute, United States Public Health Service, and by The Mona Bronfman Sheckman Foundation.

Received for publication, June 28, 1960.

REFERENCES

1. LESSER, G. T., BLUMBERG, A. G., and STEELE, J. M., *Am. J. Physiol.*, 1952, **169**, 545.
2. LESSER, G. T., BLUMBERG, A. G., and STEELE, J. M., *Proc. 2nd Internat. Conf. Biochem. Problems Lipids*, London, Butterworths Scientific Publications, 1956, 373.
3. LESSER, G. T., PERL, W., and STEELE, J. M., *J. Clin. Inv.*, 1960, **39**.
4. PERL, W., *Internat. J. Appl. Rad. and Isot.*, in press.
5. JONES, H. B., *in* Medical Physics, (O. GLASSER, editor), Chicago, Year Book Publishers, Inc., 1950, **2**, 855
6. BEHNKE, A. R., *Medicine*, 1945, **24**, 359-379.
7. KETY, S. S., *Pharmacol. Rev.*, 1951, **3**, 1.
8. BLUMBERG, A. G., LA DU, B. N., JR., LESSER, G. T., and STEELE, J. M., *J. Pharmacol. and Exp. Therap.*, 1952, **104**, 325.
9. DAVIDSON, D., EGGLETON, P., and FOGGIE, P., *Quart. J. Exp. Physiol.*, 1952, **37**, 91.
10. LESSER, G. T., and REIFENBERG, G. H., unpublished data.
11. SECHZER, P. H., DRIPPS, R. D., and PRICE, H. L., *J. Appl. Physiol.* 1959, **14**, 887.
12. ROBERTSON, J. S., *Physiol. Rev.*, 1957, **37**, 135.
13. BERMAN, M., and SCHOENFELD, R., *J. Appl. Physics*, 1956, **27**, 1361.
14. ROBBINS, B. H., *in* Cyclopropane Anesthesia, Baltimore, The Williams and Wilkins Co., 1958, 7.
15. CANDER, L., and FORSTER, R. E., *J. Appl. Physiol.*, 1959, **14**, 541.
16. SPECTOR, W. S., Handbook of Biological Data, Philadelphia, W. B. Saunders Co., 1956, 259, 283.
17. GREVILLE, G. D., *Biochem. J.*, 1943, **37**, 17.
18. PITTS, G. C., *Am. J. Physiol.*, 1956, **185**, 41.
19. LUNDIN, G., *J. Physiol.*, 1960, **152**, 167.
20. PRICE, H. L., *Anesthesiology*, 1960, **21**, 40.
21. PRICE, H. L., KOVNAT, P. J., SAFER, J. N., CONNER, E. H., and PRICE, M. L., *Clin. Pharmacol. and Therap.*, 1960, **1**, 16.
22. GOLDSTEIN, A., and ARONOW, L., *J. Pharmacol. and Exp. Therap.*, 1960, **128**, 1.
23. BEHNKE, A. R., *in* Medical Physics, (O. GLASSER, editor), Chicago, Year Book Publishers, Inc., 1950, **2**, 257
24. COMROE, J. H., JR., FORSTER, R. E., DUBOIS, A. B., BRISCOE, W. A., and CARLSEN, E., *in* The Lung, Chicago, Year Book Publishers, Inc., 1955, 48.

APPENDIX A

MATHEMATICAL TREATMENT OF MODEL

The model consists of a finite number of compartments connected in parallel *via* the blood circulation with a closed respiratory circuit of constant volume (Fig. 3). The total amount Q (moles) of cyclopropane in the system is constant and equal to the sum of the amounts $Q_i(t)$ in the various body compartments plus the amount $Q_0(t)$ in the respiratory circuit volume. In terms of the fractional amounts

$$q_\nu(t) = Q_\nu(t)/Q, \quad \nu = 0, 1, 2, 3 \tag{A1}$$

this condition is

$$q_0 + q_1 + q_2 + q_3 = 1 \tag{A2}$$

The average concentration $C_i(t)$ of cyclopropane in the ith body compartment is defined by

$$V_i C_i(t) = Q_i(t) \tag{A3}$$

The respiratory circuit volume is defined by an analogous equation

$$V_0 C_e(t) = Q_0(t) \tag{A4}$$

in which $C_e(t)$ is the average concentration of cyclopropane in the external volume, which is the part of the respiratory circuit volume, external to the subject, in which measurements were made.

The four time-dependent variables of the model are taken as $q_\nu(t)$, $\nu = 0, 1, 2, 3$. One equation connecting these variables is equation (A2). Three more can be obtained from the Fick principle of perfusion applied to each body compartment,

$$\frac{dQ_i}{dt} = F_i(C_a - C_{vi}), \quad i = 1, 2, 3 \tag{A5}$$

in which $C_a - C_{vi}$ is the arteriovenous difference of concentration of cyclopropane for the ith compartment at time t. The analogous Fick equation for the respiratory circuit volume is already included in the preceding formulation. It is obtainable from substitution of equation (A5) into the time derivative of equation (A2) and by using the equations of continuity of flow of cyclopropane on arterial and venous sides of the circulation respectively,

$$C_a F_1 + C_a F_2 + C_a F_3 = C_a F \tag{A6}$$

$$C_{v1} F_1 + C_{v2} F_2 + C_{v3} F_3 = C_v F \tag{A7}$$

In equations (A6), (A7), all circulatory shunts are neglected and the concentrations all correspond to the same time; *i.e.*, the circulatory time lags in the arterial and venous bloods between lungs and body tissues (of order 1 min. or less) are neglected relative to the uptake times of primary interest in this experiment (of order 30 to 200 min.). Hence the time dependence of all concentrations can be indicated as $C(t)$.

The arterial and venous concentrations of cyclopropane are next related to the concentrations existing in the compartments. By the assumption of solubility equilibrium between blood and tissue at the venous end of each compartment,

$$C_{vi}(t) = \frac{C_i(t)}{\lambda_i} = \frac{V_i C_i(t)}{v_i} = \frac{q_i(t)}{v_i} Q \tag{A8}$$

By the assumption of solubility equilibrium between arterial blood and the alveolar gases

$$C_a(t) = \frac{C_A(t)}{\lambda_A} = \frac{C_A(t)}{C_e(t)} \frac{C_e(t)}{\lambda_A} \tag{A9}$$

By the neglect of lung "fill-up" time, the lung volume is assumed to be in equilibrium contact with the external volume at all times. Hence the ratio $C_A(t)/C_e(t)$ is constant and equal to its value at $t = \infty$. This value is given (3) by,

$$\frac{C_A}{C_e} = \frac{80}{79} \frac{T_e}{T_A} \left(\frac{p_e - p_{vA}}{p_e - p_{ve}} \right) \tag{A10}$$

where T_e, P_e, P_{ve} are temperature, pressure, and water vapor pressure in the external volume, and T_A, P_{vA} are temperature and water vapor pressure in the alveolar volume. The temperature and pressure factors in equation (A10) are given by the elementary gas

laws while the factor 80/79 represents the respiratory quotient effect (24); *i.e.*, the increase in equilibrium concentration of an inert gas in the alveolar volume because the rate of emission of carbon dioxide into this volume is less than the rate of absorption of oxygen from it. Expressing the partition coefficient in equation (A9) in terms of the Bunsen solubility coefficient of cyclopropane in blood α_{bl}, by

$$\lambda_A = \frac{1}{\alpha_{bl}} \frac{273}{T_A} \tag{A11}$$

and substituting equations (A11), (A10), and (A4) into (A9) yields

$$C_a(t) = \frac{q_0(t)}{v_0} Q \tag{A12}$$

where

$$v_0 = \lambda_0 V_0 \tag{A13}$$

and

$$\lambda_0 = \frac{1}{\alpha_{bl}} \left(\frac{79}{80}\right)\left(\frac{273}{T_s}\right)\left(\frac{p_s - p_{vs}}{p_s - p_{vA}}\right) \tag{A14}$$

The quantity v_0 may be regarded as the solubility volume of the respiratory circuit (external volume plus lung volume). Substitution of equations (A12) and (A8) into (A5) yields the three additional equations desired

$$\frac{dq_i}{dt} = F_i\left(\frac{q_0}{v_0} - \frac{q_i}{v_i}\right), \quad i = 1, 2, 3. \tag{A15}$$

In terms of the turnover rates $f_i = F_i/v_0$, $\phi_i = F_i/v_i$, equation (A15) can be written

$$dq_i/dt = f_i q_0 - \phi_i q_i, \quad i = 1, 2, 3 \tag{A16}$$

equations (A2) and (A16) define the model mathematically. Under steady state conditions the turnover rates f_i, ϕ_i ($i = 1, 2, 3$) are constant in time. Then the equations are linear with constant coefficients and have a solution of the form

$$q_\nu(t) = q_{\nu\infty} + \Sigma_j b_{\nu j} e^{-\alpha_j t}, \quad \nu = 0, 1, 2, 3 \tag{A17}$$

where Σ_j denotes summation from $j = 1$ to 3.

The relations between the exponential parameters in equation (A17) and the turnover rates in equation (A16) may be obtained by the "old-fashioned" method of substituting equation (A17) into (A16) and (A2), equating coefficients of like exponentials, and using the initial conditions $q_0(0) = 1$, $q_i(0) = 0$ ($i = 1, 2, 3$). These relations may be exhibited in a more concise and convenient form by the Laplace transform method (13). By this method, the Laplace transform $\bar{q}_0(p)$ of $q_0(t)$ is obtained from equation (A17) in the form

$$\bar{q}_0(p) = \frac{q_{0\infty}}{p} + \Sigma_j \frac{b_{0j}}{p + \alpha_j} \tag{A18}$$

On the other hand $\bar{q}_0(p)$ is obtained from equations (A16) in the form

$$\frac{1}{p\bar{q}_0(p)} = 1 + \Sigma_j \frac{f_j}{p + \phi_j} \tag{A19}$$

By putting either expression for $\bar{q}_0(p)$ into the form of the other, the turnover rates can be expressed in terms of the exponential parameters or *vice versa*. From the Laplace transform of $q_i(t)$,

$$\bar{q}_i(p) = \frac{f_i}{p + \phi_i}\,\bar{q}_0(p), \quad i = 1, 2, 3 \tag{A20}$$

the exponential parameters of the body compartments can be expressed as

$$q_{i\infty} = \frac{f_i}{\phi_i}\,q_{0\infty} = \frac{v_i}{v_0}\,q_{0\infty}, \quad i = 1, 2, 3 \tag{A21}$$

$$b_{ij} = \frac{f_i b_{0j}}{\phi_i - \alpha_j}, \quad i, j = 1, 2, 3 \tag{A22}$$

From equations (A21) and (A2) it follows in particular that

$$q_{0\infty} = \frac{v_0}{v_0 + v_1 + v_2 + v_3} \tag{A23}$$

In the present paper the turnover rates were first obtained from the exponential parameters by an iteration method based on the "old-fashioned" approach. The results were then checked by the Laplace transform method.

APPENDIX B

APPLICATION OF MODEL TO EXPERIMENT

In applying the model to the experiment to derive physical conclusions, various theoretical quantities of the model must first be identified with those quantities which can be considered as "actually measured." The actually measured quantities are, first, $C_e'(t)$, the concentration of cyclopropane (moles/liter) in the external volume at time t; second, $Q(t)$, the amount of cyclopropane (moles) initially introduced into the external volume minus the amount subtracted up to time t in sampling; and third, a constant volume V_E (liters), measured by a nitrogen dilution technique (2). The volume V_E comprises the external volume plus an effective lung volume such that the product $V_E C_e'(\infty)$ is the amount of cyclopropane in the external volume plus actual lung volume at sufficiently long time, when the lung volume is in "equilibrium contact" with the external volume. From the preceding actually measured quantities a derived experimental quantity is constructed to represent the data,

$$q(t) = \frac{V_N C_e'(t)}{Q(t)} \tag{B1}$$

The following identifications are now made: $C_e'(t)$ with the model quantity $C_e(t)$, equation (A4); V_E with the model quantity V_0, equation (A4); $Q(t)$ with the constant Q of the model, equation (A1); and $q(t)$ with the model quantity $q_0(t)$, equation (A1) with $\nu = 0$.

By the identification of $Q(t)$ with Q a sampling error is made. In the experiments less than 8 per cent of the amount added initially was removed for chemical analysis during the entire experiment of about 8 hrs. duration. Of this amount, about one-third was removed in the last 4 hrs. By using the variable $Q(t)$ in equation (B1) instead of, for example, the constant initial amount $Q(0)$, an attempt is made to allow partially for this error. Thus the sampling error, while difficult to assess quantitatively, should be no more than a few per cent.

The identification of $q(t)$, equation (B1), with the model quantity $q_0(t)$ is not made for the time range 0 to ∞. The first and last experimental measurements of $C_e'(t)$ were made some 12 minutes and 480 minutes after injection of cyclopropane into the external volume. Hence $q(t)$ can be identified with $q_0(t)$ only in the time range 12 min. to 480 min. In this time range the five numbers q_∞, a_1, a_2, k_1, k_2 are derived by curve-fitting exponential functions to $q(t)$. These numbers are derived experimental quantities in the same sense as $q(t)$, equation (B1), is derived from actually measured quantities. They are identified with the model quantities $q_{0\infty}$, b_{01}, b_{02}, α_1, α_2 of equation (A17) with $\nu = 0$. Since these model quantities are functions of the model parameters v_0, v_1, F, F_1, this identification yields five relations from which five model parameters can be determined if the others are known or assumed.

The model was set up as a closed 4-compartment model, *i.e.*, as a constant plus three exponential model. The five numbers q_∞, a_j, k_j ($j = 1, 2$) which represent the data correspond, however, to a constant plus two exponentials. The reason for assuming the extra exponential in formulating the model was that the sum $q_\infty + a_1 + a_2$ obtained in the curve-fitting process was sufficiently less than one to warrant the assumption that another exponential existed having the model interpretation of an additional body compartment and satisfying the condition $q_\infty + a_1 + a_2 + a_3 = 1$ required by equation (A17) with $\nu = 0$, $t = 0$ (and identifying a_3 with b_{03}). This assumption is expected to result in more accurate values of the model parameters v_1, v_2, F_1, F_2, which depend primarily on a_1, a_2, k_1, k_2, than the alternative procedure of using a closed 3-compartment model and representing the experimental results by a constant plus two exponentials with altered values a_1' and a_2' such that $q_\infty + a_1' + a_2' = 1$ (this alteration could be produced by changing the time scale by the substitution $t = t' + \delta$ and regarding t' as the physically correct time interval from the time zero of the experiment). The derived value of v_3, which depends primarily on a_3, is not expected to have much quantitative significance.

APPENDIX C

COMPOSITION OF BODY COMPARTMENTS

Consider first the whole body as composed additively of a weight of fat W_f, having a solubility volume $\lambda_f V_f$, and a fat-free lean weight W_l, having a solubility volume $\lambda_l V_l$. Then the total solubility volume of the body is given by (see equation (A23)),

$$\lambda_f V_f + \lambda_l V_l = v_1 + v_2 + v_3 = \left(\frac{1 - q_\infty}{q_\infty}\right) v_0 \tag{C1}$$

The partition coefficients λ_f, λ_l are given by the ratios

$$\lambda_f = \frac{\alpha_f}{\alpha_{bl}}, \quad \lambda_l = \frac{\alpha_l}{\alpha_{bl}} \tag{C2}$$

where α_f, α_l, α_{bl} are the Bunsen solubility coefficients of cyclopropane per unit volume of fat, fat-free lean mass, and blood respectively (ml STP/ml). In terms of the solubility coefficients α_f', α_l' per unit weight of fat and fat-free lean mass (ml STP/gm, see (1, 8)), defined by

$$\alpha_f V_f = \alpha_f' W_f, \quad \alpha_l V_l = \alpha_l' W_l \tag{C3}$$

equation (C1) becomes

$$\alpha_f' W_f + \alpha_l' W_l = \alpha_{bl}(v_1 + v_2 + v_3) = \alpha_{bl} v_0 \left(\frac{1 - q_\infty}{q_\infty}\right) \tag{C4}$$

The second form of equation (C4), combined with the body weight equation

$$W_f + W_l = W \tag{C5}$$

has previously been used (3) to calculate total body fat W_f and total fat-free lean mass W_l. To make inferences concerning the composition of the ith compartment as between fat W_{fi} and fat-free weight W_{li}, the equation analogous to the first form of equation (C4) is used.

$$\alpha_f' W_{fi} + \alpha_l' W_{li} = \alpha_{bl} v_i, \quad i = 1, 2, 3 \tag{C6}$$

As an example, for subject EB, Table III, and with the solubility coefficients (1, 3, 8), $\alpha_f' = 11.26$, $\alpha_l' = 0.33$, $\alpha_{bl} = 0.40$, equations (C6) are

$$11.26\ W_{f1} + 0.33\ W_{l1} = 195.4, \quad (F_1 = 0.67 \text{ liter/min.}) \tag{C7}$$

$$11.26\ W_{f2} + 0.33\ W_{l2} = 28.4, \quad (F_2 = 0.68 \text{ liter/min.}) \tag{C8}$$

$$11.26\ W_{f3} + 0.33\ W_{l3} = 8.03, \quad (F_3 = 5.29 \text{ liter/min.}) \tag{C9}$$

in which the corresponding blood flow rates to the respective body compartments (Table III) have been indicated on the right. The total body fat W_f and fat-free lean mass W_l can be expressed additively in terms of values for the three body compartments as

$$W_{f1} + W_{f2} + W_{f3} = 18.9 \text{ kg} \tag{C10}$$

$$W_{l1} + W_{l2} + W_{l3} = 57.1 \text{ kg} \tag{C11}$$

Since the sum of equations (C7 to C9) is equation (C4) which has been used in deriving equations (C10), (C11), only four of the five preceding equations are independent. Consider the four independent equations to be equations (C7), (C9), (C10), (C11). There are six unknowns, W_{fi}, W_{li} ($i = 1, 2, 3$). Hence, two more conditions are needed. These are taken as

$$W_{f1} = x_1(W_{f1} + W_{l1}) \tag{C12}$$

$$W_{f3} = x_3(W_{f3} + W_{l3}) \tag{C13}$$

For given x_1, equations (C7), (C12) can be solved for W_{f1}, W_{l1}. For given x_3 equations (C9), (C13) can be solved for W_{f3}, W_{l3}. Then equations (C10), (C11) can be solved for W_{f2}, W_{l2} respectively. The results for subject EB are shown in Table IV.

The qualitative nature of the three compartments, which indicates the x_1, x_3 range of interest, is suggested by equations (C7), (C9), and the corresponding blood flow rates. Consider first equation (C7), corresponding to compartment 1. The right hand sides of equations (C7) to (C9) are proportional to the amounts of cyclopropane in the respective compartments. If the entire 57.1 kg of fat-free lean mass of the body were in compartment 1, only $0.33 \times 100 \times 57.1/195.4 = 9.7$ per cent of the cyclopropane in this compartment would be accounted for. The remainder, 90.3 per cent, requires $W_{f1} = 0.903 \times 195.4/11.26 = 15.7$ kg of fat to be present, which is 83.0 per cent of the total body fat. Such a combination of W_{f1} and W_{l1}, however, which amounts to almost the entire body, is anatomically incompatible with the derived blood flow rate of 0.67

liter/min. to this compartment. The composition of compartment 1 becomes compatible with its derived blood flow rate if W_{t1} is decreased substantially and W_{f1} increased slightly.

Consider, next, equation (C9) corresponding to compartment 3. If this compartment contained all fat and no fat-free lean mass, the entire cyclopropane content of the compartment would be accounted for by a fat content of $W_{f3} = 8.03/11.26 = 0.71$ kg. Such a combination of W_{f3} and W_{t3}, a very small proportion of the body, is anatomically incompatible with the derived blood flow rate of 5.29 liter/min. to this compartment. The composition of compartment 3 becomes compatible with its derived blood flow rate if W_{f3} is reduced to slight proportions and W_{t3} is increased substantially.

EXPLANATION OF IMPORTANT SYMBOLS

a_j = amplitude exponential parameter representing experimental data
$b_{\nu j}$ = amplitude coefficient of exponential in model solution
$C(t)$ = concentration of cyclopropane at time t, moles/liter
$C_e'(t)$ = experimentally measured concentration of cyclopropane in external volume
F = rate of blood flow, liters/minute
f_i = F_i/v_0, rate of blood flow per unit respiratory circuit solubility volume, minute^{-1}
k_j = rate constant exponential parameter representing experimental data, minute^{-1}
$P_i(t)$ = fractional partial pressure of cyclopropane in ith body compartment at time t
p = Laplace transform complex frequency variable
Q = constant total amount of cyclopropane in system in model, moles
$Q(t)$ = total amount of cyclopropane in system at time t in experiment, moles
$Q_\nu(t)$ = amount of cyclopropane in νth model compartment, moles
$q(t)$ = experimentally derived ratio of amount of cyclopropane in respiratory circuit volume to total amount of cyclopropane in system at time t
$\dot{q}(t)$ = dq/dt, time derivative of $q(t)$
$q_\nu(t)$ = $Q_\nu(t)/Q$, fractional amount of cyclopropane in νth model compartment
$q_\nu(p)$ = Laplace transform of $q_\nu(t)$
q_∞ = constant equilibrium value of $q(t)$ at $t = \infty$
$q_{\nu\infty}$ = constant equilibrium value of $q_\nu(t)$ at $t = \infty$
T_j = $0.693/k_j$, half-time of exponential representing experimental data, minutes
$T_{\alpha 3}$ = $0.693/\alpha_3$, half-time derived in model analysis, minutes
t = time, minutes
V = volume, liters
V_R = experimentally determined respiratory circuit volume, liters
v = λV, solubility volume, liters
W = weight, kilograms
α = Bunsen solubility coefficient of cyclopropane, milliliters STP/milliliter
α' = Bunsen solubility coefficient divided by density, milliliters STP/gram
α_j = rate constant of exponential occurring in model analysis
λ = α/α_{bl}, partition coefficient of cyclopropane
ϕ_i = F_i/v_i, solubility volume perfusion, minute^{-1}

Subscripts

i = 1, 2, 3, body compartment
0 = respiratory circuit volume
ν = 0, 1, 2, 3, either respiratory circuit volume or body compartment
j = 1, 2, 3
A = alveolar volume
e = external volume
f = fat (lipid)
l = fat-free tissue (lean)
fi = fat in ith body compartment
li = fat-free tissue in ith body compartment
bl = blood

MICROEXUDATES FROM CELLS GROWN IN TISSUE CULTURE

MURRAY D. ROSENBERG
From The Rockefeller Institute

ABSTRACT Cellular substrata of known molecular structure and measurable dimensions can be constructed as transferred films from Langmuir troughs or as adsorbed films. In addition, large molecules in culture media form measurable adsorbates. With the techniques of ellipsometry and surface chemistry it is possible to characterize and measure (within ± 3A) as a function of several parameters a microexudate of molecular dimensions deposited when tissue cultured cells contact certain substrata. The selective attraction of substratum and cell for microexudate has been determined, and the time course of deposition in Eagle's medium is characterized by a rapid initial accretion of material. During this period, microexudate can diffuse several cell diameters and cannot be detected in the culture medium. In Eagle's medium the cells cannot be detached from glass surfaces by versene or trypsin unless the surface of cell or substratum is coated with certain molecules. Trypsin becomes adsorbed to cell surfaces, continues to be enzymatically active on the surface, and digests protein components of microexudate and substratum. Microexudate appears to be a complex mosaic of molecules (including protein) synthesized within or on the surfaces of cells and secreted by cells or transferred from their surfaces to specific substrata. It is proposed that this mosaic plays, on the molecular level, a significant role in cell-to-cell interactions, cell locomotion and adhesion, and the selective application and spreading of cells on various surfaces.

INTRODUCTION

The experimental study of the development and activity of cells *in vitro* requires consideration of several parameters such as cell strain, internal and surface condition of the cell, the culture medium, cellular contacts, and the substratum upon which the cell rests. In addition, the experimenter must be cognizant of the complex interplay between these parameters, as well as the modifications introduced when the behavior of cells is subjected to laboratory investigations.

An early example of the interdependency between the above parameters was presented by Weiss (1945). He demonstrated that an explant of cells in liquid culture produced a microscopic colloidal exudate or "ground mat" whose fine fibrillar network determined the orientation and arrangement of the cells growing outward

from the explant. Thus, the cells in conjunction with their growth medium modified their environment in such a way that their pattern of locomotion was affected. Another example of this interdependency among the parameters which bear upon cellular behavior are the alterations by cellular products of the growth medium and substratum, which in turn modify the surfaces and activities of the cells (changes in pH, accumulation of toxic products, etc.). Thus, a cell and its environs are generally in a state of dynamic equilibrium, one modifying the other in complex ways.

The investigations described in this report were undertaken to determine whether, in view of the presence of the aforementioned exudate of microscopic dimensions, the cell can alter its substratum through the deposition of a microexudate of molecular dimensions, nondetectable by light microscopy (see Rosenberg (1960)). By adapting to biological systems several of the techniques commonly used in the construction and measurement of monomolecular films, it was possible to demonstrate that cells cultured *in vitro* can produce upon contact with a substratum a microexudate that alters the molecular carpet upon which the cell rests. The characteristics of this microexudate are the subject of this paper.

The first section describes the techniques used to observe this microexudate as well as the methods used to prepare the cells and control the substrata for the cells. Later sections on the results are divided into two parts: part I deals primarily with observations and measurements of physical characteristics of the microexudate; part II deals with the chemical composition and source of this material. In a final section the role of this molecular material is discussed, and it is proposed that the microexudate is composed, in part, of molecules previously adsorbed to the surface of cells.

To clarify the presentation, the following definitions of terms are presented.

Colloidal exudate: An exudate of microscopic dimensions (greater than 0.1 micron) produced by cells cultured *in vitro*.

Microexudate: A substance of submicroscopic dimensions (roughly 20 to 40A) given off by cells cultured *in vitro*.

Cell population surface density (also designated by the symbol CPSD): The average of several counts of the number of cells covering a surface area of 1 mm^2.

Relative cellular cross section (also designated by the symbol RCS): The product of the average cross-sectional area of the spherical, unspread cell (in square millimeters) and the cell population surface density (CPSD).

Mean microexudate thickness: The thickness (in angstroms) of the microexudate averaged over an area of 1 mm^2.

MATERIAL AND METHODS

The basal medium (with no serum components) described by Eagle (1955), and henceforth referred to as Eagle's medium, was used in these investigations. The cells for the experiments were obtained from stock cultures of several strains reared in

Eagle's medium supplemented with 10 per cent horse serum or from freshly dissociated tissues of chick embryos. The stock cultures, prior to use, were washed with calcium- and magnesium-free Earle's solution. They were detached either enzymatically with 0.05 per cent trypsin or with 0.05 per cent sodium versenate (disodium ethylenediaminetetracetate) at 37°C (pH approximately 7.8) for 3 to 5 min. The loosened cells were centrifuged for 5 min at 600 R.P.M., the supernatant was discarded, and the pellet of cells was washed carefully with Eagle's medium. For immediate use the pellet was resuspended by gentle pipetting in the test medium, or suspended in the standard culture medium and maintained for several hours in a roller tube for later use. Cells resuspended in Eagle's medium must be used without delay or kept in a roller tube since they rapidly adhere to glass.

The fresh embryonic tissue was dissociated enzymatically with 0.5 per cent trypsin-pancreatin for 10 to 15 min at 37°C, centrifuged, and used as above.

The test slides are made of glass with a vacuum-deposited chrome coating that is nontoxic to the growth and spreading of cells. Each slide is cleaned with cerium oxide, dried with a jet of filtered air, and sterilized under ultraviolet light for 10 min. No adsorption of ozone has been detected. Base readings on all slides are obtained with an ellipsometer.

The ellipsometer as developed by Rothen[1] (1945) can be used to measure the overall thickness of molecular films with a precision of a fraction of 1 A. The instrument is designed on the principle that when light, linearly polarized in a plane making an angle other than 0 or 90° with the plane of incidence, impinges upon a metallic surface, the reflected light is elliptically polarized. The shape and orientation of the ellipse depend upon the angle of incidence and the optical constants of the metal. The parameters of the ellipse will be altered if the metallic surface is covered with a thin transparent film, and these alterations can be measured and calibrated in terms of the thickness of the transparent film. The error due to changes in the index of refraction of the transparent film will in general be very small. The field of view of the optical system is 1 mm^2, and measurements of film thickness, therefore, represent an average or mean over this area. Hence, the measured thickness of a surface film will be determined by the configuration, orientation, dimensions, and surface concentration of the molecules of which the film is composed.

0.5 ml of the cellular suspension to be studied is placed on the slide. The material is kept in a saturated atmosphere of 5 per cent CO_2, 95 per cent air to maintain a pH of 7.4 at the test temperature. During each experiment a duplicate set of control slides is covered with the same amount of cell-free test medium. As additional controls, samples of the supernatant medium that bathes the cells resting upon the slide, are transferred to clean chrome-plated test slides to determine the presence of adsorbable molecules.

To measure the CPSD, the test slide is examined microscopically, and cell counts are made over several regions of the slide and then averaged.

At designated times the cells are removed mechanically from the slides by means of a jet of isotonic saline and/or doubly distilled water. This procedure is fully effective in removing the attached cells. Many cells thus removed from the surface can be recultured.

Upon removal of the cells, the slides are air-dried and their surface is studied in the ellipsometer to determine the presence and mean thickness of any thin films. Slides upon which films of microexudate have been deposited then can be used for additional experiments.

---

[1] The author is highly indebted to Dr. A. Rothen of The Rockefeller Institute for the loan of the equipment required for the study of molecular films.

Precautions. Several precautions are essential to ensure reproducible measurements. (1) All slides must be carefully cleaned with a mild abrasive such as cerium oxide. (2) The slides must be used shortly after cleaning. (3) Experiments should be conducted in an air-conditioned, sterile atmosphere to reduce contaminants. (4) Cells suspended in protein-free media must be mildly agitated since they adhere very rapidly to the surfaces of containers. (5) The cells must be prepared with a minimum of centrifugation and pipetting to reduce the possibility of mechanical damage to the cells, resulting in the leakage of materials that could then adsorb to the surface. If these precautions are adopted, measurements can be repeated with an accuracy of $\pm$ 3 A.

RESULTS—PART I

A. *Observations.* By means of the aforementioned procedures it has been possible to detect on the test slides a microexudate given off by cells. The surface of the slide, as viewed through the ellipsometer, appears to be covered with a relatively uniform film dotted with small "high spots" representing the locations from which the cells were detached. Thus, the microexudate can be divided into two surface regions; a subcellular one and an intercellular one of varying molecular concentrations. If the density of cells on the surface is small such that the mean intercellular distance is greater than four or five cell diameters, it is possible to measure the *average* thickness of the intercellular microexudate; with greater densities of cells, the measured thickness is an *average* of that of the subcellular and intercellular microexudates. This instrumental averaging must be taken into account in evaluating the measurements discussed in the next section.

Besides the above instrumental limitation, one must also be mindful that the culture medium may modify the surface that is examined for the presence of molecular material. The common growth media for the *in vitro* culture of cells usually contain components of serum or other large molecules which readily adsorb to surfaces. Thus, the medium itself may rapidly alter the substratum for the cells, and it is likely that in many situations the cell surface might be similarly modified as a result of adsorption. These alterations of the substratum are measurable with the ellipsometer, but make the detection of microexudates from cells far more difficult and ambiguous. To prevent this difficulty and to obtain reproducible and meaningful measurements, it was necessary to use for relatively short periods a synthetic culture medium containing no adsorbable molecules, namely, Eagle's medium.

The cells used in the experiments described below, namely, fresh embryonic chick skin and retina, and tissue culture strains of rat kidney, human epidermoid carcinoma, and human conjunctiva, during the experimental time interval (4 hrs.) exhibited in Eagle's medium none of the morphological changes associated with cellular degeneration such as withdrawal of processes, increased refractiveness of granules and nucleoli, vacuolization, or pyknosis of nuclei. Except for chick retina, the cells showed good attachment, spreading, and process formation on glass surfaces.

In addition, the human conjunctiva cells (grown in our laboratory for the past 2 years) could be maintained and subcultured in Eagle's medium for several days with excellent spreading and process formation on glass surfaces but little, if any, multiplication. Moreover, if these cells were then transferred to a standard growth medium (Eagle's mixture supplemented with 10 per cent calf serum), they again resumed proliferation. For these reasons, human conjunctiva cells in Eagle's medium were used for the longer time intervals (up to 29 hrs.).

The methods used to detach or dissociate these cells (see section on methods) can result in certain morphological changes. Under phase microscopy the surfaces of trypsin-treated cells can be seen to have both fine and coarse corrugations whereas the surfaces of cells treated with versene (as described above) appear considerably smoother. In addition, the versene-treated cells appear to spread more rapidly, although no actual quantitative tests have been carried out to verify this impression.

Cells in Eagle's medium allowed to attach and spread on a clean glass surface can no longer be detached by digestion of protein with trypsin or removal of the cations, magnesium and calcium, with versene, although the application of trypsin often results in the withdrawal of processes. On the other hand, if either the cells or the substratum are first washed with a 1 per cent solution of bovine gamma globulin or horse serum so as to form an adsorbed molecular film on the surface of the cell or the glass, and the cells are then resuspended in Eagle's medium and allowed to spread, they become detachable with either trypsin or versene treatment. The relationship between this observation and the presence of a microexudate is obscure, although the experiments to be described suggest certain explanations.

B. *Measurements*

1. *Time Course of the Deposition of Microexudates.* As exemplified in Fig. 1, the average thickness of microexudate increases as a function of time, the time course varying for different types of cells. The cells had previously been detached or dissociated with trypsin (see methods section), and then suspended in Eagle's medium. Since each cell type differs in its mean diameter and mean cross-sectional area, the CPSD was selected so that the RCS is roughly equal for all curves. For this figure an approximate value of 5 per cent was chosen; a value at which the cells are sufficiently distant (roughly four cell diameters) from one another, prior to spreading upon the chromed surface, for ellipsometer measurements to include essentially intercellular regions. Thus, the initial rapid rise in average thickness most likely results from an accumulation of molecules intercellularly rather than a change in dimensions, orientation, configuration, or stacking of molecules. The mean diameters of the cell types in Fig. 1 are as follows: embryonic skin (curve A), 10 microns; human conjunctiva (curve B), 14 microns; human epidermoid carcinoma (curve C), 15 microns; embryonic chick retina (curve D), 7 microns. It has been possible to reproduce curve B for human conjunctiva cells on three separate occasions with an accuracy of ± 2 A. The other curves have not been

studied for reproducibility. It is difficult to assess accurately the detailed differences between these curves, that is, whether the time course of the deposition of microexudate of a given cell type or strain is specific for that particular material. An appraisal of specificity must await the results of more detailed studies currently in progress. However, a major point of interest is that the cells upon contact with the indicated substratum very rapidly produce material of molecular dimensions. The time curve for this intercellular material has a high initial slope, and the rate of increase of its average thickness then decreases with time, the maximum rate of change of curvature occurring at 1 to 2 hrs.

If the RCS is markedly increased such that the ellipsometer measurement then averages the thicknesses of both the subcellular and intercellular microexudates, an interesting, as yet unexplained, phenomenon results. This is illustrated in Fig. 2, where the RCS is roughly greater than 15 per cent (intercellular distance approximately two cell diameters), and the cell types and their mean diameters are: embryonic chick skin (curve A), 10 microns; rat kidney (curve B), 14 microns; embryonic chick retina (curve C), 7 microns. These time curves show an initial peak followed by a temporary dip. Although the spreading and interactions of cells in the case of high surface concentrations, may lead to considerable modifications in the microexudate, these factors, in themselves, have not as yet been adequate to explain the bizarre configuration of these curves.

TABLE I

ADSORBABLE MATERIAL IN SUPERNATANT OF HUMAN CONJUNCTIVA CELLS

Time (hours)	0.25	0.5	1.0	2.0	3.0	4.0	5.0	20.0	23.0	25.5	29.0
Average thickness (angstroms)*	4 5	4 5 1	4 5 1	4 6	4 4 1	3 4	2 2	0	2	6	1

* Multiple determinations.

Finally, curve E of Fig. 1 and curve D of Fig. 2 illustrate control readings, obtained when cell-free Eagle's medium is allowed to remain on the test slide for designated periods of time. The small variations are less than 3 A and demonstrate how errors due to contaminants in the atmosphere or in the medium may be minimized if great care is taken. In addition, as described in the methods section, the medium supernatant to the cells was studied for the presence of adsorbable molecules. The results of this study, illustrated in Table I, indicate that the adsorbate so obtained is essentially negligible.

2. *Microexudates in Different Culture Media.* With certain alterations in the culture medium the time curve of average microexudate thickness undergoes the changes illustrated in Fig. 3. If Eagle's medium is supplemented with horse serum, the large serum molecules are very rapidly adsorbed to the substratum, forming a layer roughly 23 A thick. This alteration of the cellular substratum will occur when-

ever adsorbable molecules are present in the medium, and there are good indications, presented in a later section, that these molecules adsorb to and thus modify also the surface of the cell. The problem then arises as to whether a microexudate can still be detected as an overlay on the adsorbed layer.

Curve B of Fig. 3 is the typical time curve for trypsinized human conjunctiva cells cultured in Eagle's medium (375 cells/mm^2). If the same cell strain after trypsin treatment is cultured in Eagle's medium supplemented with 5 per cent horse serum (370 cells/mm^2), curve A results. The almost instantaneous adsorbate, 23 A in thickness, pictures the adsorption of molecules from the medium, but above this layer there seems to be a gradual overlay of material, possibly of microexudate. In any case, the appearance of microexudate as a result of cellular contact with the modified substratum is markedly retarded.

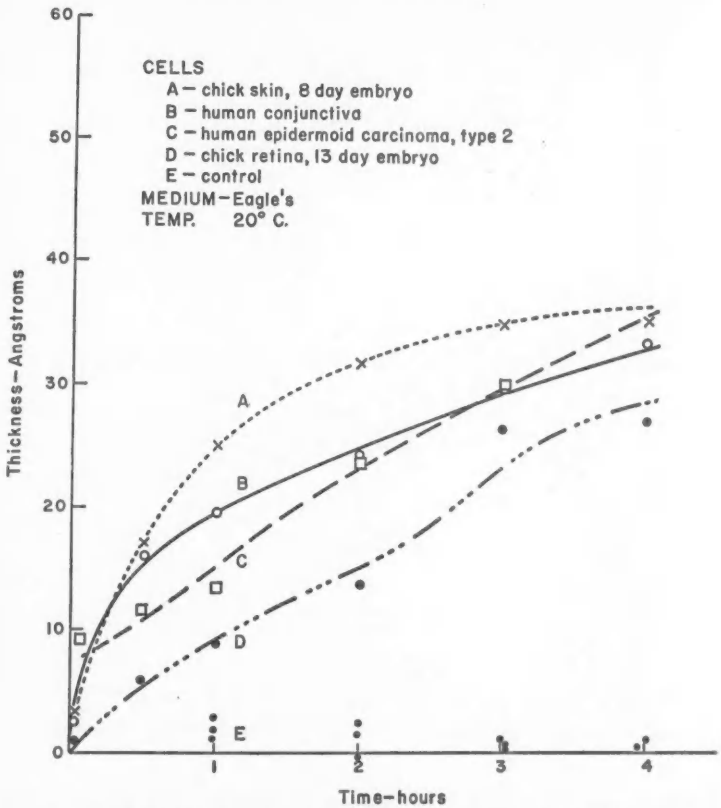

FIGURE 1 Average thickness of microexudate (in angstroms) as a function of time for various cell strains. (Low concentration of cells.)

Curve C depicts, on the other hand, microexudate production when the same strain of cells is cultured in Eagle's medium supplemented with 5 per cent bovine ultrafiltrate. This ultrafiltrate consists of small nonadsorbable molecules; that is, if a cell-free sample of the ultrafiltrate is allowed to remain on a test slide for a 15-min. period and is then washed off, no change in the surface of the slide can be detected by means of ellipsometry. For both curve B and curve C, the cells contact the same substratum, but it is not possible to determine whether the slight differences in configuration of the curves are in response to the changes in the culture medium. Far more elaborate studies are required. However, the striking decrease in microexudate that occurs when serum in the medium adsorbs to surfaces led to a study of the effects of controlled substrata.

3. *Formation of Microexudates on Different Substrata.* Several tech-

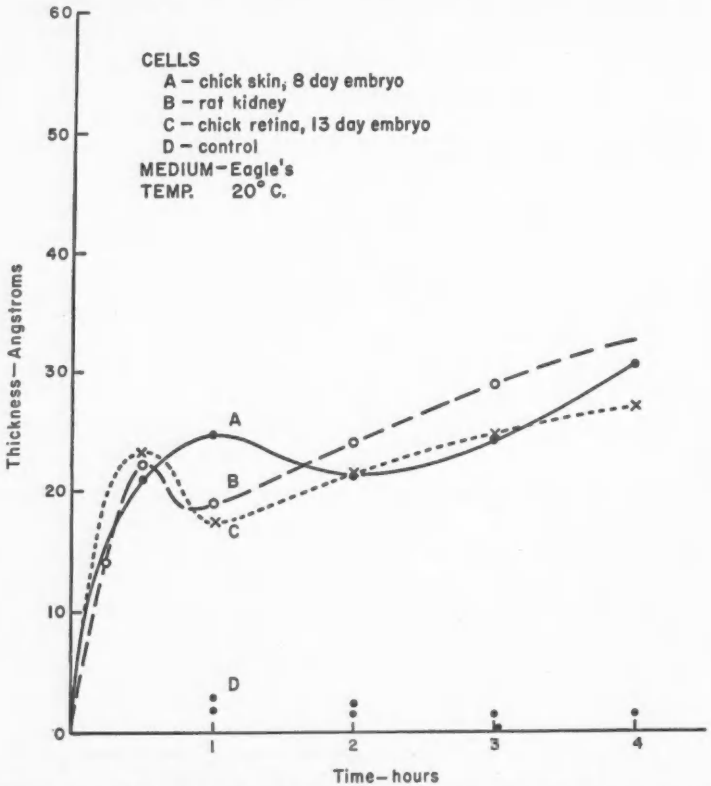

FIGURE 2 Average thickness of microexudate (in angstroms) as a function of time for various cell strains. (High concentration of cells.)

niques are commonly used in the field of surface chemistry to prepare thin films of known molecular structure and thickness. One technique is to adsorb molecules directly to surfaces; another is to use a Langmuir trough, containing a buffered solution upon whose surface is placed a small amount of the material to be studied. Many materials form a monomolecular film on the surface of the buffer, and by application of lateral pressure along the surface, the monomolecular film can be transferred to clean surfaces. By means of repeated transfers, a transferred film can be prepared with a thickness varying from one to several thousand molecular layers. For a review of these techniques, see Rothen (1956).

Such adsorbed or transferred films can then serve as specific substrata of known molecular structure, thickness, and orientation for the study of surface reactions of cells. The presence and average thickness of the films prior to the additions of

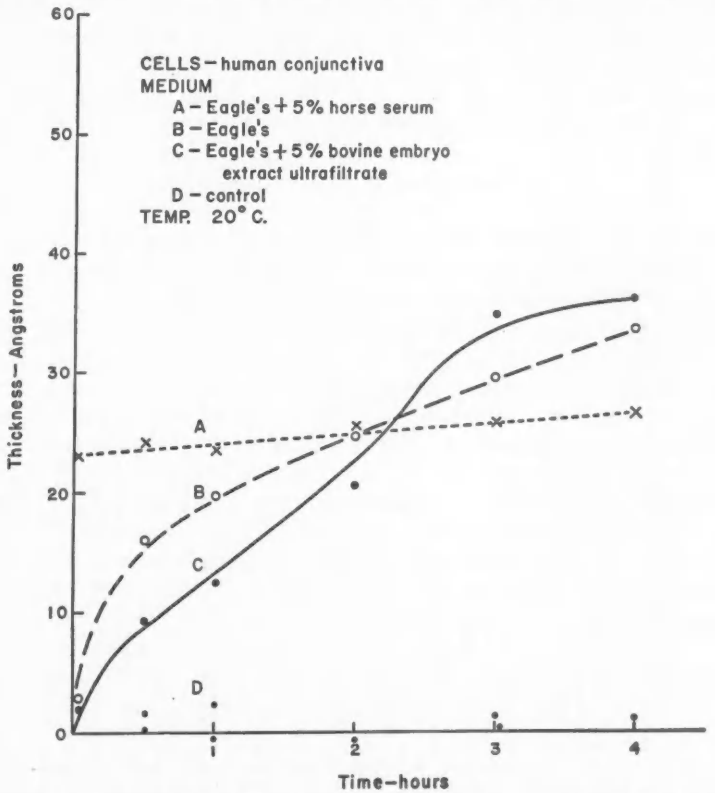

FIGURE 3 Average thickness of microexudate (in angstroms) as a function of time for various growth media.

cells and medium can be readily ascertained with the ellipsometer. Any subsequent changes in average thickness after the addition of cells are then attributable to cellular effects. Fig. 4 portrays the changes in average thickness when human conjunctiva cells, detached from tissue culture flasks by trypsin, are allowed to grow in Eagle's medium on specified substrata for 2 hours and then removed.

The average thicknesses of transferred and adsorbed monolayers are given in the lower portion of the figure with glass as the reference substratum. The second-

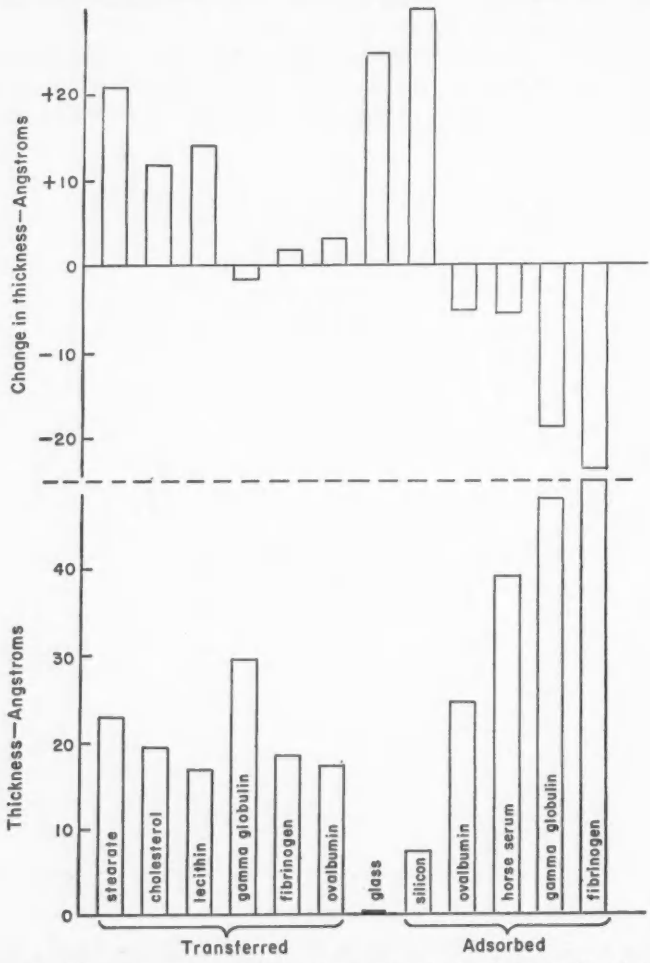

FIGURE 4 Change in average thickness (in angstroms) of various transferred or adsorbed substrates after growth of trypsin-dissociated cells for 2 hrs.

ary changes in average thickness after the addition of cells are given in the upper portion of the figure. After 2 hrs. the cells have deposited on the hydrophilic glass the previously described microexudate, of an average thickness of 24 A. A similar deposit has occurred on the hydrophobic adsorbed layer of organic silicone. On transferred monolayers of stearate, cholesterol, and lecithin there is an increase in average thickness apparently attributable to microexudate, the magnitude of the change being somewhat less on transferred lecithin and cholesterol. However, transferred films of bovine gamma globulin, fibrinogen, and ovalbumin underwent no changes in average thickness, and this indicates that no significant amounts of microexudate had been deposited by the cells on these substrata. Finally, when the cells were grown on adsorbed protein layers of bovine gamma globulin and fibrinogen, the average thickness of the substratum underwent significant reduction.

These experimental results show that the appearance and mean thickness of the microexudate is signally dependent upon the molecular constitution of the substratum on which the cell rests, and that trypsin-treated cells are capable of reducing adsorbed protein films by substantial amounts. In addition, these observations suggest that the production and deposition of the microexudate could be a function of a selective and competitive attraction for the microexudate by the cell and the substratum, and that trypsin-treated cells retain trypsin activity.

Let us consider the latter suggestion. Northrop (1926) demonstrated that there is no uptake of trypsin by the cytoplasm of live cells. Rothen (1948) has shown that protein films, acted upon by trypsin, continue to exhibit trypsin activity even after transfer of the film. It, therefore, appears reasonable to assume that the cell retains trypsin activity as a result of adsorption of trypsin to its surface. This assumption can be tested experimentally. One would expect versene-treated cells or cells whose adsorbed trypsin has been inactivated to cause little, if any, reduction in the average thickness of an underlying adsorbed film of protein. In addition, if microexudate includes some protein components, the average thickness of material produced by trypsin-treated cells should be less than that available from versene-treated cells. The experiments described in the next section verify these predictions.

4. *Microexudate and Cell Treatment.* The adsorption to a chromed glass surface of trypsin, in contrast to versene, can be demonstrated by means of the ellipsometer. When solutions of versene or trypsin were placed upon the cleaned surface and removed after 15 min. the results tabulated in Table II were obtained. Thus trypsin is adsorbed, whereas versene is not.

By the methods described in section 3, one can investigate the interaction between trypsin- or versene-treated cells and known substrata. Trypsin-treated or versene-treated cells were cultured for 2 hrs. in Eagle's medium on controlled substrata of adsorbed layers of serum or protein. In addition, some trypsin-treated cells were washed with a 10 per cent solution of calf serum to inhibit or inactivate the trypsin on the surface of the cell, and the cells were then suspended in Eagle's medium. The striking results are detailed in Fig. 5. Three primary adsorbed films were

examined, namely, calf serum, fibrinogen, and bovine gamma globulin. The average thickness of the adsorbed films is shown in the lower portion of the figure; the secondary changes in average thickness after the addition of cells are shown in the upper portion. The results of control readings on a glass surface, consistent with previously described measurements, are shown on the far right.

This figure clearly illustrates that the presence of trypsin-treated cells has led to digestion of the underlying protein, whereas the presence of cells coated with a trypsin inhibitor or versene-treated cells have had no effect. In fact, the amount of

TABLE II

ADSORPTION OF TRYPSIN OR VERSENE TO GLASS

Material	Average thickness of adsorbed layer (angstroms)*
Trypsin	6
	7
Versene	0
	0

* Multiple determinations.

reduction in average thickness is comparable to the amount of material removed when 0.05 per cent trypsin at pH 7.6 is applied directly to an adsorbed film for 15 min. at 37°C (see Table III). These data substantiate the proposition that trypsin molecules are adsorbed to the surface of cells, continue to be enzymatically active at that site, and suggest that trypsin then creeps over the substratum.

A corollary to this finding is that if microexudate is in part composed of protein, the time curves for its average thickness should vary with the method of prior cellular treatment. This variation is detailed in Fig. 6, which shows that, as a function of time, molecular material of greater average thickness is deposited by versene-treated cells. It appears that the reduced average thickness of the microexudate

TABLE III

CHANGE IN AVERAGE THICKNESS OF ADSORBED LAYERS AS A RESULT OF TRYPSIN ACTION

Molecular film	Average thickness of film (angstroms)*	Change in average thickness after trypsin (angstroms)*
Calf serum	21	−6
	19	−4
Fibrinogen	48	−20
	46	−18
Bovine gamma globulin	77	−26

* Multiple determinations.

produced by the trypsin-treated cells is a consequence of the digestion of protein components by adsorbed trypsin.

DISCUSSION

The techniques described above clearly demonstrate how the interactions between cell, substratum, and medium, as well as the adsorption of enzymes to cell surfaces can be studied quantitatively. The data, so obtained, support the following conclusions:

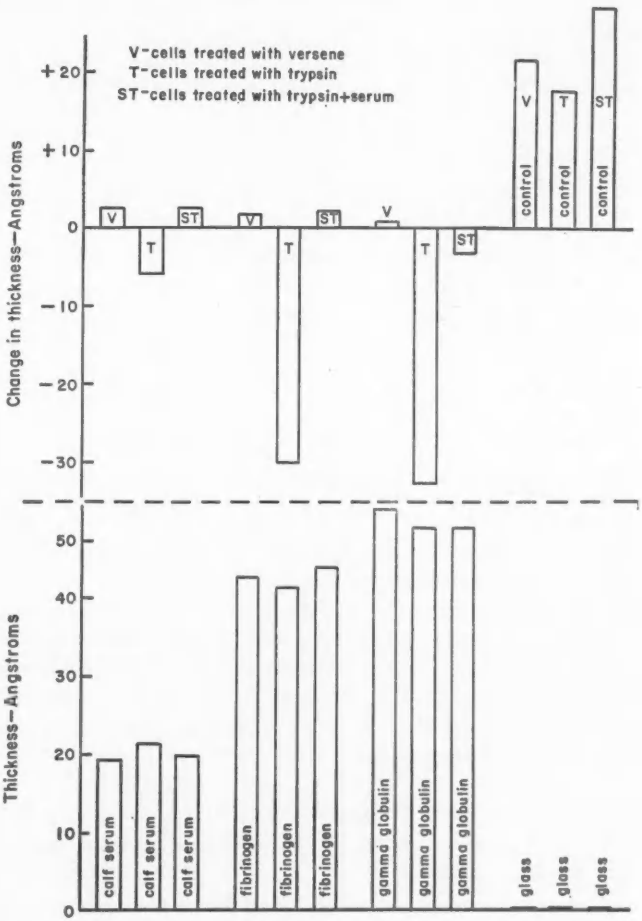

FIGURE 5 Change in average thickness (in angstroms) of various adsorbed substrates after growth of trypsin-, versene-, or trypsin-serum-dissociated cells for 2 hrs.

1. Cells can produce a microexudate or a film of molecular dimensions that coats and modifies their substratum (Figs. 1, 2).
2. The culture medium, through adsorbable components, alters both the surface and substratum of cells (Fig. 3).
3. Changes in substratum affect the deposition of microexudate, possibly as a result of the selective attractions of the substratum and cell surface for this material (Figs. 3, 4).
4. Trypsin becomes adsorbed to the surface of cells, continues to be enzymatically active on the surface, and leads to changes in the microexudate (Figs. 5, 6; Table II).

Although these results point out the significant and complex role played by molecular mechanisms when cells are maintained in tissue culture, they leave many

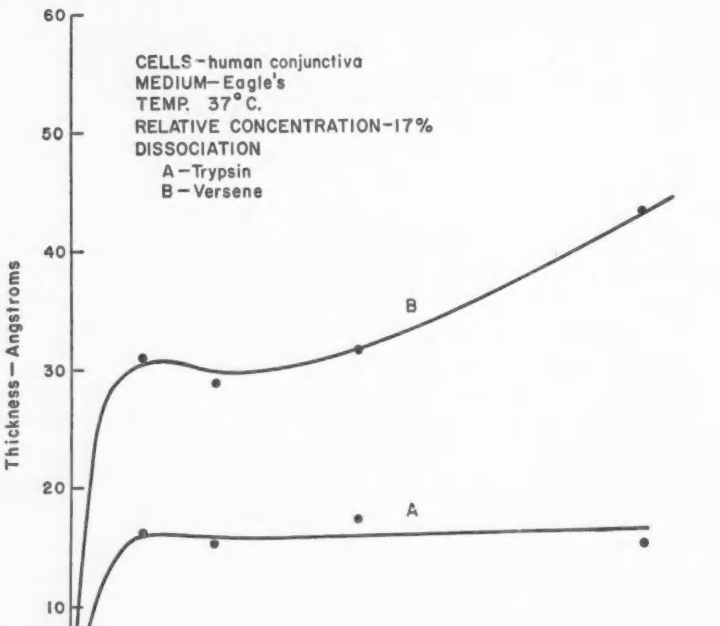

FIGURE 6 Average thickness of microexudate (in angstroms) as a function of time for trypsin- and versene-dissociated cells.

important questions unanswered. Information regarding the specificity, source, role in cellular behavior, or composition of this microexudate or molecular film is incomplete and inconclusive. For the moment several of these questions will have to remain unanswered. However, experiments have been completed which render some speculations regarding the composition and source of this material more probable than others. These results are discussed in part II below.

RESULTS—PART II

A. *Measurements*

1. *Some Chemical Characteristics of Microexudate.* (*a*) *Enzymatic tests.* Fig. 6 has shown that less molecular material is produced by trypsin-treated cells in contrast to versene-treated cells. The conclusion reached in part I has been that trypsin is adsorbed to the surface of cells and digests some protein components of microexudate. A supplementary experiment to demonstrate the presence of protein in microexudate is summarized in Table IV. The tabulated data establish that

TABLE IV

CHANGE IN AVERAGE THICKNESS OF MICROEXUDATE AS A RESULT OF TRYPSIN ACTION

Cells	Average thickness of microexudate (angstroms)*	Change after trypsin (angstroms)*
Trypsin-treated	27	1
	28	1
Versene-treated	44	−14
	49	−15

* Multiple determinations.

trypsin (0.05 per cent, pH 7.6) can lead to a reduction in average thickness of microexudate from versene-treated cells, but none in that from trypsin-treated cells. In fact, the effect of trypsin is to reduce the average thickness to a level similar to that obtained with trypsin-treated cells. Thus, the action of trypsin in digesting some protein components of microexudate is apparently similar whether the enzyme is adsorbed to the cellular surface or applied directly to the microexudate.

On the other hand, applications of solutions (0.05 per cent) of the enzymes lipase and hyaluronidase at 37°C, pH 7.4, led to no significant change in average thickness of the molecular material.

(*b*) *Tests by acids and bases.* The average thickness of material composing the microexudate remains essentially unaltered by the action of 0.01 N to 1.0 N HCl, NaOH, and $NaHCO_3$ at 23°C for 45 min. 1 N NaOH or HCl at 100°C readily removes a major portion of material in 15 min.

(*c*) *Isolation if microexudate.* In view of the action of strong acids and bases at 100°C, an effort was made to hydrolyze some components of the material. Human

conjunctiva cells were grown for 4 hrs. in Eagle's medium on 150 clean glass slides, and after removal of the cells, the glass was washed and subjected to the hydrolytic action of 1 N HCl at 100°C. The hydrolysate was then evaporated to dryness, and both water and chloroform-methanol-soluble fractions of the residue were chromatographed. In general the results of these experiments were poor. Some amino acids and lipid material were detected, but it was not possible to maintain fully satisfactory controls. More effective experiments are now underway, and perhaps the sole conclusion to be drawn at present is that the microexudate is most likely a complex molecular mosaic that includes protein.

2. *Dependence of Microexudate upon Other Physical Variables.* The determination of sources for the microexudate poses several problems. The deposition may result from a stripping off of a molecular coat from the cell surface or may consist of cellular secretions, excretions, cell debris, or cytoplasmic fragments; extracellular synthesis may also be involved. Because of the difficulty of isolating each of these possible sources, it was decided to measure the average thickness of microexudate deposited during longer time intervals, and to determine its functional dependence on additional physical variables such as CPSD and temperature. It was hoped that these studies together with the aforementioned data would provide indications of the source of the molecular deposit. The results of these tests are presented in the subsequent paragraphs.

(*a*) *Time course of the deposition of microexudate.* The average thickness of molecular material deposited on test slides by human conjunctiva cells in either pure Eagle's medium or in Eagle's medium supplemented with 10 per cent calf serum is tabulated in Table V (for the latter medium, the number of angstroms in excess of the 20 A adsorbed layer of calf serum is given). As noted in the section on observations, part I, these cells have been maintained successfully in Eagle's medium for periods in excess of 29 hrs.

In a standard growth medium (row 3) the over-all measurement was only slightly greater than the average thickness of an adsorbed layer of calf serum in the

TABLE V

AVERAGE THICKNESS OF MICROEXUDATE *VERSUS* TIME (HUMAN CONJUNCTIVA CELLS; TEMPERATURE 37°C; VERSENE TREATMENT; RELATIVE CELLULAR CROSS SECTION 20 PER CENT)

Time (hours)	0.5	1.0	2.0	3.0	4.0
Average thickness in Eagle's medium (angstroms)*	25 24 20	31 27 29	—	40 37 37	—
Average thickness in Eagle's medium supplemented with 10 per cent calf serum (angstroms)*	6 7	10 10	4 6	9 11	8 8

* Multiple determinations.

TABLE VI

AVERAGE THICKNESS OF MICROEXUDATE *VERSUS* RELATIVE CELLULAR CROSS SECTION (HUMAN CONJUNCTIVA CELLS; TEMPERATURE 37°C; VERSENE TREATMENT; GROWTH PERIOD 29 HRS.)

Relative cellular cross section (per cent)	0	0.25	0.5	1	4	11	19	47
Average thickness (angstroms)*	1	5	15	23	51	54	58	73
	0	7	15	23	54	61	67	81

* Multiple determinations.

absence of cells. In contrast, cells in pure Eagle's medium apparently yield the microexudate almost immediately upon contact with the clean glass surface, and the maximum average thickness of the film is reached in 1 to 3 hrs.

(*b*) *Microexudates at various relative cellular cross sections* (*RCS*). The functional dependence of the average thickness of microexudate upon the RCS is of interest in that the surface coverage by the deposited material seems to be complete even when intercellular distances are considerable. Table VI presents data to substantiate this statement.

At fairly low values of RCS (5 to 10 per cent), when the intercellular distance is approximately three to four cell diameters, the average thickness is close to its peak. At these concentrations the measured average thickness (see observations, part I) is that of the film of intercellular material. With increasing concentration, the subcellular area increases, and the fact that the readings represent instrumental averages of both subcellular and intercellular material is no longer negligible. For the highest concentration tabulated, the spread cells cover essentially the entire surface of the test slide, so that the average thickness is that of subcellular material. Prior to speculating on the significance of these results, some additional experiments are considered.

(*c*) *Microexudate versus temperature.* Fig. 7 illustrates how the average microexudate thickness varies with temperature. Only a slight increase with increasing temperature indicates that the rate of deposition of this material is not a function of cellular metabolic activity.

TABLE V—*concluded*

6.0	20.0	23.0	25.0	29.0	45.0	53.0	69.0	77.0
—	39	47	53	47	—	—	—	—
	42	51	56	47				
	41							
4	11	5	—	8	11	5	7	13
6	9	11		8	8	6	9	15

(*d*) *Adsorbable material in supernatants.* Table I, in an earlier section of this paper, contains data showing that Eagle's medium, supernatant to human conjunctiva cells spread upon test slides, contains few, if any, adsorbable molecules. It is presumed that if adsorbable molecules are given off by cells, they are in sufficiently small quantity so as to be present only on surfaces, rather than in the bulk of the medium. The results of an additional experiment, supporting this contention, are presented in Table VII. Human conjunctiva cells were maintained in suspension

TABLE VII

AVERAGE THICKNESS OF MOLECULAR LAYER ABSORBED FROM EAGLE'S MEDIUM USED FOR ROLLER TUBE CULTURE (HUMAN CONJUNCTIVA CELLS; TEMPERATURE 37°C; VERSENE-TREATED)

Time in roller tube (hours)	2	26	2†
Average thickness	5	8	3
(angstroms)*	3	7	4
	3	9	4

* Multiple determinations.
† High concentration of cells.

in Eagle's medium in roller tube cultures. The total cross-sectional area of cells in suspension was far in excess of the total surface area of glass in contact with the suspension. At designated periods, aliquots were centrifuged, and the supernatant tested for the presence of adsorbable molecular material. Few, if any, molecules were adsorbed from the supernant medium unless the cells had been in the roller tube for at least 26 hrs. The small amount of adsorbable material after 26 hrs. is possibly a result of cellular damage due to agitation.

The question that must now be examined is whether the foregoing empirical results weave a consistent pattern suggestive of the source and composition of microexudate. The following discussion concentrates on this question.

DISCUSSION

As noted above, the microexudate is most likely a complex mosaic of molecules (including protein) which is synthesized within or on the surface of cells and secreted or transferred such that it can be detected as a molecular film on the cellular substratum. The most likely sources for this material are cellular secretions or the transfer of molecules from the cellular surface to the surface upon which the cell rests. Both of these hypotheses are supported in varying degrees by the experiments described above and analyzed in the following summary.

1. The microexudate appears only if cells contact certain kinds of substrata, such as clean glass, silicone, or transferred stearate films. Little if any material is given off when cells rest upon transferred or adsorbed films of protein or

serum (Figs. 4, 5). The selective attraction of various substrata, therefore, appears to play an important role in the spreading of this material.

2. One would expect secreted or transferred material to appear rapidly beneath the cell and to diffuse gradually outward from the cell. In fact, an approximate calculation based upon an RCS of 10 per cent (intercellular distance of approximately three cell diameters) and a diffusion coefficient of 10^{-7} cm^2/sec. leads to the prediction that the molecular fabric of the microexudate should rapidly spread intercellularly during the first 15 min. (This estimate is based solely upon physical adsorption; no chemadsorption is assumed.) The results of this calculation are certainly of the correct order of magnitude and partly in agreement with the data illustrated in Figs. 1 and 2 and Table V, although for high concentrations of cells the initial rate of microexudate appearance is not as rapid as might be expected.

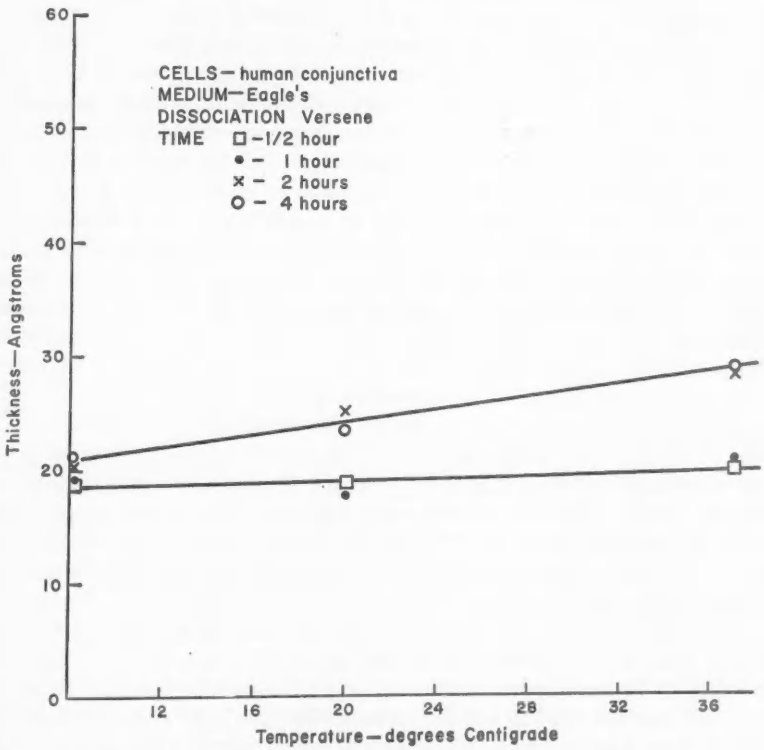

FIGURE 7 Average thickness of microexudate (in angstroms) as a function of temperature.

3. The maximum average thickness of intercellular microexudate is attained already at low values of the RCS (Table VI). Assuming a maximum film thickness of 40 A and assuming further that at the equilibrium point 30 to 40 per cent of the intercellular region has been covered with a molecular fabric, the cells would have had to give off only 0.2 to 0.6 per cent of their total weight to cover this area. This amount of material is in no way excessive and is consonant with the hypothesis that microexudate results from cellular secretion. Similarly, inasmuch as the surface area of a spherical cell is four times its cross-sectional area, a sufficient number of molecules could be transferred from the surface of the cell to bring about reasonable coverage of the intercellular spaces. Thus, the hypothesis of displacement or transfer of molecules from the surface of the cell is also in accord with these data.
4. The supernatants of attached or suspended human conjunctiva cells contain very little adsorbable material (Table I, VII). One would not expect molecular transfer from surfaces of cells to be followed by the appearance of adsorbable molecules in the medium. On the other hand, cellular secretions are more likely to add adsorbable material to the suspending medium, unless the quantity of secreted material is so minimal as to be completely adsorbed.
5. Both molecular transfer between surfaces and the physical liberation of secretions could be relatively independent of temperature, consistent with the data diagrammed in Fig. 7.

In summary, the experiments performed up to now suggest two possible sources for the molecular fabric that comprises the microexudate. Either molecules normally present on cellular surfaces as a result of adsorption, secretion, or synthesis are transferred to the substrate; or the material is directly secreted by the cell onto the substratum. The relative shares of these two sources in the total deposits cannot be assessed pending the development of additional experimental techniques.

GENERAL DISCUSSION

The experiments described in this report show that cells upon contact with a surface can deposit a complex molecular carpet on surfaces that have strong attractive forces for this material. It appears likely that this molecular film or microexudate of cellular origin consists of a combination of cellular secretions and molecules transferred from the surfaces of the cells.

In view of the predominant function of cellular secretions in tissue repair, wound healing, and cell growth and development, one would expect secretory products to contribute to the composition of microexudate. On the other hand, the likelihood that molecules adsorbed to cellular surfaces also contribute to the formation of microexudate is an unexpected yet highly significant outcome from these investigations. If microexudate is composed, in part, of molecules whose prior region of activity was the cell surface, a determination of its physical and chemical properties

should reveal significant information about the surfaces of cells, regions of poor accessibility. It then may be possible to quantitate chemically and immunologically the complex problem of specificity with respect to cell surfaces.

The suggestion has been made often that protein is adsorbed to the lipoid components of the cell membrane. Danielli (1958) contended that in addition to a primary adsorbed denatured monomolecular layer of protein, there is an overlying secondary layer of globular native protein. Weiss (1960) recently proposed that the cell surface is occupied by a network of filiform macromolecules in essentially planar array. Allison and Valentine (1960) have shown that virus particles adsorb to cell surfaces at a rate that is less than expected on the basis of Brownian collisions. The investigations described in this paper show how one protein, trypsin, is adsorbed to the surface of cells and remains enzymatically active on the surface. One exception seems to be the surface of erythrocytes which possess envelopes unlike tissue-cultured cells. According to Abramson, Moyer, and Gorin (1942), erythrocytes do not appear to adsorb protein, a property which may be necessary for their biological survival in the circulatory system (see Bangham, Pethica, and Seaman (1958)). It appears very likely, however, that the surfaces of most cells have configurations and charge distributions such that molecular adsorption can take place. The investigations described in this paper reemphasize the significance of these adsorbed materials, and suggest for the first time that these molecules actively participate in the formation of molecular films, termed microexudates, on cellular substrata.

In evaluating possible roles for this microexudate, one must view it as both a possible representative of molecular substances previously adsorbed to cell surfaces, and as a molecular film that can modify surfaces in contact with the cells. The effects of molecular adsorption to cell membranes on the chemical and physical properties of the surface are obscure. Bangham, Pethica, and Seaman (1958) discussed the functional relationship between electrophoretic mobility and the charged group at the interfaces of some blood cells. Schmitt (1941) proposed that an adhesive lining mediates cell-to-cell interactions. Weiss (1941, 1950) described the selective surface stickiness ("fasciculation") appearing in pioneering nerve fibers after making peripheral connections. The investigations on microexudate indicate that adsorbed materials can be involved in cell-to-cell interactions and cell contacts. The further study of microexudate as a specimen of materials previously adsorbed to cellular surfaces, as well as additional studies on the interactions between cell and microexudate may help clarify some aspects of the complex phenomena of cell contact.

In addition, microexudate can result in alterations of the cellular substratum. In this capacity it may act as an ultrafine "ground mat," several orders of magnitude smaller than the colloidal exudate described by Weiss (1945) and discussed in the introduction to this report. This molecular carpet could then directly influence cell locomotion, adhesion to surfaces, and the selective application and spreading of cells on various surfaces. Some recent data of Taylor (1960) on the attachment and

spreading of cells partly corroborate this assumption. Crisp and Ryland (1960) have shown how films affect the settlement of marine organisms, and Zvyegintsev (1959) has considered their influence on the adsorption of microorganisms. It seems, therefore, that molecular films or microexudates can assume the role of a ubiquitous mediator of interactions on the molecular level.

Several investigators (Steinberg (1958), Lieberman and Ove (1958)) have proposed that a surface protein and polyvalent cation are intimately related to the processes of attachment and flattening of cells on surfaces. Lieberman and Ove (1958) also suggested that attachment with basic peptides does not appear to involve a polyvalent cation, since such bonds can be released with trypsin but not with versene. The bridge of microexudate, however, between the cell and glass differs in that it is resistant to both trypsin and versene, even though microexudate contains some trypsin-digestible components. Thus, it appears that microexudate could act as an ionic bridge, or what is more likely, that the bonding mechanism involves London-van der Waals forces (see Curtis (1960)) or modifications of these forces described by Yos, Bade, Jehle (1957), Lifshitz (1955), Derjaguin, Abrikossova, Lifshitz (1956), and Overbeek (1952).

Undoubtedly several mechanisms are at play on the molecular level. Steinberg (1958), Weiss (1958), and Curtis (1960) have reviewed many of them, such as the steric interactions of complementary sites, short-range electrostatic forces, calcium bonding, intercellular bridges, long-range London-van der Waals forces, mechanical linkages of surface microfibrils, and some specific cellular exudates. The experiments described in this report are limited to the study of molecular materials produced by cells contacting specified surfaces. Major questions regarding the chemical characteristics of microexudate, its role in biological systems, its specificity and structure are left open and await clarification. These investigations, however, exemplify and establish the usefulness of surface chemistry techniques in studying these questions. It is hoped that answers can be provided by further research to supplant any premature formulations.

The author is indebted to Dr. Alexander Rothen for helpful discussions and the loan of equipment used to measure molecular films. He is exceedingly grateful to Mrs. Sybil Bush for her technical assistance in executing the above experiments.

This research is part of a program supported by grants from the American Cancer Society and the National Institutes of Health (United States Public Health Service) to Dr. Paul Weiss as Principal Investigator.

Received for publication, August 11, 1960.

REFERENCES

1. ABRAMSON, H. A., MOYER, L. S., and GORIN, M. H., *in* Electrophoresis of Proteins, New York, Reinhold Publishing Corp., 1942.
2. ALLISON, A. C., and VALENTINE, R. C., *Biochim. et Biophysica Acta*, 1960, **40**, 393.
3. BANGHAM, A. D., PETHICA, B. A., and SEAMAN, G. V. F., *Biochem. J.*, 1958, **69**, 12.
4. CRISP, D. J., and RYLAND, J. S., *Nature*, 1960, **185**, 119.
5. CURTIS, A. S. G., *Am. Naturalist*, 1960, **94**, 37.
6. DANIELLI, J. F., *in* Surface Phenomena in Chemistry and Biology, New York, Pergamon Press, 1958, 246.
7. DERJAGUIN, B. V., ABRIKOSSOVA, I. I., and LIFSHITZ, E. M., *Quarterly Revs.*, 1956, **10**, 295.
8. EAGLE, H., *Science*, 1955, **122**, 501.
9. LIEBERMAN, I., and OVE, P., *J. Biol. Chem.*, 1958, **233**, 637.
10. LIFSHITZ, E. M., *J. Exp. and Theoret. Physics*, 1955, **1**, 94.
11. NORTHROP, J. H., *J. Gen. Physiol.*, 1926, **9**, 497.
12. OVERBEEK, J., Th.G., *in* Colloid Science, (H. R. KRUYT, editor), Amsterdam, Elsevier, 1952.
13. ROSENBERG, M. D., *Abstracts, 4th Ann. Meeting, Biophysic. Soc.*, 1960.
14. ROTHEN, A., *Rev. Sc. Instr.*, 1945, **16**, 26.
15. ROTHEN, A., *J. Am. Chem. Soc.*, 1948, **70**, 2732.
16. ROTHEN, A., *in* Physical Techniques in Biological Research, (G. OSTER, and A. W. POLLISTER, editors), New York, Academic Press, 1956, 156.
17. SCHMITT, F. O., *3rd Growth Symp.*, 1941, **5**, 1.
18. STEINBERG, M. S., *Am. Naturalist*, 1958, **92**, 65.
19. TAYLOR, A. C., *Abstracts, 4th Ann. Meeting, Biophysic. Soc.*. 1960.
20. WEISS, P., *3rd Growth Symp.*, 1941, **5**, 163.
21. WEISS, P., *J. Exp. Zool.*, 1945, **100**, 353.
22. WEISS, P., *J. Exp. Zool.*, 1950, **113**, 397.
23. WEISS, P., *Internat. Rev. Cytol.*, 1958, **7**, 391.
24. WEISS, P., *Proc. Nat. Acad. Sc.*, 1960, **46**, 993.
25. YOS, J. M., BADE, W. L., and JEHLE, H., *in* Molecular Structure and Biological Specificity, *Am. Inst. Biol. Sc.*, publication No. 2, 1957.
26. ZVYEGINTSEV, D. G., *Mikrobiologiya*, 1959, **28** (1), 104.

ANALYSIS OF CERTAIN ERRORS IN SQUID AXON VOLTAGE CLAMP MEASUREMENTS

ROBERT E. TAYLOR, JOHN W. MOORE, *and* KENNETH S. COLE
From the National Institutes of Health, Bethesda

ABSTRACT Localized membrane current and potential measurements were made on the squid giant axon in voltage clamp experiments. Spatial control of potential was impaired by the use of axial current supplying electrodes with surface resistance greater than 20 ohms for a centimeter length of axon. No region of membrane which was indeed subjected to a potential step showed more than one inward current peak. Other patterns were results of space clamp failure. Membrane current and potential patterns during space clamp failure were approximately reproduced in computations on a model containing two membrane patches obeying the equations of Hodgkin and Huxley. Non-uniformities in the axon or electrodes are not necessary for non-uniform electrical behavior. An extension of the core conductor model which includes the axial wire and external solution has been analyzed. The space constant of electrotonic spread is less than 0.5 mm with a usable electrode. Errors of about 5 per cent are introduced by ignoring the external solution. Resistance between the membrane and the control electrodes reduces the control and a few ohm cm^2 could lead to serious errors in interpretation.

The principles and ideals underlying the use of the voltage clamp concept for the study of the electrical properties of the squid giant axon, and the degree of success which has been obtained in their realization are discussed in another paper from this laboratory (Cole and Moore, 1960).

Current patterns which differed qualitatively from those reported by Cole (1949) and by Hodgkin, Huxley, and Katz (1949) were observed by Cole and Moore (unpublished) in 1954. They sometimes found that a "notch" of inward current flow occurred (as in Fig. 2*b*) between the usual peak inward current and the plateau of outward current, following a depolarizing step of 20 to 50 mv from the resting potential. These notches were not systematically investigated at that time, but appeared to be associated with the use of comparatively high resistance axial current supplying electrodes, and were thought to be largely caused by leakage of action potentials produced in the regions beyond one or both of the guard sections. This type of behavior closely resembles that reported by Frankenhaeuser and Hodgkin (1957) and, in those cases in which they used a point control system, by

Tasaki *et al.* (Tasaki and Spyropoulos, 1958). Frankenhaeuser and Hodgkin presented convincing evidence that their extra, delayed, inward current peaks were due to action potential invasion, but their discussion does not apply to the point control system used in this laboratory. Notched patterns of this type have been reported when action potential invasion was eliminated with the use of urethane in the guard regions (Tasaki and Bak, 1958*a*) or with the use of the "double clamp" (Tasaki and Spyropoulos, 1958).

Experimental and theoretical work has been in progress in this laboratory for some time concerning the interpretation of these anomalous results. It appeared at the outset that the notches, and the trains of oscillations reported by Tasaki and coworkers, would have to be explained either by a drastic revision of the concepts which emerged from the earlier work, or on the basis of non-uniform potential control and/or non-uniform membrane properties.

In this paper we shall discuss several ways in which the measured membrane current under attempted voltage clamp conditions fails to represent what the average would be over an area which was in fact subjected to a step of constant potential. It will be assumed that, for a membrane area of more than a few square microns, the accuracy with which the membrane potential may be forced to be spatially constant is limited only by the realizability of low resistance electrodes placed close enough to the membrane. Experimental results are presented which strongly support the conclusion that in any voltage clamped region, notches or oscillations will not appear, and that no new fundamental interpretations of the voltage clamp data are required at this time.

METHODS

The methods used in the experimental work presented here have been described (Cole and Moore, 1960). A schematic representation of the experimental arrangement is shown in Fig. 1 and includes all the kinds of electrodes which were used. The external differential electrodes and the internal probe were not used simultaneously. In some experiments an additional pipette electrode was placed outside the axon near the internal probe in order to increase the accuracy of the measurement of the membrane potential by this probe. Further clarification will be included as the occasion arises.

ANOMALOUS CURRENT PATTERNS

Following the observations of Cole and Moore in 1954 of notches in the pattern of membrane current during a depolarizing pulse such results have been observed from time to time. Some representative patterns are shown in Fig. 2. The notches appear only over a range of membrane potentials during the pulse which corresponds approximately to the region of apparent negative resistance in the peak inward current *versus* potential curve; they are sometimes, but not typically, associated with a "threshold;" using a point control system there are never more than

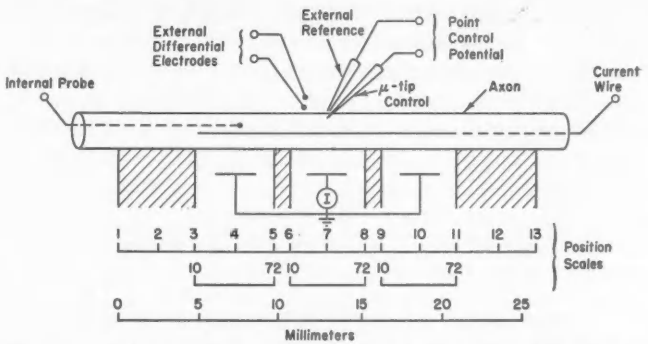

FIGURE 1 Schematic representation of experimental arrangement for point control voltage clamp experiments. The position scales refer to the positions of the external differential electrodes and the internal probe. The total current through the center chamber electrode is referred to as I_o in the text. The axial current electrode was a 75 micron diameter platinized platinum wire. Dashed lines indicate insulated wires.

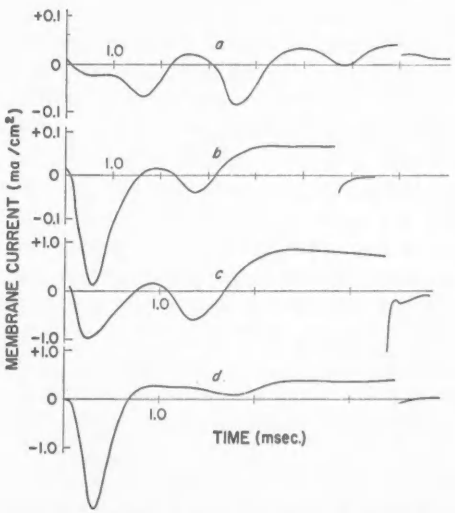

FIGURE 2 Representative center chamber current patterns having the additional peaks of inward (negative) current referred to as notches. These curves were obtained by the deliberate use of high surface resistance axial electrodes. Axons in normal artificial sea water, except *a*, which contained 2 mM K^+. *a*, membrane potential step from −55 mv to −35 mv. *b*, potential step from −75 mv to −37 mv. *c*, 40 mv depolarizing step, initial potential not recorded. *d*, Potential step from −70 mv to −40 mv. Membrane potentials with respect to external solution; *i.e.*, control micro-tip minus external reference.

two additional inward peaks. When axial current supplying electrodes of very low surface resistance are used the notches seldom occur. Our interest here is not in the notches *per se,* but in the implications with respect to the adequacy of the clamping and the concepts underlying the interpretation of the results. In order to investigate these matters, axial electrodes of deliberately high surface resistance were prepared and it was with the use of these electrodes that the curves of Fig. 2 were obtained.

CORRELATION OF NOTCHES WITH AXIAL ELECTRODE RESISTANCE AND MAXIMUM INWARD CURRENT

There are very good reasons (see below) why an increase in the surface resistance of the axial current supplying electrode would be expected to favor the appearance of anomalies in the current patterns. An analysis was made of all the experiments from the summer of 1958 for which the relevant data were recorded to determine how good the correlation was between the appearance of notches, the axial electrode resistance, and the maximum peak inward current obtainable. Most of the electrodes were 75 micron diameter platinized platinum wires. The surface resistance was measured before and after each experiment by applying a step of constant current and observing (through a reference electrode) the potential at the beginning of the step and at 10 milliseconds later. The ratio of potential to current obtained at zero time will be referred to as R_0; at 10 msec. as R_{10}. These values contain a certain amount of resistance due to the solution (about 12 ohm cm; *cf.* Cole and Moore, 1960, Appendix B) so that they are maximum values. No corrections were made. The electrodes used fall into two groups—those for which the resistance was as low as possible, and those which had a deliberately high resistance. In the high resistance group (R_0 greater than 30 ohm cm; R_{10} greater than 100 ohm cm) notches occurred in every case. For the routinely used electrodes R_0 varied from 12 to 23 ohm cm (average 18.3); R_{10} from 27 to 59 ohm cm (average 40.6). Notches occurred in 37 per cent of 47 experiments with no correlation between notches and resistance within the group. There is thus only a rough correlation of notches with axial electrode resistance. Attempts to correlate notches with the maximum peak inward current for any nerve were completely unsuccessful.

On almost any theory, the effect of the electrode surface resistance should be closely related to the potential drop from the inside of the metal wire to the interior surface of the axon membrane (*cf.* two patch theory below). To the extent that the radial current flow was uniform this potential drop would have a maximum given by the product of the total radial resistance times the maximum peak inward current. The radial resistance of the axoplasm for a 75 micron diameter electrode and a 500 micron diameter axon is about 12 ohm cm. This value is close to that added to the measured electrode resistance by the solution in which

they were measured, so that the measured values are close to the total radial resistance with the electrode in the axon. With these approximations, the results are shown in Fig. 3. The coordinates (on logarithmic scales) are the maximum peak inward current and the average of the zero time axial electrode resistance as measured before and after each experiment. The values for the axial electrode resistance have been converted to units of ohm cm² (ohms for a square centimeter of membrane, not electrode surface) so that the product of the coordinates of any point is in millivolts. Any 45° line represents some approximate maximum value for the radial potential drop. Axon-electrode combinations which were capable of pro-

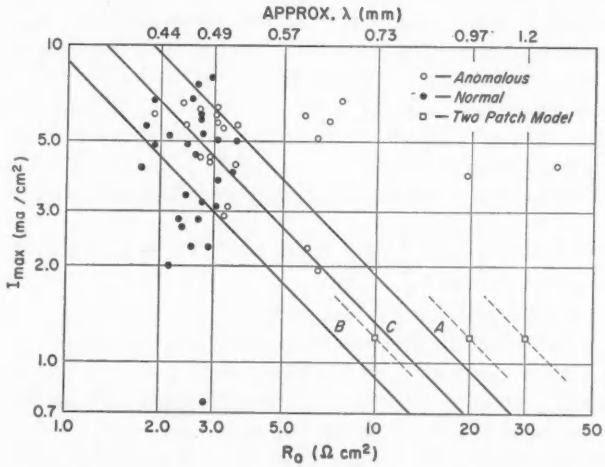

FIGURE 3 Appearance of notches (open circles) in membrane current during some depolarizing membrane potential step compared to normal, simple patterns (solid circles) in which no notches occurred for any value of potential during the step, for all 1958 experiments for which the relevant data were obtained. Coordinates are the maximum value for the peak inward current (I_{max}) for each particular axon, at the time of the observations, and the value of the axial electrode high frequency surface resistance (R_0). R_0 was measured as described in the text and converted here to units of ohms per square centimeter of axon membrane. Diagonal lines thus represent loci of constant potential which approximate that between the inside of the axial wire and the inside surface of the membrane at the time of the maximum peak inward current. Along the top of the graph are the values of the space constant (λ) calculated for a 500 micron diameter axon with external isopotentiality assumption and nominal values of axon parameters given in text for a resting membrane. Two patch model results (squares) are for uniform case with series resistance of 10, 20, and 30 ohms (see later text). Maximum peak inward current for the two patch model is plotted for comparison as 1.24 ma/cm² after multiplication by a scale factor of 0.516. This scale factor is the ratio of the peak inward current for the H-H axon as used in the computations (2.4 ma/cm²) to that of the average of the experiments shown here (4.65 ma/cm²).

ducing a notch in the current pattern are represented by the open circles, those which were not capable of producing a notch by solid circles.

The ten experiments for which the product of resistance and maximum inward current was the largest (greater than line A, about 20 mv) showed 80 per cent notches; the ten least products (less than line B, about 9 mv) showed no notches. The remaining thirty points are divided by line C at the median. In this group there were 53 per cent notches above the median, 47 per cent below. The lack of correlation in this group indicates that there are other variables involved. There is little doubt but that these were non-uniformities in axon diameter, axon membrane properties, and electrode surface impedance. The important conclusion is that no anomalous current patterns were observed under conditions when the maximum radial potential drop internally was less than about 9 mv but in almost every case when this potential drop was greater than about 20 mv. There is no indication whatever that the axons which were weak differed in any qualitative manner from those which could produce large inward currents. The conclusion is that the latter are merely more difficult to control. These remarks are in no way meant to imply that it is the magnitude of the inward current itself which makes control difficult.

MEMBRANE CURRENT AND POTENTIAL DISTRIBUTION —EXPERIMENTAL

Localized Membrane Current Measurements. A powerful method for investigating the spatial distribution of membrane current (originating in discussions with J. Lettvin; and see Cole and Moore, 1960) is to measure the external radial potential gradient in the immediate vicinity of the membrane. Measurements were made with a pair of 50 micron diameter electrodes spaced 200 to 300 microns apart (Cole and Moore, 1960) and oriented perpendicular to the membrane surface. It is plausible that the membrane current in the surrounding region will influence the potential between these electrodes to an extent which decays rapidly with distance to a negligible value at a few times the electrode separation.

A resolving power of about 225 microns was calculated (from measurements with a 500 micron diameter wire) as the separation between two narrow stripes on a 500 micron axon which would just give a dip in the observed apparent current density at a point midway between the two stripes. The calibration of these electrodes was only approximate and we will employ an arbitrary scale factor and consider only the time course and distribution of membrane current measured in this manner.

The kinds of results which were obtained are illustrated in Figs. 4 to 8. Figs. 7 and 8 are isometric plots of the data shown in Figs. 5 and 6 respectively. Fig. 4 is from an axon with relatively high maximum inward current (5.0 ma/cm^2) and relatively low resistance axial electrode ($R_0 = 20$ ohm cm). There was no obvious deviation of the pattern of membrane current averaged over the center chamber region from those described earlier (Cole, 1949; Hodgkin, Huxley, and Katz,

1949) and used by Hodgkin and Huxley (1952) in their empirical formulations. However, for a depolarizing pulse of + 50 mv (from a holding potential of −74 mv) the inward current at 0.5 msec. was about 30 per cent greater near the ends of the center chamber than in the middle and there is a large reduction in the center of the guard region. The much smaller variation in the steady state current at 5.0 msec. indicates that this is not the result of a gross injury.

Localized membrane current measurements on two nerves which did show a notch in the average center chamber current are shown in Figs. 5 and 6 and

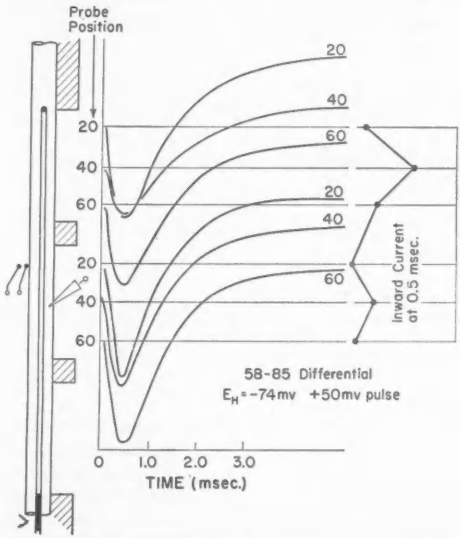

FIGURE 4 Distribution of current (in left guard and center chamber) as measured with external differential current measuring electrodes at the positions indicated on the schematic diagram at the left. This axon did not show a notch under any conditions. Profile at right shows value of inward current at each position at 0.5 msec. after beginning of potential step. E_H is the "holding potential" at which the control point was held prior to the initiation of the depolarizing pulse.

8 in which several important points are illustrated. The first, and the most important result of the present investigation, is that the second hump of inward current becomes smaller as the point control region is approached (position 7, Fig. 5; position 41, Fig. 6). This result was found in every case. Because the electronic feed-back apparatus was capable of maintaining constant membrane potential at the control point during the pulse, and that it did so was known from direct measurement, the conclusion is inescapable that the anomalous current patterns seen as the current electrode pair is moved away from the control point are directly associated with a failure of the "space clamp." It is, of course, highly desirable to understand the

reasons behind the space clamp failure in these cases—and it is necessary to do so in order to deal with the problem effectively—but it is stressed that neither a theoretical explanation nor measurements of membrane potential variations are required in order for the above experimental results to demonstrate with almost complete certainty, for the squid axon in sea water, that regardless of what kind of experimental arrangement is employed no "notches" or "oscillations" in the current pattern occur during an applied potential step.

Although a kind of action potential invasion might be responsible for the patterns seen in Fig. 6, positions 71, 61, 51, it is difficult to see how this could be the case for any of the other patterns in Fig. 5 or 6. The patterns in Fig. 5, position 2,

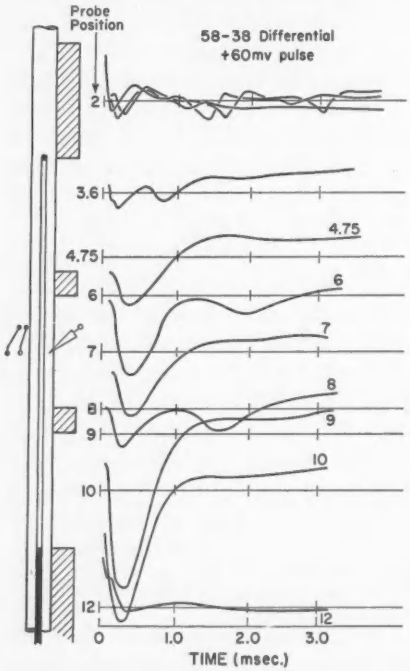

FIGURE 5 Distribution of external differential electrode current measurements for an axon, electrode, and depolarizing pulse which resulted in a notch in the center chamber current. Note the absence of the notch at position 7, near the control microelectrode. Curves at position 2 are three superimposed traces showing action potentials which did not invade the center chamber. These data are shown in isometric projection in Fig. 7.

show that a repetitive response was occurring beyond the end of the guard region (three separate traces) but there is no indication that these action potentials actually invaded into the center chamber region. Action potential invasion will be further discussed below.

Localized Membrane Potential Measurements. A large number of measurements were made of the distribution of potential in axons under a variety of conditions, with the use of internal and external micropipette electrodes and longi-

tudinal insertion of a platinum wire insulated except at the tip (*cf.* Cole and Moore, 1960). We are particularly concerned with gross effects resulting from space clamp failure using high resistance axial current electrodes, but even under apparently moderately good conditions with no apparent anomalies in the total membrane current measured over the center chamber (4.6 mm), the uniformity of membrane potential may be far from ideal. This situation is illustrated in Fig. 9 in which the axial electrode resistance was $R_0 = 14$ ohm cm (2.12 ohm cm² of membrane),

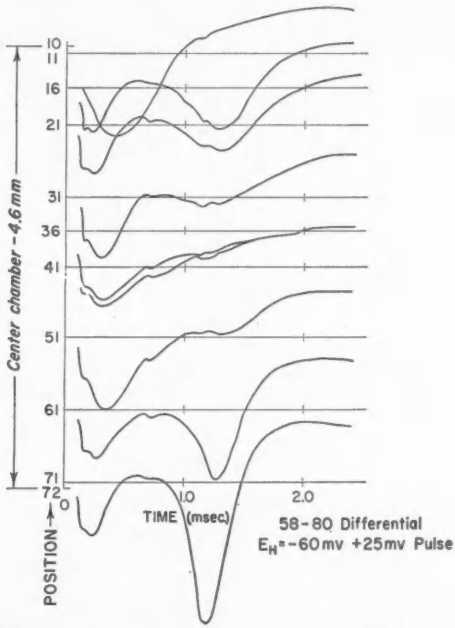

FIGURE 6 Distribution of membrane current as in Fig. 5, but for center chamber only. A notch appeared in the center chamber current under these conditions. Microelectrode potential control was close to position 41 (double trace shows current at beginning and end of this series of measurements). The pronounced notches away from the control point do not occur at position 41.

$R_{10} = 59$ ohm cm (8.95 ohm cm²) and no indication of a notch in the membrane current. Membrane potential measurements at three positions in the center chamber were made with the internal wire probe and an external pipette; the maximum variation at various values of potential during the pulse (E_p) is plotted as delta V_m in Fig. 9. Values at the time of the peak inward current are denoted by the diamonds, at the steady state by the open triangles. These have been corrected for deterioration by a linear interpolation based on the curves of peak inward current,

also shown on Fig. 9, taken before and after the period (about 20 minutes) of membrane potential measurements. The maximum variation of membrane potential over the center chamber clearly occurs at the value of potential during the pulse which is in the region where the peak inward current is changing most rapidly. The

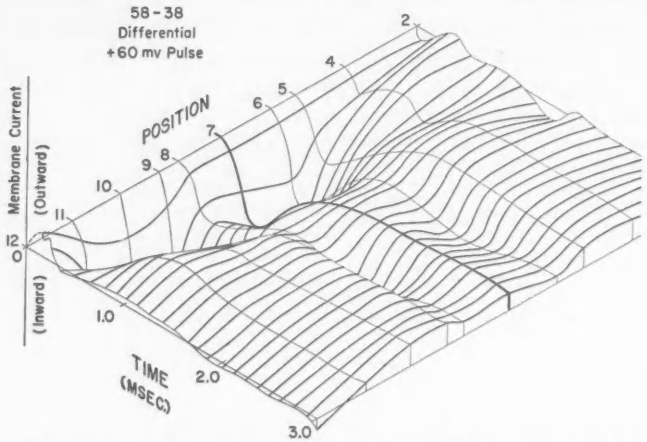

FIGURE 7 Membrane current distribution. Isometric projection of data shown in Fig. 5. Lines roughly paralleling position axis are lines of constant time, drawn freehand.

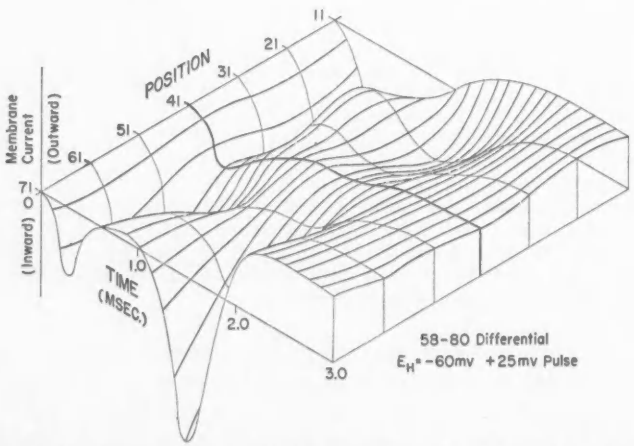

FIGURE 8 Membrane current distribution. Isometric projection of data shown in Fig. 6. Notch at positions 51, 61, and 71 might be the result of an action potential arising beyond the end of the cell and interacting with the potential-current behavior in the cell. The notches at positions 21 and 31 do not appear to be the result of an external action potential.

variation during the steady state (3.3 msec. after the beginning of the step) increases with the amount of depolarization; within the limits of error it could be proportional to the pulse magnitude. Although many significant results might be obtained with an axon such as this one a membrane potential variation reaching 16.5 mv in the center chamber cannot be considered an ideal space clamp. Presumably this axon was very non-uniform—perhaps an injury had occurred somewhere—but in the past there has been no simple, practical procedure by which it could have been eliminated from an experimental series.

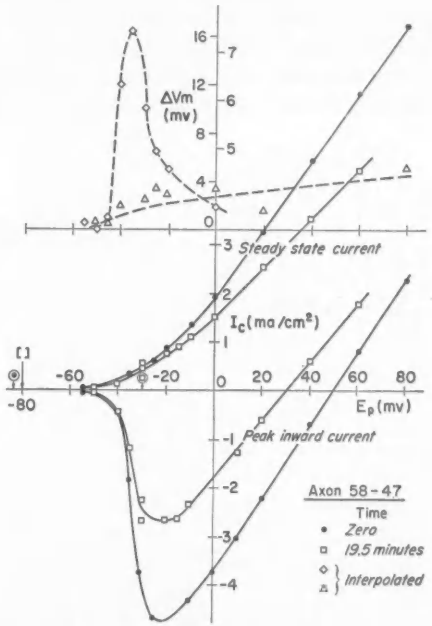

FIGURE 9 Upper graph, the variation in membrane potential (V_m) among three positions in the center chamber during a depolarizing pulse. Membrane at control microelectrode was subjected to a potential step from an initially hyperpolarized value of −80 mv (square brackets) to the value as indicated (E_p). Diamonds, variation at time of total center chamber peak inward current. Open triangles, variation at the time of the steady state outward current.

No notch occurred in the center chamber current for any value of depolarizing pulse.

Lower graph, peak inward and steady state outward center chamber (I_c) for comparison with upper graph. Two sets of data taken before potential measurements (solid circles) and after (open squares, average of 19.5 minutes later). Values given in upper graph were corrected for the deterioration of the axon by a linear interpolation, based on the data in the lower graph. The circled points on the potential axis are the resting potentials of the axon measured before and after the two current curves.

The distribution of membrane potential under conditions of extreme space clamp failure resulting from the use of very high resistance axial current supplying electrodes is illustrated in Figs. 10 to 13 (the isometric projection of Fig. 11 is from the same data as those of Fig. 10). These data were obtained by taking the difference in potential between a longitudinally inserted probe and the microtip electrode used for potential control. Adequate controls were made in each case to insure that the potential between the microtip control and the external reference electrode was indeed a step. Thus the inner probe minus microtip curves approximate the variation in the membrane potential, as a function of time, from the ideal space clamp. For a perfect space clamp these records would be zero at all times. The approximation is inexact because (*a*) the radial position of the inner probe could not be precisely controlled so that the radial voltage drop in the axoplasm which is present in the records varies with longitudinal position. Neither the magnitude

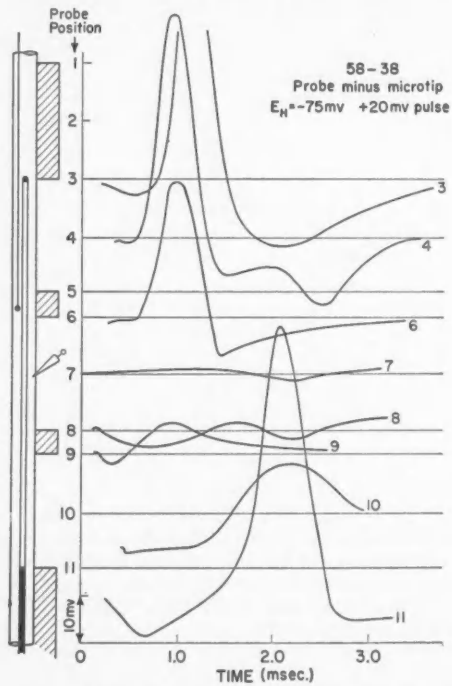

FIGURE 10 Space clamp failure. Deviation from base line is the potential of internal probe minus the control microtip potential. This is approximately the difference between the membrane potential and the potential at which the clamping was attempted. Deliberately high resistance axial electrode used to impair space clamp. Control microtip near position 7. Depolarizing pulse of 20 mv from initially hyperpolarized value of −75 mv.

nor the time course of this error is calculable since the membrane current and thus the radial current are certainly not uniform with distance. The magnitude of this error could reach maximum values of 10 to 15 mv (a few milliamperes per square centimeter of membrane times the radial axoplasm resistance of about 2 ohm cm^2), and (*b*) the potential of the external solution along the outer surface of the axon is not constant to within more than a few millivolts under conditions of extreme space clamp failure. For these reasons, and because the analysis of the distribution of voltage and current in such a complicated system has not been attempted in detail, exact quantitative considerations are not possible. However, in spite of the approximations involved, several relevant conclusions emerge from these results. These are: (*a*) the deviations are not confined to depolarizing pulses in a restricted potential range as the obvious anomalies in the current patterns are; (*b*) very large deviations from the membrane potential changes impressed at the control point occur in

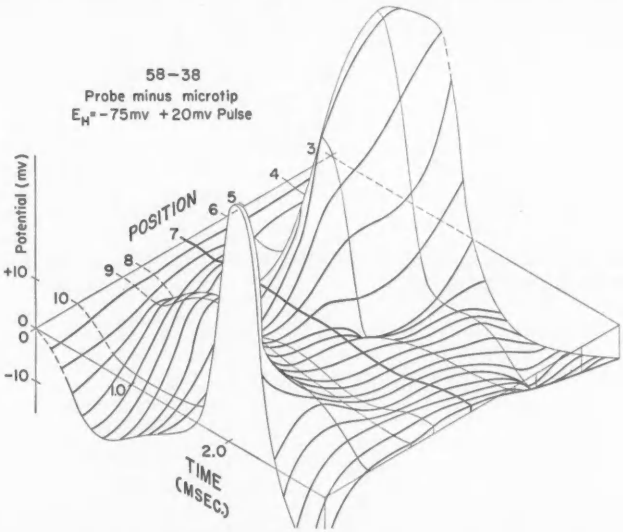

FIGURE 11 Isometric projection of data in Fig. 10.

regions not more than a millimeter distant; (*c*) the behavior of the membrane potential on one side of the control point bears no constant relation to that on the other; and (*d*) the deviations are usually di- and sometimes triphasic.

The curves of approximate membrane potential *versus* time and distance along the axon presented in Fig. 12 have been converted into curves of the potential between the axial wire and the inner probe. This was done with the use of the curve of the potential between the axial wire and control microtip for this particular depolarizing step, which is not illustrated; *i.e.*, axial wire minus inner probe equals

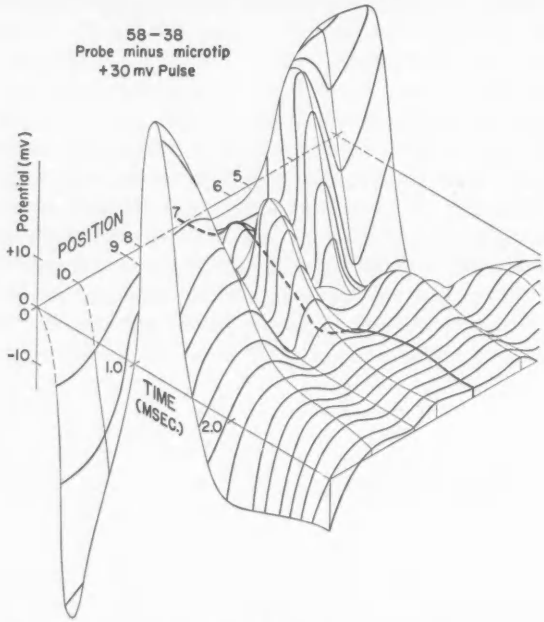

FIGURE 12 Isometric projection of space clamp failure results as in Figs. 10 and 11, but for 30 mv depolarizing pulse.

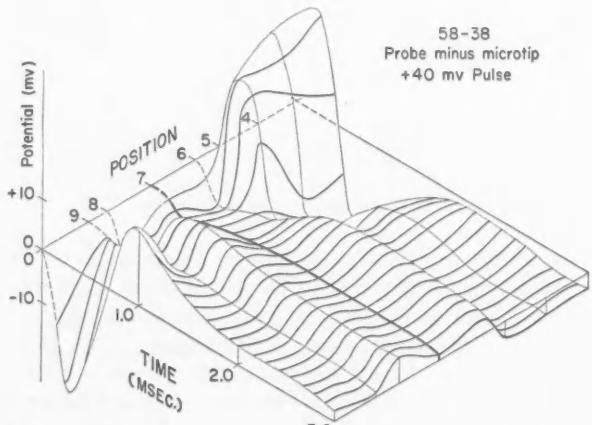

FIGURE 13 Isometric projection of space clamp failure results as in Figs. 10 and 11 but for 40 mv depolarizing pulse.

the difference between the axial wire minus microtip and inner probe minus microtip. The results are shown in Fig. 14. These curves have been computed in an effort to obtain an approximation to the membrane current which is flowing at any point at the same time that the potential measurements were made. Such data were not obtained with the simultaneous use of external differential electrodes because of the complexity of the experimental setup required. However, the axial wire minus inner probe potential measurements approximate the use of internal differential

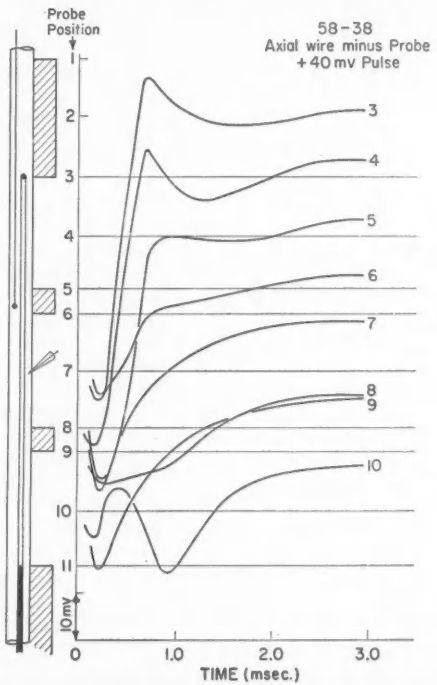

FIGURE 14 Approximate membrane current distribution during space clamp failure. These curves are the potential between the axial wire and the internal probe derived from the data shown in Fig. 13, and see text.

electrodes. If there were no longitudinal currents flowing in the axoplasm, nor any axial electrode polarization, these curves would be an exact measure of the radial current leaving the axial wire and passing through the membrane of the axon. Longitudinal currents are present, and could be estimated from the data of Fig. 13. This has not been attempted because of the errors discussed above. However, bearing in mind the presence of some inaccuracies, certain of the curves of Figs. 13 and 14 are compared in Figs. 15 and 16 and represent approximate curves of simultaneous membrane potential and current during space clamp failure. We note that

there is a tendency for the current curves (axial wire minus inner probe) to have the shape ordinarily seen in a proper voltage clamp experiment when the curve of membrane potential (inner probe minus microtip) is fairly flat. This is not always exactly true, and the presumption is that the discrepancies are due to longitudinal axoplasm currents. Other general tendencies occur: a well developed notch in the membrane current is associated with a membrane potential which is diphasic with the first phase negative going (Fig. 15) and not when the first phase is positive

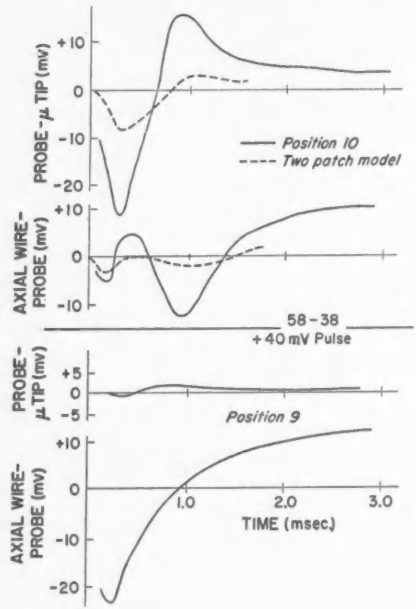

FIGURE 15 Simultaneous approximate membrane potential deviation (probe minus microtip) and membrane current (axial wire minus probe) from Figs. 13 and 14. Note that at position 9 the potential deviation is small and the current has only one inward peak. At position 10 the potential variation is initially negative going and current has pronounced notch. Dotted curves are results of computations on the two patch model which illustrate the same type of relationship. See text below.

going as in Fig. 16. The dotted curves in Figs. 15 and 16 are computed potentials and currents in the "two patch" model discussed below. The relationships shown here are understandable on the basis of the two patch model but this is not meant to be in anyway exact or comprehensive. For example, it is surmised that the effect of the propagation of an action potential into the chamber from the end at just the right time might produce potential and current patterns which were indistinguishable from some of those computed on the basis of this model.

THE SPACE CLAMP — THEORETICAL

We shall consider how well one may be expected to be able to maintain a spatially uniform and known potential over an extended region of the squid axon membrane, assuming perfect electronic control of the potential between the microtip and exter-

nal reference control electrodes (see Fig. 1). We shall not analyze in any detail the results to be expected using an extended control system. Some of the results to follow apply to either system and some do not. The effects of the lateral guards will not be considered in detail.

It is important to realize at the beginning that in either the point control or extended control systems the means by which the membrane potential control is attempted is *only* through the potential which is applied between the internal and

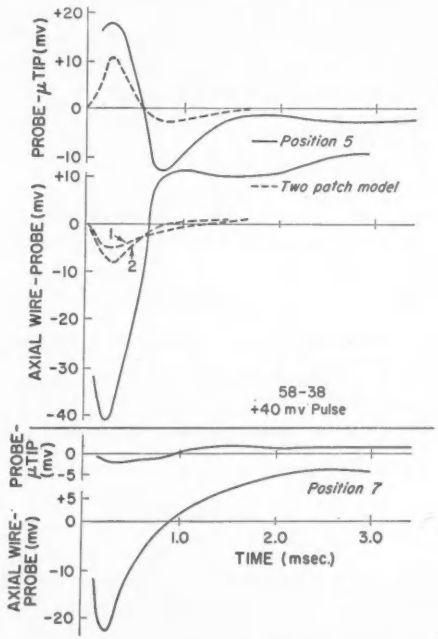

FIGURE 16 Curves as in Fig. 15. At position 7, near the microtip control the current has one inward peak. At position 10 the potential deviation is initially positive going and the membrane current has a large inward peak and no pronounced notch. Dotted curves from two patch model computations illustrate this type of relationship. Dotted current curve labeled (1) is for the controlled, (2) for the uncontrolled, patch. This is an example of a no-notch error discussed below.

external current supplying electrodes. These electrodes represent the effector organ of the feedback apparatus.

Electrotonic Spread with Axial Wire. An extension of the usual simple core conductor model approximation has been devised by one of us (KSC) which includes the effect of the axial wire and the external fluid. An element of length of this model is shown in Fig. 17. Applying Ohm's and Kirchhoff's laws to the

circuit of Fig. 17 and allowing the length of this element to approach zero we may write

$$d^2V_2/dx^2 = -r_2[(V_a - V_2)/r_1 - i_3]$$
$$d^2V_4/dx^2 = -r_4(i_3 - V_4/r_5) \quad (1)$$

where:

V_a is the potential, in volts, of the axial wire relative to a ground electrode considered to be equivalent to a cylinder surrounding the axon;
V_2 is the potential, in volts, relative to ground, at a point inside the axon;
V_4 is the potential, in volts, relative to ground, of a point outside the axon;
r_1 is the equivalent radial resistance, in ohm cm, between the axial wire and the point at which V_2 is taken; it includes r_a, the axial electrode surface resistance;
r_2 is the equivalent longitudinal resistance, in ohm/cm of the axoplasm, considered to be lumped along a line;
r_3 is the equivalent radial resistance, in ohm cm, between points at which V_2 and V_4 are taken, including the membrane resistance;
r_4 is the equivalent longitudinal resistance of the external solution, in ohm/cm;
r_5 is the equivalent radial resistance of the external solution, in ohm cm, between the point at which V_4 is taken and ground;
i_j is the current through r_j, in appropriate units for any j, positive from left to right, or top to bottom in the model as shown in Fig. 17;
x is distance along the model from some reference point, positive to the right.

Equations (1) require no assumptions about the electrical properties of the membrane. In the steady state (in time) the membrane may be represented by an equivalent battery (V_3) in series with a resistance (r_m), in which case we may write the further relations

$$i_3 = (V_2 - V_4 - V_3)/r_3 \quad (2)$$

$$V_m = V_3 + i_3 r_m \quad (3)$$

The quantity $(V_2 - V_4)$ will differ from the membrane potential V_m by an amount which will only be large if the membrane resistance r_m is small compared to r_3 (note $r_m < r_3$). Equation (3) may be written as

$$V_m = (V_2 - V_4)r_m/r_3 + V_3(1 - r_m/r_3). \quad (4)$$

and it will be convenient to consider $(V_2 - V_4)$ instead of V_m in most cases.

In the event (see later) that the errors introduced by neglecting the potential variations in the external solution can be tolerated, the relevant equations are obtained by setting $r_4 = 0$ in equation (1).

The solutions of the equations for electrotonic spread in the usual simple core conductor model are characterized by the fact that the variable x is always multiplied by a constant, $1/\lambda$, where λ is referred to as the "space constant" or "characteristic length" of the nerve. It is a complication of the model shown in Fig. 17 that instead of one space constant being sufficient, two are required. The solution of equations (1) under steady state conditions (in time) given by equation (2) and

the condition that V_2 and V_4 are bounded, for an infinite length of nerve, x greater than zero, is

$$V_2(x) - V_2(\infty) = Ae^{-x/\lambda_1} + Be^{-x/\lambda_2},$$
$$V_4(x) - V_4(\infty) = Ce^{-x/\lambda_1} + De^{-x/\lambda_2}, \tag{5}$$

where λ_1 and λ_2 are the positive roots of the equation

$$\left[r_2\left(\frac{1}{r_1}+\frac{1}{r_3}\right)-\frac{1}{\lambda^2}\right]\left[r_4\left(\frac{1}{r_3}+\frac{1}{r_5}\right)-\frac{1}{\lambda^2}\right]-\frac{r_2r_4}{r_3^2}=0. \tag{6}$$

Values for the Model. The resistivity of axoplasm will be taken to be about twice that of sea water and assumed to be 40 ohm cm. For a 500 micron diameter axon the longitudinal internal resistance will be about 15,000 ohm/cm; the convergence resistance between a 75 micron diameter axial wire and the axon membrane will be about 12 ohm cm. The values to be used for the external resistances were arrived at by fitting the model to the results of measurements of the distribution of current outside a 500 micron diameter wire which was insulated except for one narrow ring, and positioned in the cell in place of the axon. A space constant of about 0.1 cm was found at a distance of about 100 microns from the surface of the wire and at about 0.1 cm from the surface of the wire the lines of current flow were

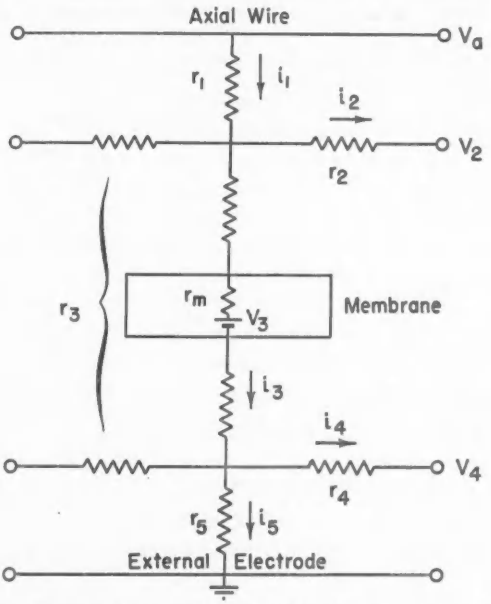

FIGURE 17 An element of length of the model taken to represent a squid axon containing axial wire. The external fluid is represented by resistances r_4, r_5, and a portion of r_3. For details see text.

virtually parallel. The values for r_4 and r_5 were chosen so that the model fits these data in the limit where the membrane resistance (hence r_3) is infinite. Thus, for r_3 infinite, equation (4) gives $1/\lambda^2$ as equal to r_4/r_5 or r_2/r_1. We take $1/\lambda^2_2$ to be (for r_3 infinite) r_4/r_5 and $1/\lambda^2_1$ to be r_2/r_1. We thus have $r_4/r_5 = 100$. r_4 is taken to be 300 ohm cm as being close to the longitudinal resistance of an annular cylinder with inner diameter 500 microns, outer diameter 2500 microns. Thus $r_5 = 3$ ohm cm. We do not lose any generality by assuming that the sea water at a distance of 0.1 cm is at ground potential. The values for the model thus become: $r_1 = (r_e + 6)$ ohm cm; $r_2 = 15{,}000$ ohm/cm; $r_3 = (r_m + 9)$ ohm cm; $r_4 = 300$ ohm/cm; $r_5 = 3$ ohm cm, where r_e is the axial electrode surface resistance, in ohm cm.

We are now in a position to calculate results from the model and to answer the question of the error introduced by simplifying the model by assuming the external fluid to be isopotential everywhere. Representative values of λ_1 and λ_2 are shown in Table I according to equation (6). Approximate values for the space constant

TABLE I

AXON MODEL SPACE CONSTANTS

λ_1 and λ_2 are the positive roots of equation (6). Parameter values used (see Fig. 17) are: $r_1 = (r_e + 6)$ ohm cm; $r_2 = 15{,}000$ ohm/cm; $r_3 = (r_m + 9)$ ohm cm; $r_4 = 300$ ohm/cm; $r_5 = 3$ ohm cm. The membrane resistance (r_m) is taken to be 5000 ohm cm for the resting state and 50 ohm cm for the active state. The surface resistance of the axial electrode (r_e) is considered for a perfect electrode ($r_e = 0$), a hopeless electrode for space clamping ($r_e = 50$ ohm cm), and for no electrode ($r_e = \infty$). The single space constant approximation is for the assumption of external isopotentiality.

r_e ohm cm	r_m ohm cm	λ_1 cm	λ_2 cm	λ (single space constant approximation) cm
0	50	0.0191	0.0978	0.0191
50	50	0.0436	0.0990	0.0438
∞	50	0.0624	0.1016	0.0627
0	5000	0.0200	0.1000	0.0200
50	5000	0.0624	0.1000	0.0608
∞	5000	0.1000	0.5778	0.5779

assuming external isopotentiality for the appropriate axial electrode surface resistances are included in Fig. 3. The coefficients (A, B, C, D) in Equation 5 are determined by the parameters of the system and include two arbitrary constants, which could be, for example, $V_2(0)$ and $V_4(0)$. The relative values of these coefficients determine the relative contributions of the term involving λ_1 and λ_2 and this relationship is not constant for the various conditions listed in Table I. It is for this reason that the value of λ for the single space constant approximation in Table I varies from being almost equal to λ_1 for a low resistance electrode and the active state to being almost equal to λ_2 for a high resistance electrode and the resting state.

The error introduced by the isopotential assumption is illustrated by considering specifically the error which would be introduced for the case in which the membrane properties are the same everywhere and a short circuit is introduced across r_3 at some point. Call this point $x = 0$. We then have that $V_2(0) = V_4(0)$. By integrating the current through r_1 from minus to plus infinity and putting it equal to the integral of the current through r_5 we arrive at another relation between $V_2(0)$ and $V_4(0)$. We shall not present the algebra here, but represent this relation by

$$M_1[V_2(0) - V_2(\infty)] + M_2[V_4(0) - V_4(\infty)] = 0,$$

and we have

$$V_2(0) = V_4(0) = \frac{M_1 V_2(\infty) + M_2 V_4(\infty)}{M_1 + M_2}.$$

We can derive an expression for the isopotential assumption error as

$$\frac{V_4(0) - V_4(\infty)}{V_2(\infty) - V_4(\infty)} = \frac{1}{1 + M_2/M_1} = R. \tag{7}$$

Actually carrying out the above indicated steps we get

$$\frac{M_2}{M_1} = \sqrt{\frac{r_1 r_2}{r_4 r_5}}\left[\frac{\sqrt{r_2 r_5[1 + (r_1 + r_5)/r_3]} + \sqrt{r_1 r_4}}{\sqrt{r_2 r_5} + \sqrt{r_1 r_4[1 + (r_1 + r_5)/r_3]}}\right]. \tag{8}$$

Now, equation (7) gives the variation in the external potential divided by the potential across the membrane far from the short circuit. This is a measure of the fractional error introduced if we should take the external fluid to be isopotential. Note that R does not depend upon the values of V_a, the axial wire potential, or of V_3, the open circuit membrane potential. Using the values given above we may calculate R for various cases. Allowing the axial electrode surface resistance (r_e) and the membrane resistance (r_m) to vary, we reach a maximum error for zero r_e ($r_1 = 6$) and infinite r_m, in which case $R = 0.09$, or about 10 per cent error. The minimum r_e which is realizable, however, is about 20 ohm cm, for which, with r_m infinite the maximum R is 0.045, or about 5 per cent error. A lower bound for R, which is easily computed is with $r_3 = 0$. Under these conditions, equation (8) reduces to r_2/r_4 and thus $R = 0.0196$, independent of electrode resistance. The range of error to be expected is thus between 2 and 5 per cent. This amount is felt to be small enough so that for most cases the assumption of external fluid isopotentiality is justified. We shall refer to the model under these conditions as the single space constant model.

For the condition of external fluid isopotentiality the differential equations (1) reduce to

$$\frac{d^2V_2}{dx^2} = r_2(1/r_1 + 1/r_3)V_2 - (r_2 V_a/r_1 + r_2 V_3/r_3), \tag{9}$$

which may be written

$$\lambda^2 \frac{d^2V_2}{dx^2} = V_2 - V_2(\infty), \tag{10}$$

where λ is the characteristic length, or space constant and $V_2(\infty)$ is the value of V_2 which would obtain if the membrane potential were uniform with distance. We see from (9) and (10) that

$$\lambda^2 = \frac{1}{r_2(1/r_1 + 1/r_3)} \tag{11}$$

and

$$V_2(\infty) = (r_3 V_a + r_1 V_3)/(r_1 + r_3). \tag{12}$$

Thus we have a model which is equivalent to the usual core conductor model, for the steady state in time, if we replace the membrane resistance by the parallel resistance of r_1 and r_3 and the open circuit membrane potential by the expression (12). For the most part we shall consider V_2 as if it were the membrane potential, but we must keep in mind that it is actually the potential between some point in the axoplasm and ground. We may, if necessary, use the correct expression (equation (4) with $V_4 = 0$ for the external isopotential case).

THE TWO PATCH MODEL

Genesis of the Model. In any attempted voltage clamp arrangement the membrane potential and current in one region of the axon will exert an effect at some other region in two different ways; by the direct flow of current in the axon and by the influence that one region may have on the potential of the axial wire *via* the external feedback apparatus. Because the results of the above analysis indicate a rather short space constant for passive electrotonic spread (*cf.* Fig. 3 and Table I), in the neighborhood of 0.5 mm, which we have confirmed experimentally (Cole and Moore, 1960), it would seem reasonable that regions separated by more than this distance might interact mainly by the second of the two ways mentioned. This is equivalent to neglecting the coupling due to that part of the membrane between the regions considered; *i.e.*, assuming a space constant of zero. These considerations led one of us (RET) to devise the simplified models shown in Fig. 18 to represent the axon for a point control arrangement (Fig. 18*A*) and an extended control arrangement (Fig. 18*B*). Even on the assumption of a zero space constant the extended control system is not adequately represented by only two patches. No extensive computations have been made for this model and we shall not consider it in detail. For the point control system and the zero space constant approximation, however, two patches are sufficient. For the squid axon in sea water the empirical equations of Hodgkin and Huxley are considered to be appropriate for each individual patch because of the observation that the membrane current measured with external differential electrodes in a region known to be voltage-controlled appears to behave in this way (*cf.* Figs. 5 to 8 and Cole and Moore, 1960).

Computations with the Model. For computations with the model we consider patches (Fig. 18*A*) with the lumped characteristics of 1 cm² of membrane

as given by the empirical equations of Hodgkin and Huxley at 6.3°C. In every case the applied potential step is from an initially hyperpolarized value of −20 mv (with respect to resting potential). The purpose of the computations was to determine the potential across and the current through the second patch when the first patch was subjected to a potential step. These computations were done in December, 1958, with the use of the analog computer which R. FitzHugh has been using to analyze the properties of the Hodgkin-Huxley equations (FitzHugh, 1960). A preliminary report has appeared (Taylor and FitzHugh, 1959).

As was anticipated, the current through the second patch did not necessarily fol-

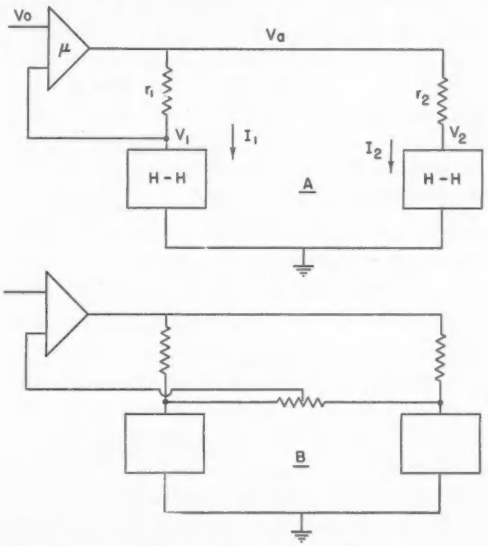

FIGURE 18 The two patch model. *A*; the zero space constant approximation for a point control voltage clamp arrangement. Boxes represent patches of membrane, one of which (subscript 1) is controlled by the electronic feedback apparatus. The other (subscript 2) is any other region of membrane. *B*; simplified model for extended control voltage clamp arrangement. This model (*i.e.*, two patches) would not be sufficient even for the zero space constant approximation, but would probably oscillate if the properties of the boxes were taken to be the Hodgkin-Huxley equations.

low that through the first, even when the two patches were identical and the values of the series resistances r_1 and r_2 were the same.

In addition to the equations of Hodgkin and Huxley which relate the current and potential for the equivalent membrane patches we have the following relations

$$V_1 = V_o \quad \text{(perfect clamp)}$$
$$V_a = V_1 + r_1 I_1$$
$$V_a = V_2 + r_2 I_2$$

where (see Fig. 18*A*) V_1, V_2, I_1, I_2 are the potentials across and the currents through the first and second patches respectively (currents and potentials are defined relative to resting conditions; outward current and depolarization positive), r_1 and r_2 are the total series resistances between the axial wire (at potential V_a) and the patches. Any three terminal network consisting only of pure linear resistances may be connected to the three points at which V_a, V_1, and V_2 are defined and the model as shown in Fig. 18*A* will be an exact representation (r_1 and r_2 depending on the network) so long as the potential V_1 is controlled. The computations were done by first solving the H-H equations for the first patch for a step of potential from −20 mv to V_1 at time zero. The resultant pattern of current $I_1(t)$ was then fed into the computer at a later time, multiplied by r_1, added to V_1, and the H-H equations were again solved by the computer for the condition that the pattern of potential $V_a = V_1 + I_1 r_1$ was equal to $V_2 + I_2 r_2$. The final output of the computer was either the potential $V_2(t)$ or the current $I_2(t)$. It was not possible to record these potential and current curves simultaneously, so that those critical cases in which the solution was not necessarily the same for successive computer runs, I_2 and V_2, may not correspond exactly to the same solution.

The current through the membrane capacity was not included in these computations. This component of the membrane current would alter the solutions in two ways: Firstly for short times compared to the time during which the membrane properties change with potential, if the feedback apparatus produced a step in V_1, the potential V_a which produces this step cannot itself be a step. It was taken to be, but auxiliary computations showed that the initial departure of V_a from a step when the capacity current was included was a transient which decayed rapidly enough not to influence the solution at times of interest here. Secondly, for longer times, the value of V_a would include a term $C_m r_2 dV_2/dt$. This correction was also included in the computations in certain cases and found to be small.

A final simplification was the manner in which the non-uniformities in the actual situation were represented in the model. This was done by altering the ratio r_1/r_2. A perfectly uniform axon would be represented by a value of unity for this ratio. Other values represent either a non-uniformity in the surface resistance of the axial electrode, the axon diameter, or the condition of the membrane. For the first two the representation is accurate in the case that the membrane properties were uniform, in the third case it would only represent an alteration in membrane properties which were such that all the parameters which determine the membrane conductances in the H-H equations were multiplied by a common factor. There are many ways in which the H-H equations might be modified to represent non-uniformities. This way was chosen because of the ease with which the ratio r_1/r_2 could be changed in the computer, and while it is important to consider the effect of possible non-uniformities in membrane properties there are no data available to indicate what these might in fact be.

The Two Patch Computer Results. Figs. 19 to 23 are reproductions of

the computer results which illustrate five situations in which the current through the second, uncontrolled patch was not the same as that through the first. In each case the value of V_1 and of V_2 was -20 mv before zero time. Those cases in which the currents and potentials were the same in each patch are not illustrated. (The computations were not undertaken with a view toward completely mapping the regions of the r_1, r_2, V_1 space in which various kinds of anomalous current patterns would occur, but to demonstrate that, for the model, a notch could indeed occur in the pattern of $I_2(t)$, as had been concluded from rough and intuitive arguments.)

The Uniform Model. All the r_1, r_2, V_2 combinations tried are listed in Table II. The uniform cases are those for which $r_1 = r_2$. A small notch occurred in

TABLE II

TWO PATCH MODEL COMPUTER RESULTS

r_1, series resistance of controlled patch (see Fig. 18*A*). r_2, series resistance of uncontrolled patch. V_1, potential of controlled patch during depolarizing step from an initially hyperpolarized value of -20 mv. The appearance of a notch in the current through the uncontrolled patch is indicated by "notch," a difference between the *shape* of the current pattern in the controlled and uncontrolled patches but without a notch, by "no-notch," and no difference by "same." "Unstable" indicates that in a series of computer runs both notch and no-notch patterns occurred. Underlined entries are those for which Figures appear in this paper.

r_1 ohms	r_2 ohms	V_1 mV			
		+25	+30	+40	+50
	5	Notch	Notch	Notch	—
10	10	Notch (small)	Notch (small)	Same	—
	20	No-notch	No-notch	No-notch	—
	10	—	Notch	Notch	Notch
	15	—	Notch	Notch	—
	18	—	Notch	Notch	—
	20	—	Unstable	Same	Same
20	22	—	No-notch	—	—
	24	—	No-notch	—	—
	25	—	No-notch	No-notch	—
	26	—	No-notch	—	—
	40	—	No-notch	No-notch	No-notch
	25	—	Notch	—	Notch
	30	—	Notch	—	Same
30	35	—	Unstable	—	No-notch (small)
	40	—	Unstable	—	No-notch
	60	—	Unstable	—	—
40	40	—	—	—	Notch (Not reproducible)

the current through the second patch for values of $r_1 = r_2 = 10$ ohms. Increasing this value to 20 ohms gave the results shown in Fig. 19 for potential during the step of $V_1 = +30$ mv. A more or less pronounced notch is seen in successive computer runs. The variability in the results for successive runs is related to noise in the computer. It is not known whether the sensitivity in certain cases was the result of the particular way in which the computer was programmed or is inherent in the H-H equations, but in any case the variability did not appear in those cases (large depolarizing steps) in which the current through the two patches was expected to be identical. A small bias was probably introduced because the curve follower which was used to reintroduce the curve of $I_1(t)$ into the computer slightly underestimated this function; *i.e.*, added a small increment of current in the inward direction. For this reason a strictly uniform case might be better represented by a small difference between r_1 and r_2 and the value for r_1 and r_2 at which notches just begin to appear might be slightly larger than 10 ohms. None of these considerations, however, alters the fact that for $r_1 = r_2 = 20$ ohms a very definite and pronounced notch occurred (Fig. 19). Increasing these resistances to 30 and 40 ohms (Fig. 20) accentuated the notch. The three points represented by the open squares in Fig. 3 are the (corrected) values for peak inward current and series resistance which are appropriate to the two patch computed results for series resistances in the model of 10, 20, and 30 ohms respectively, from left to right. In other words, the two patch model computations indicate that, for a uniform axon notches might be expected to begin to appear for points above and to the right of the 45° line passing through the first square on the left. The uniform model computations only resulted in anomalous current patterns of the notch type except that in the case $r_1 = r_2 = 20$ ohms, $V_1 = +30$ mv, a no-notch pattern would occasionally occur. (A no-notch pattern is illustrated in Fig. 22 and discussed in the next paragraph.) Although not illustrated in Fig. 19, this case is listed as "unstable" in Table I. A slight jar of the curve follower during the initial period of the computation was sufficient to change the course of the solution from a notch to a no-notch anomaly.

Non-uniform Model. As described above, non-uniformities are represented in the model by making r_1 differ from r_2. In every case tried, a non-uniformity of this kind introduced an anomalous current pattern in the second patch for some value of V_1 during the step. The limits of this effect were not accurately delineated (see Table II), but it is clear that for values of r_1 greater than some value which is less than 20 ohms the limits are very narrow. For example, with $r_1 = 20$ ohms, depolarizing pulse to +40 mv, a change in r_2 from 20 to 18 ohms (Table II and Fig. 21 for $r_2 = 15$ ohms) was sufficient to introduce a notch in the second patch. For larger amounts of non-uniformity the limits on the values of r_1 and r_2 are more severe as illustrated by the fact that a notch occurred for the case $r_1 = 10$ ohms, $r_2 = 5$ ohms (see Table II). A different, and potentially more dangerous, type of anomaly occurred in the computed results for the non-uniform cases when r_2 was greater than r_1. This type is illustrated in Fig. 22 and will be referred to as a "no-

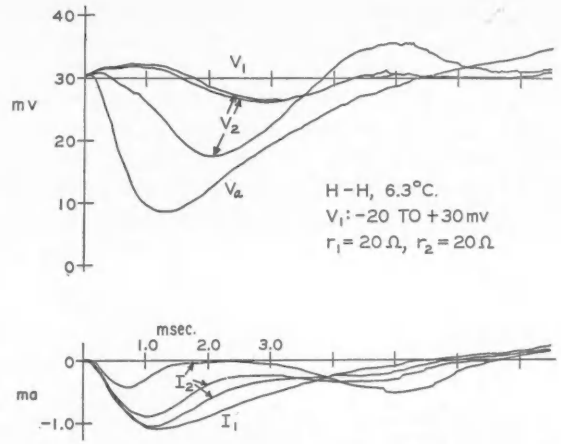

FIGURE 19 Two patch model analog computer results. Uniform case. Currents and potentials relative to resting, outward current and depolarization positive. V_1, I_1 refer to controlled patch; V_2, I_2 to uncontrolled patch; V_a is the potential of the axial wire. The three curves of I_2 and V_2 are for successive computer runs.

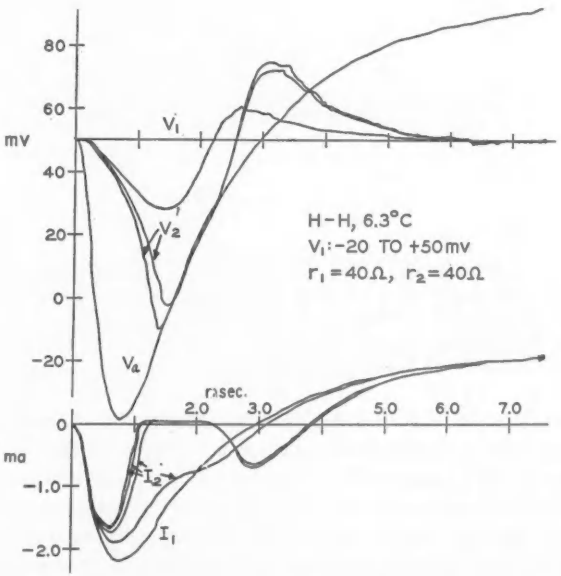

FIGURE 20 Two patch model computer results. Uniform case. Same as Fig. 19 but larger series resistances and depolarizing pulse.

notch" error. It is characterized by a current pattern in which the peak inward current may be greater or less than it would be for a perfect clamp and the potential across the second patch is greater (more depolarized) at the time of the peak inward current than the potential at which the first patch is controlled.

Discussion of Model Behavior. The behavior of the two patch model with the Hodgkin-Huxley equations is rather thoroughly understood, but an extended discussion would be too lengthy to include here. In certain cases the behavior is reasonable on the basis of some simple arguments. Reference to Fig. 24 will

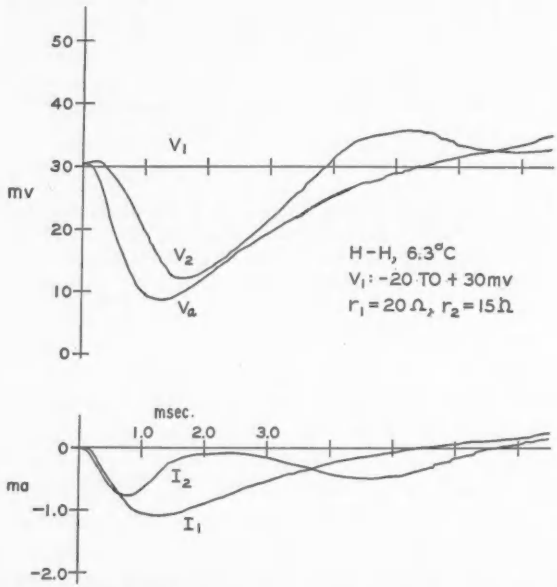

FIGURE 21 Two patch model computer results. Non-uniform case. Resistance in series with uncontrolled patch less than with controlled which favors a notch type error. This arrangement is (except for a scale factor on I_a and $V_a - V_2$) exactly equivalent mathematically to reducing all the conductances in the H-H equations for the uncontrolled patch by a common factor.

prove useful. This figure shows the peak inward current for various potentials during a step from a hyperpolarized value of −20 mv for the Hodgkin-Huxley equations as we used them. Strictly speaking the points on this curve bear only accidental relation to each other, because the various points are gotten under quite different conditions of potential and time. As a heuristic device let us consider a two patch model in which the current-voltage characteristic of each patch is independent of time and identical with the peak inward current curve shown in Fig. 24. Clamping the controlled patch at a potential V_0 would result in a current through this

patch given by the intersection of the vertical line through V_o and the curve. If the series resistance for this patch were 20 ohms the potential V_a would be given by the intersection of the line through this point of slope 1/20 with the zero current axis as indicated. Consider the second patch with identical series resistance of 20 ohms. The current and potential for the second patch will be given by the intersection of the curve and the line through V_a of slope 1/20 (labeled $r_1 = 20$ ohms in Fig. 24). However, because no feedback is involved, the intersection at the potential V_o will be *unstable*. In the presence of noise the current through the sec-

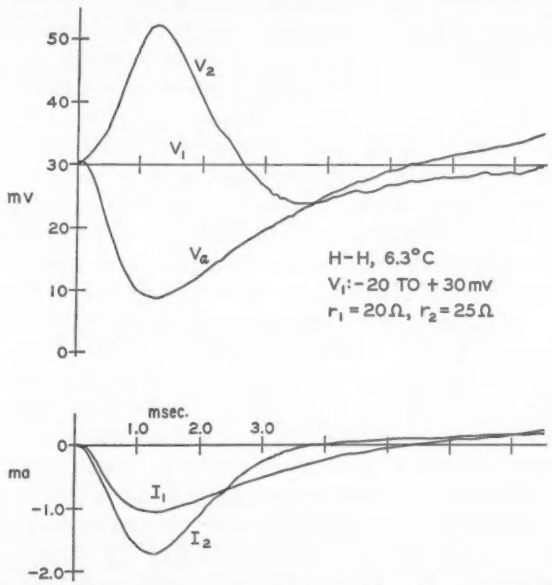

FIGURE 22 Two patch model computer results. Non-uniform case. Resistance in series with uncontrolled patch greater than controlled, favoring a no-notch type of error. This is equivalent mathematically (except for a scale factor on I_a and $V_a - V_2$) to increasing the conductances in the H-H equations for the uncontrolled patch by a common factor. In this case the inward current through the uncontrolled patch is greater than the controlled, but it may be less in other cases.

ond patch cannot be identical with that through the first, but must be the value given by one of the other two, stable, points of intersection. The final state will depend on the initial conditions and/or the exact time course of the noise. Large enough noise could drive the system from one stable condition to the other in a random fashion. If the electrical properties of the patches depend upon potential and time, as they do in the axon membrane, the entire time course of the current and potential for the uncontrolled patch may be greatly influenced by noise. This is presumably the cause of the variation which sometimes occurred in the computer

solutions on successive runs. An extreme case of this result is illustrated in Fig. 23.

The dashed lines in Fig. 24 represent non-uniform conditions. For this example, with time independent patch characteristics and $r_2 = 15$ ohms, the current and potential of the uncontrolled patch must lie on the line of slope 1/15 passing through V_a and $I = 0$. We note that this line intersects the patch characteristic in only one point, which is near V_a. In a very rough sense this is one kind of situation which leads to the production of notches while the other case illustrated, for $r_2 = 40$ ohms, is the kind of situation which leads to the production of no-notch errors.

Let us now consider the two patch model with the patches obeying the Hodgkin-Huxley equations for the case represented by Fig. 21 where $r_1 = 20$ ohms, $r_2 = 15$ ohms with an applied step in V_1 from -20 mv to $+30$ mv. For times greater than zero the axial wire potential V_a must follow a time course given by $V_a = V_1 + r_1 I_1$ where $V_1 = +30$ mv. At short times the current through the first system, I_1, is becoming more negative, hence V_a will be less than V_1. Assume that the current through the second system, I_2, is equal to I_1. Because r_2 is less than r_1 the potential drop $r_2 I_2$ will be too small to keep V_2 equal to V_1, reducing the amount of depolarization, hence the inward current, for the second patch. This is a regenerative process leading toward the current in the second patch being very small and therefore V_2 will approach V_a. Following the time of the peak inward current through the first patch V_a will become larger, depolarizing the second patch and resulting in a transient, delayed, inward current, which we have called a notch. Because V_1 is under control and the inward current in the controlled patch is of limited duration there is no time for a second notch to occur. This requirement is not present in the extended control system and it is suggested that this is the reason that a train of oscillations may be observed under these conditions (Tasaki and Bak, 1958*a*). Computations have not been done for the system shown in Fig. 18*B*, nor for the extended, continuous model of which this is a severe simplification. Rough and intuitive arguments suggest that the system of Fig. 18*B* would oscillate under certain conditions.

In some cases the current pattern through the second patch not only varied for successive computer runs, but would sometimes show a notch and sometimes a no-notch error. These cases are represented in Table II as unstable and one of them is shown in Fig. 23.

Extensions of the Two Patch Model. Various modifications of the two patch model have been considered in an attempt to gain further insight into the space clamp problem. Some of these have been of value, but none have yielded results which are sufficiently more comprehensive than the two patch model to make them worth including here.

Conclusions from the Model. The most important conclusion from considerations of the two patch model is the very strong support that the computations provide for the assertion that the behavior of the squid axon (in sea water) in the voltage clamp arrangements which have been employed is, *without exception,*

predictable from the assumption of the validity of the H-H equations. Even though the general space clamp problem is too complex to envision an early complete theoretical analysis the results to date indicate that the appearance of notches and/or oscillations during the clamping pulse provides no reason to doubt the validity of the current concepts embodied in the H-H equations and is rather to be taken as prima facie evidence of space clamp failure.

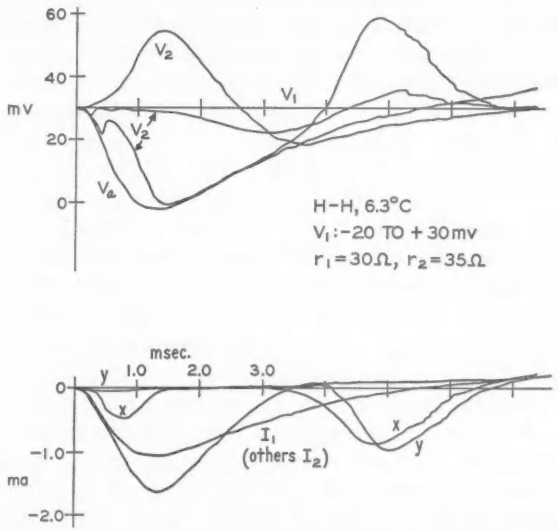

FIGURE 23 Two patch model computer results. Case where solution was unstable, sometimes giving a notch and sometimes a no-notch error on successive runs. Currents and potentials were recorded on different runs.

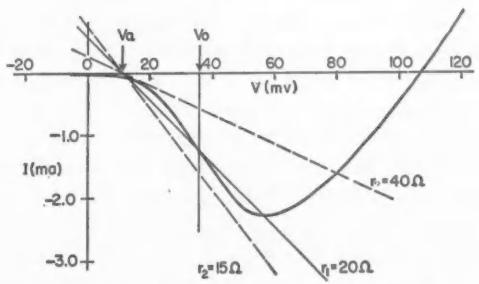

FIGURE 24 Curved line, value of peak inward current during a depolarizing step from a hyperpolarized value of −20 mv (relative to resting potential) to the value V, given by the Hodgkin-Huxley equations as used for the two patch model computations. For significance of other lines and further details see text.

EXTERNAL ACTION POTENTIAL INVASION

If a region of nerve in good condition extends beyond the end of the axial electrode, in any of the voltage clamp arrangements, an action potential will be initiated in this region for a sufficiently large depolarizing pulse and under certain conditions might invade the measuring region and produce a non-uniformity in the membrane potential, or add to that already present. Invasion of external action potentials may be avoided by eliminating the nerve in the region beyond the axial electrode (Frankenhaeuser and Hodgkin, 1957); eliminating the action potential with a drug which does not lower the membrane resistance or potential, such as urethane (Tasaki and Bak, 1958*a*), with the use of the double clamp (Tasaki and Spyropoulos, 1958, p. 312), or by the use of low surface resistance axial electrodes as we have done (Cole and Moore, 1960). The type of interaction described by Frankenhaeuser and Hodgkin (1957) will not occur with the point control system because an invading action potential must reach the immediate vicinity of the control microelectrode in order to influence the feed-back control.

An invading action potential could not reach the current measuring chamber by purely passive electrotonic spread unless the surface resistance of the axial current wire were so high that one would not expect the membrane potential to be uniform in any case. For example, for a 100 mv action potential to be attenuated to 1 mv over a distance of 6 mm the space constant would have to be 0.13 cm which, for a maximum membrane resistance of 5000 ohm cm, gives a minimum value of 254 ohm cm for the surface resistance of the axial wire, a hopeless value for a space clamp, even for a uniform axon. This is a somewhat artificial point of view, except when the applied depolarizing pulse is large enough so that all parts of the membrane which are capable of becoming "active" have done so by the time that the invading action potential appears. In this case the argument is rigorous and eliminates the possibility of notches occurring in this way for depolarizing pulses larger than those for which the peak inward current is a maximum.

For completeness we shall dispose of another possibility. If the axon were very non-uniform the inward current, during a depolarizing pulse to some value, might be small in the guard chamber, compared to its value in the center measuring chamber, but capable of becoming much larger due to the added depolarization of an invading action potential, delayed in time. Some of this current would then be drawn through the gap in the partition and appear as an extra, delayed inward current hump in the current measured in the center chamber. The magnitude of this effect depends upon the resistance of the gap, but for a value of 300 ohms (our system without grease or axon) it would have a maximum in the neighborhood of 0.1 ma/cm^2, referred to a square centimeter of membrane for a 500 micron diameter axon.

We are still left with the possibility of the interaction of an invading action potential for depolarizing pulses larger than that necessary to initiate them beyond the axial wire and smaller than that necessary to produce the maximum peak inward

current. A complete understanding of this region has not been achieved. This is a complex problem, augmented by the fact that the potential range, as well as the suspected axial electrode resistance range, is the same as that for which the two patch model indicates the possibilities of notches under conditions of small amounts of non-uniformity in membrane properties. The most reasonable conclusion at the present time appears to be that there might be a range of axial electrode resistance values such that for a uniform axon the space clamp might fail and a notch might be produced only when action potentials are present beyond the ends of the axial electrode. Uniform, in this case, clearly must refer to the average properties over regions comparable in size to the axon radius. Moderate amounts of non-uniformity in membrane properties would narrow this range if it exists.

ERRORS INTRODUCED BY SMALL RESISTANCE BETWEEN VOLTAGE CONTROL POINTS

Ideally the potential which is being controlled should be the potential across the membrane capacity, but in practice it is not possible to do this without the use of compensated feed-back. A consideration of the effects of a small resistance between the control points, in series with the membrane capacity, is necessary for the evaluation of the importance of the steps taken to reduce this resistance and for a consideration of the possible effects of the presence of a suspected residual series resistance when all known series resistances are accounted for.

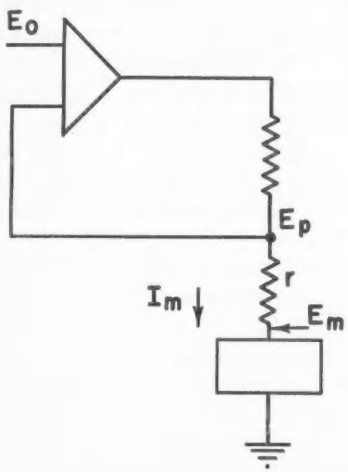

FIGURE 25 A simplified equivalent circuit relevant to the effect of a resistance in series with the membrane capacity between the potential control electrodes.

A simplified representation of the relevant equivalent circuit is shown in Fig. 25. We shall assume that $E_o = E_p$. Clearly $E_m = E_p - I_m r$. If r is very large, then during a clamping pulse to certain potentials threshold phenomena or/and repetitive ac-

tivity may result. However, for solutions of the equations of Hodgkin and Huxley for the squid axon, Fitzhugh and Moore (unpublished data) have found that the magnitude of the resistance required for threshold phenomena (considerably less than that required for repetitive activity) is about twice the reciprocal of the steepest part of the peak inward current *versus* clamping potential curve. The value of this reciprocal negative slope for the Hodgkin-Huxley axon is (independent of temperature) 24 ohm cm^2 for a holding potential equal to the resting potential and 16 ohm cm^2 for a 20 mv hyperpolarized holding potential (see Fig. 24). In our experiments, for twenty-two axons for which the data are available, this value averaged 3.42 ohm cm^2, varying from 1.6 to 8.2. This difference cannot be a direct result of the greater peak inward currents in our experiments. For these twenty-two axons the maximum peak inward current averaged 3.89 ma/cm^2, as compared to 2.4 ma/cm^2 for the H-H axon prepolarized by 20 mv, or a ratio of 0.617, while the ratio of the reciprocal negative slopes is 3.42/16, or 0.214. There is no known reason, of course, why these ratios should be the same. If the axons which we used behaved in a fashion comparable to the H-H axon, and if the steepness of the peak inward current curve was not the result of a large series resistance, then serious trouble from instability would occur for an additional series resistance of 7 ohm cm^2. This value can be compared to the 50 ohm cm^2 for the H-H axon without prepolarization.

Errors are introduced for values of series resistances well below these which lead to instability. The 7 to 9 ohm cm^2 estimated by H-H and Katz (1952) to be present in the experiments with uncompensated feedback introduced errors, but probably not of a serious nature. In our experiments this resistance has been decreased (Cole and Moore, 1960) by the use of an internal microtip just under the surface of the membrane and an external reference electrode just outside the membrane, for voltage control. It is not known what the value of the final resistance is, but it should be close to the irreducible minimum without the use of compensated feedback.

Fig. 26 (axon 58-63) shows the effect of increasing this series resistance by removal of the external reference electrode on the curves of peak inward current, plotted against the clamping potential during the pulse.

Removal of the reference electrode (squares) decreases both the peak inward current and the steady state current for rather large depolarizations, while the shape of the peak inward current curve is distorted for smaller values of depolarizing pulses. The time to the peak inward current is not changed much, except for a slight increase in the region of $E_p = -40$ to -50 mv. These effects of the addition of a small series resistance are to a very good approximation completely duplicated by the results of a similar "experiment" done by FitzHugh and Moore (unpublished data) on the analog computer with the empirical equations of Hodgkin and Huxley. Similar results were found for three other nerves and for one in which an external lumped resistance was inserted between the voltage control points.

To properly evaluate the kinds of error which might result in future experiments it is worth while to consider the explanation of the effects seen in Fig. 26.

For the steady state outward current the situation is relatively simple. The line through the open circles in Fig. 26 is the steady state relation between E_p and I_m when the series resistance is zero and $E_p = E_m$. When a series resistance is introduced the current for a given E_p should be the intersection of the steady state $I_m - E_p$ curve for $r = 0$ and the load line $E = E_m = E_p - I_m r$. It follows that the reciprocal of the slope of the $I_m - E_p$ curve for $r = 0$ should differ from the same quantity for the $I_m - E_p$ curve for $r = r$ by the amount r, evaluated at the same I_m. In particular a straight line will remain a straight line and the reciprocal slopes will differ by r. This will be true no matter what kinds of non-linear elements are present so long as they give a straight line current voltage characteristic in the steady state. For this particular experiment, the slopes of the open circle line ($r = 0$) and the open squares line (series resistance in) differ by 2.7 ohm cm². This value thus

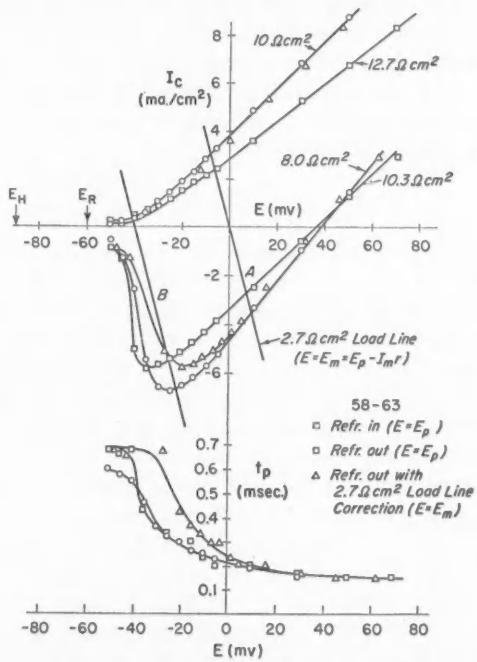

FIGURE 26 Effect of added series resistance between the potential control electrodes on the curves of peak inward and steady state outward current during depolarizing steps. Lower curve, time to peak inward current. In this case the resistance was added by removal of the external reference control electrode. Open circles, reference connected, no added series resistance. Open squares, reference removed, resulting in the addition of 2.7 ohm cm² series resistance. Open triangles, result of a simple "load line" correction (straight lines) for a series resistance of 2.7 ohm cm². Theoretically the load line correction should be possible either for the steady state or if the current voltage relation is a straight line.

represents the resistance between the point at which the reference electrode was in the solution, and ground (the nerve in the measuring chamber had an area of 0.075 cm² giving 36 ohms for the actual resistance).

The open square curves for the peak inward and steady state outward currents are plotted in Fig. 26 against the value of E_p. Correcting these curves for the presumed 2.7 ohm cm² gives the open triangles for I_m *versus* E_m. The same convention has been employed for the curves of the time to the peak inward current (t_p) in the same figure. When the currents and times are plotted against the membrane potential (E_m) the straight line portion of the peak inward current is the same with and without the series resistance and the times to the peak are the same over this range of potentials. However, for E_m between −40 and zero the peak currents and times differ considerably. The situation here is not simple, but the effects are intuitively reasonable and essentially duplicated by the analog computations with the Hodgkin-Huxley equations. It can be shown that a consequence of the H-H equations is that the sodium conductance at the time of the peak inward sodium current during a potential step from an initially hyperpolarized value ($m_o = 0$) is a function of the ratio of the time constants of the sodium off (τ_h) and the sodium on (τ_m) processes; *i.e.*, the peak current is given by

$$I_p = (E_p - E_{Na}) F(\tau_h/\tau_m) g_{Na} m_\infty{}^3 h_0 .$$

In the region of large depolarizations the ratio of time constants remains almost constant for different values of E_m as does m_∞. We thus find an almost straight line for the peak inward current *versus* potential curve, and (when plotted against E_p) the inverse slope of this line changes by the amount of the added series resistance. In the range of small depolarizations, the ratio of time constants is not constant with potential, nor is m_∞. With the presence of a series resistance the potential across the capacity, E_m, will vary with time during a step in E_p and thus the ratio τ_h/τ_m and M_∞ will also vary with time. The resultant peak inward current will no longer have any simple significance and will be a compromise between the values for no series resistance corresponding to $E_m = E_p$ and $E_m = I_m r$ with I_m evaluated for $r = 0$. In the example of Fig. 26, for a depolarizing step to $E_p = -40$ mv and a series resistance of 2.7 ohm cm² the membrane potential must always be on the load line labeled B. The limiting values for the peak inward current are that for no series resistance and $E_m = -40$ mv (−2.6 ma/cm²) and that for the intersection of load line B and the curve for no series resistance (−6.7 ma/cm²). The simple average of these limiting values is −4.65 ma/cm², compared to the measured peak inward current of −5.17 ma/cm². There is no simple way to arrive at *accurate* values for the effect of a small series resistance on the inward current in this range of potentials. It is probably not possible to uniquely correct for the errors introduced by a known series resistance. Distortions of the current patterns as represented in Fig. 26 might not be serious, depending upon the use to which the data are put. It is clear that in some of our experiments the addition of as little as 1 to 2 ohm cm² (or

7 to 14 ohm cm for a centimeter length of measuring region) would distort the peak inward current curve to such an extent that one might conclude that it was discontinuous.

Compensation. The addition of a negative resistance between the voltage control points (compensated feedback, see Hodgkin, Huxley, and Katz, 1952) will properly remove the effect of an added positive resistance. Fig. 27 represents the results of one such experiment. Removal of the reference electrode introduced a net

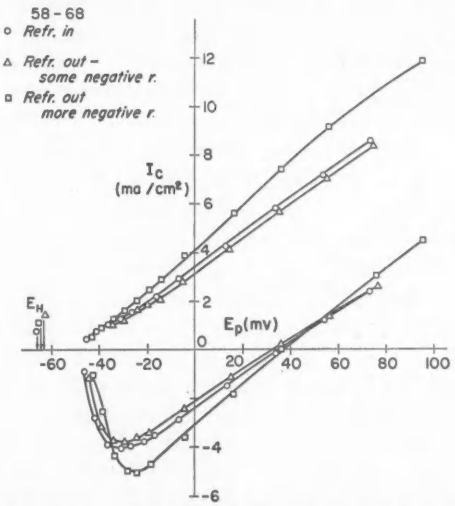

FIGURE 27 Peak inward and steady state outward currents versus potential during a depolarizing step (from a holding potential indicated by E_H). Open circles, normal conditions. Open triangles, reference removed (introducing 3.5 ohm cm² series resistance) and compensated by the introduction of negative resistance. Open squares, addition of a further 3 ohm cm² of negative resistance.

series resistance of 3.5 ohm cm² (not shown in the figure). Addition of a negative resistance yielded the peak inward and steady state outward current curves (open triangles) which are virtually identical with the original (open circles) curves (neither a positive or a negative resistance added). The times to the peak inward current were also identical. Addition of still more negative resistance resulted in the curves through the open squares. This represents the addition of about 3 ohm cm². Since the nerve remained stable, one suspects that at least 3 ohm cm² was present originally between the voltage electrodes and the membrane capacity. That is to say, the open square curves are probably more accurate than the circle curves.

DISCUSSION

If the membrane current during an applied potential step consisted of a number of peaks, or a continued oscillation, there would be no apparent justification for the

use of the membrane potential as a controlled variable in attempting to determine the electrical characteristics of the membrane. And the use of a voltage clamp apparatus would hardly seem to be an appropriate substitute for a desk calculator for eliminating the membrane capacity current. There is no reason, other than the experimental results themselves, to expect that the current through the squid axon membrane, following a step of membrane potential, would have the simple form described by Cole (1949) and Hodgkin, Huxley, and Katz (1949). It is of the greatest importance, however, to know whether this is indeed the case. Hodgkin and Huxley (1952) were able to fit their data for the currents during a potential step in terms of three *independent* processes (sodium on, sodium off, potassium on), each of which is describable by a linear, first order differential equation in which the parameters depend only on the membrane potential. This would not be practical for a system in which the current was oscillatory for constant potential; each additional current peak would require at least one more "simple" process.

While to our knowledge, everyone who has atempted to use the voltage clamp method has at some time observed notches or oscillations in the measured current patterns, we have never found a membrane current pattern with more than one peak when we were certain that the membrane potential was constant over the region in which the current was measured. One must conclude, then, that the anomalous current patterns are the result of a failure to obtain sufficient spatial control of the membrane potential. From the results given in this paper we may form a rather good idea of how it is that the attempted spatial control may fail and how the anomalous current patterns arise. Although the results presented here refer only to the squid axon in sea water for a particular kind of electrode arrangement, similar difficulties would arise in the attempt to voltage clamp any system, biological or otherwise. The empirical equations of Hodgkin and Huxley were employed in computations because they exist, and are relevant to our system, but they are incidental to the problem of the space clamp. If the oscillations were not artifacts the problems of spatial control would be essentially the same.

It is useful to distinguish between spatial control difficulties which are the result of non-uniformities in membrane properties and those which would occur in a uniform system. For our purposes a uniform membrane would be one for which the properties were the same averaged over any region comparable in size to one space constant (about 0.5 mm). Non-uniformities of significantly finer detail would not be directly measurable in terms of membrane potential. This is a fundamental limitation on the measurement of the electrical properties of any interface.

For a uniform system the spatial control would be perfect if the resistance between the axial electrode and the membrane were smaller than some given value. What this value is remains uncertain, but it is probably not greatly different from the reciprocal of the maximum negative slope of the curve of peak inward current *versus* clamping potential measured at the controlled point. In the computations on the two patch model with the Hodgkin-Huxley equations, an incipient notch oc-

curred in the uncontrolled patch for a series resistance of 10 ohms (see Table II), while the reciprocal of the maximum negative slope of the inward current in the controlled patch was 16 ohms. Because of the presence of a known small bias in the computer (see page 186), this example may not in fact represent a perfectly uniform case, but it cannot be concluded that the limiting resistance is greater than 16 ohms (for 1 cm^2 of membrane).

In the presence of non-uniformities of membrane properties or axial electrode resistance there is no lower limit for the appearance of errors in the current through an uncontrolled region of membrane. These errors in the non-uniform case might be small and give rise to no obvious anomalies in the current-time patterns, but their complete elimination is impossible and the requirements for stability are severe. Thus a well developed notch occurred in the uncontrolled patch in the two patch model computations for a series resistance of 10 ohms in the controlled patch and 5 ohms in the uncontrolled. A rough conversion of these values to those appropriate for the axons which were used in the present investigation gives values for radial resistance which are comparable to the radial axoplasm resistance between a 75 micron diameter wire and a 500 micron diameter membrane. We must conclude that it is not possible to confidently predict the existence of an adequate space clamp for a squid axon using a 75 micron diameter axial electrode, even if it has zero surface resistance. It would appear that an independent check on the adequacy of spatial clamping must be made for each axon or the region over which the membrane current is measured must be reduced to a size comparable to an axon radius. At the present time the only feasible check on the adequacy of the space clamp and the uniformity of the axon appears to be the measurement of the membrane current distribution with external differential electrodes. If this distribution is not uniform, then almost nothing can be said about the system. A non-uniform result would certainly not indicate anything about the uniformity, or lack of uniformity of the membrane properties. Spatially uniform membrane current, however, should constitute strong evidence both that the membrane properties were uniform and that the clamp was good. An unbelievable combination of error cancellations would have to occur in order to give uniform membrane current with non-uniform membrane properties.

Extensions of Two Patch Model. From the experimental results presented here it does not appear that the stability properties of the squid axon in the point control arrangement are appreciably different from those which the two patch model would suggest. Analysis of the complete, continuous model has not been attempted and is probably impractical although some intermediate models may be useful for certain purposes. Further analysis of the behavior of the membrane in the immediate vicinity of the control point would be helpful.

A reasonable analysis of the extended control voltage clamp arrangements does not seem to be possible without the development of Hodgkin-Huxley analogs which are compact enough to be incorporated into a resistor board model for the axon.

The Node of Ranvier. It is important to know whether the membranes of

other cells may show oscillations in the membrane current under conditions of constant potential for the same reasons as discussed for the squid axon. Such oscillations were not reported in nerve cell bodies by Hagiwara and Saito (1959) or by Frank *et al.* (1959) but were reported by Tasaki and Bak (1958*b*) for the frog node. However, the most careful work on the node has been done by Dodge and Frankenhaeuser (1958) and with improvements in technique, particularly with regard to the accurate measure of nodal membrane potential, the oscillations, which they had observed initially, disappeared. The situation is much the same as for the squid, the more reliable the membrane potential measurement over the current measuring region, the less the tendency to oscillate. In addition (Dodge, 1960, and personal communication), certain likely sources of error have been identified. The most important of these is probably the capacity between the outer pools in the usual gap technique methods. The existence of 10^{-14} farads of capacity in this position is sufficient to introduce differences of 10 mv between the recorded and actual membrane potential. The deviation is proportional to the first derivative with respect to time of the membrane current and appears to be adequate to explain the reported oscillations. Here, as elsewhere in this paper, we are assuming a perfect electronic system which maintains the recorded membrane potential at any predetermined value. The final conclusion from the work of Dodge and Frankenhaeuser is that it is possible to adequately voltage clamp the node of Ranvier but that special methods must be employed for the measurement of the membrane potential. Other difficulties are present in the membrane current supply and are discussed by Dodge and Frankenhaeuser (1958).

SUMMARY

An experimental and theoretical examination has been made of certain technical difficulties which may limit, and in some cases negate, the attempt to deduce the electrical characteristics of the squid axon membrane with the use of the "voltage clamp" technique. In order that data obtained with the use of this technique have any clear meaning the potential across the capacity of the membrane must be known in time (potential-time clamp) and uniform over the entire region in which the (average) membrane current is measured. Uniformity of membrane current under these conditions is not a requirement for the measuring system, but a property of the nerve membrane about which no reliable information is available at this time.

Extreme space clamp failure was induced with the use of deliberately high resistance axial current supplying electrodes and the distribution of membrane potential and current under these conditions is described. It was found that when more than one inward going membrane current peak occurred during a potential step all but the first decrease to a small value, or disappear, when the region over which the current was measured was known to be under good potential control. It is concluded that the appearance of notches or oscillations in the membrane cur-

rent during a clamping pulse is sufficient evidence for space clamp failure and that under these conditions the data cannot be used to deduce the membrane electrical characteristics. The absence of obvious anomalies in the current patterns, however, is not sufficient evidence for the conclusion that the space clamp is adequate.

Most features of the observations made during space clamp failure have been reproduced by computations using a two patch model and the empirical equations of Hodgkin and Huxley (Taylor and FitzHugh, 1959). Incomplete and largely intuitive extension of these results to the actual system provides very strong support for the conclusion that no data now available for the squid axon in sea water are inconsistent with the basic ideas embodied in the Hodgkin-Huxley equations.

Both experimentally and on the basis of incomplete but convincing theoretical arguments it is concluded that current supplying axial electrodes with surface resistance greater than about 25 ohm cm are useless for space clamping a uniform axon which can produce as much as 5 ma/cm^2 peak inward membrane current. The presence of non-uniform membrane properties would reduce the maximum allowable electrode resistance below 25 ohm cm; possibly to zero. For data to be acceptable reasonable evidence for adequate spatial clamping over the entire current measuring region must be provided. This may be done by reducing the area over which the current is measured to something less than an axon diameter, or by the measurement of membrane current distribution with external differential electrodes and rejection of any axon for which this distribution is not uniform.

The effects of a resistance between the potential reference points and in series with the membrane capacity have been described. The results are in agreement with the predictions of the empirical equations of Hodgkin and Huxley, and lead to the conclusion that a few ohm cm^2 of series resistance would result in errors which are probably uncorrectable in principle. These errors could be minor, but a series resistance of about 7 ohm cm^2 could lead to serious instability problems and might mislead one into concluding that the peak inward current *versus* potential curve was discontinuous.

We wish to thank Dr. Jose del Castillo for his collaboration during the course of the experimental work, Mr. John Gebhart for help in the construction and maintainance of the electronic equipment, and Mr. Ernest Whitcomb for his technical assistance. We are grateful to Dr. R. FitzHugh, Dr. W. K. Chandler, and Dr. W. J. Adelman, Jr., for many helpful suggestions and criticisms.

The experiments presented in this article were conducted at the Marine Biological Laboratory, Woods Hole, Massachusetts.

Received for publication, September 16, 1960.

REFERENCES

COLE, K. S., 1949, Dynamic electrical characteristics of the squid axon membrane, *Arch. sc. physiol.*, **3**, 253.

COLE, K. S., and MOORE, J. W., 1960, Ionic current measurements in the squid giant axon membrane, *J. Gen. Physiol.*, **44**, 123.

DODGE, F. A., JR., 1960, Simple nerve-membrane analog, *Abstr. Biophysic. Soc.*, 11.

DODGE, F. A., JR., and FRANKENHAEUSER, B., 1958, Membrane currents in isolated frog nerve fibre under voltage clamp conditions, *J. Physiol.*, **143**, 76.

FITZHUGH, R., 1960, Thresholds and plateaus in the Hodgkin-Huxley nerve equations, *J. Gen. Physiol.*, **43**, 867.

FRANK, K., FUORTES, M. G. F., and NELSON, P. G., 1959, Voltage clamp of motoneuron soma, *Science*, **130**, 38.

FRANKENHAEUSER, B., and HODGKIN, A. L., 1957, The action of calcium on the electrical properties of squid axons, *J. Physiol.*, **137**, 218.

HAGIWARA, S., and SAITO, N., 1959, Voltage-current relation in nerve cell membrane of *Onchidium verruculatum*, *J. Physiol.*, **148**, 161.

HODGKIN, A. L., and HUXLEY, A. F., 1952, A quantitative description of membrane current and its application to conduction and excitation in nerve, *J. Physiol.*, **117**, 500.

HODGKIN, A. L., HUXLEY, A. F., and KATZ, B., 1949, Ionic currents underlying activity in the giant axon of the squid, *Arch. sc. physiol.*, **3**, 129.

HODGKIN, A. L., HUXLEY, A. F., and KATZ, B., 1952, Measurement of current-voltage relations in the membrane of the giant axon of *Loligo*, *J. Physiol.*, **116**, 424.

TASAKI, I., and BAK, A. F., 1958*a*, Discrete threshold and repetitive responses in the squid axon under "voltage clamp," *Am. J. Physiol.*, **193**, 301.

TASAKI, I., and BAK, A. F., 1958*b*, Current-voltage relations of single nodes of Ranvier as examined by voltage-clamp technique, *J. Neurophysiol.*, **21**, 124.

TASAKI, I., and SPYROPOULOS, C. S., 1958, Nonuniform response in the squid axon membrane under "voltage clamp," *Am. J. Physiol.*, **193**, 309.

TAYLOR, R. E., and FITZHUGH, R., 1959, A source of anomalous current patterns in the "voltage clamped" squid axon, *Abstr., Biophysic. Soc.*, G. 6.

LETTERS TO THE EDITOR

Dear Dr. Brink:

Readers of the Biophysical Journal may be interested in some of the details of its physical form.

The type face chosen, Times Roman, was one of three recommended in 1950 for use in scientific periodicals by a Committee of the Royal Society under chairmanship of Sir Solly Zuckerman. Though it was designed for *The Times* of London in 1932, it has only recently become available for Monotype composition in this country. The full range of sizes and special characters that make it so suitable for scientific printing in England are not yet available here, so that for a few issues typographic-minded readers may notice some improvisations in the mathematical formulae and tables.

We have adopted a few innovations to give the reader "swiftest access to the author's thought" in the words of Stanley Morrison, designer of Times Roman and sometime typographic adviser to *The Times*, Cambridge University Press, and the Monotype Corporation. The conventional "running heads" on each page have been dropped to the foot of the page. We believe the reader is not likely to forget what he is reading as he turns a page so we do not interrupt his eye as he resumes reading the text. Should a reader wish to write a note regarding the article, however, he will find at the foot of each pair of facing pages all that will be needed for most references. Similarly, the date of receipt of the manuscript and acknowledgments of grant support are placed at the end of the text but before the references. Finally, on the contents page (which is placed on the back cover for ready accessibility) the page numbers follow immediately after the last word in the title, instead of being aligned in a column down the right edge of the page. By not forcing the eye to jump a long gap from title to page number, a source of error is avoided.

The proportions of the page approximate the Pythagorean Golden Section $(1:\frac{1}{2}\{\sqrt{5}-1\})$, a matter largely of esthetics, but the length of line, the space between lines, and the size of type provide what is believed to be optimum legibility. Closer spacing, smaller type or shorter lines (the familiar double-column format) might save something in over-all economy, but at the price of lower legibility and some awkward (and costly) problems with long equations.

These matters need not concern readers, as long as they are handled well, but I report them with the thought that biophysicists may be interested in details of the design of a relatively efficient and noise-free new channel for transmitting scientific information from one laboratory to many.

CHARLES I. CAMPBELL, Director
The Rockefeller Institute Press

Brief letters to the Editor that make specific scientific reference to papers published previously in the BIOPHYSICAL JOURNAL are invited. Receipt of such letters will not be acknowledged but those containing pertinent scientific comments and scientific criticisms will be published.

ANNOUNCEMENTS

Placement Service Change of Address

The *new* address for the Placement Service of the Biophysical Society is P. O. Box 668, Frederick, Maryland.

Announcements of direct interest to the Biophysical Society will be acceptable. Receipt of announcements will not be acknowledged but appropriate ones will be printed. Conciseness and clarity are factors in the decision to print an announcement.